Volume 71C
Number 2
Apr.–June 1967

Engineering and Instrumentation

U.S. DEPARTMENT OF COMMERCE

SECTION C

JOURNAL OF RESEARCH

NATIONAL BUREAU OF STANDARDS

Journal of Research
of the
National Bureau of Standards

C. Engineering and Instrumentation

Apr.–June • 1967

VOLUME • 71C

NUMBER • 2

Editor: Martin Greenspan

Associate Editors: G. F. Montgomery, R. V. Smith, A. F. Schmidt

Publication dates:
Feb. 15, May 15, Aug. 15, Nov. 15, 1967

JOURNAL OF RESEARCH

The National Bureau of Standards Journal of Research reports research and development in the fields of activity shown at right. Also included from time to time are survey articles on topics closely related to the Bureau's scientific and technical program.

The Journal is published in three separate sections as follows:

A. Physics and Chemistry

Contains papers of interest primarily to scientists working in these fields. Issued six times a year. Annual subscription: domestic, $5.00; foreign, $6.00. Single copy, $1.00.

B. Mathematics and Mathematical Physics

Presents studies and compilations designed mainly for the mathematician and the theoretical physicist. Issued quarterly. Annual subscription: domestic, $2.25; foreign, $2.75. Single copy, 75¢.

C. Engineering and Instrumentation

Reports research and development results of interest chiefly to the engineer and the applied scientist. Issued quarterly. Annual subscription: domestic, $2.75; foreign, $3.00. Single copy, 75¢.

U.S. DEPARTMENT OF COMMERCE
Alexander B. Trowbridge, Acting Secretary
NATIONAL BUREAU OF STANDARDS
A. V. Astin, Director

The National Bureau of Standards is a principal focal point in the Federal Government for assuring maximum application of the physical and engineering sciences to the advancement of technology in industry and commerce. Its responsibilities include development and maintenance of the national standards of measurement, and the provisions of means for making measurements consistent with those standards; determination of physical constants and properties of materials; development of methods for testing materials, mechanisms, and structures, and making such tests as may be necessary, particularly for government agencies; cooperation in the establishment of standard practices for incorporation in codes and specifications; advisory service to government agencies on scientific and technical problems; invention and development of devices to serve special needs of the Government; assistance to industry, business, and consumers in the development and acceptance of commercial standards and simplified trade practice recommendations; administration of programs in cooperation with United States business groups and standards organizations for the development of international standards of practice; and maintenance of a clearinghouse for the collection and dissemination of scientific, technical, and engineering information. The scope of the Bureau's activities is suggested in the following listing of its three Institutes and their organizational units.

Institute for Basic Standards. Applied Mathematics. Electricity. Metrology. Mechanics. Heat. Atomic Physics. Physical Chemistry. Laboratory Astrophysics.* Radiation Physics. Radio Standards Laboratory:* Radio Standards Physics; Radio Standards Engineering. Office of Standard Reference Data.

Institute for Materials Research. Analytical Chemistry. Polymers. Metallurgy. Inorganic Materials. Reactor Radiations. Cryogenics.* Materials Evaluation Laboratory. Office of Standard Reference Materials.

Institute for Applied Technology. Building Research. Information Technology. Performance Test Development. Electronic Instrumentation. Textile and Apparel Technology Center. Technical Analysis. Office of Weights and Measures. Office of Engineering Standards. Office of Invention and Innovation. Office of Technical Resources. Clearinghouse for Federal Scientific and Technical Information.**

*Located at Boulder, Colo. 80302.
**Located at 5285 Port Royal Road, Springfield, Va. 22151.

Order all publications from the Superintendent of Documents
U.S. Government Printing Office, Washington, D.C. 20402.

Use of funds for printing this publication approved by the Director of the Bureau of the Budget (June 22, 1966).

JOURNAL OF RESEARCH of the National Bureau of Standards—C. Engineering and Instrumentation
Vol. 71C, No. 2, April–June 1967

An Apparatus for Measuring Thermal Expansion at Elevated Temperatures

B. D. Rothrock and R. K. Kirby

Institute for Basic Standards, National Bureau of Standards, Washington, D.C. 20234

(November 23, 1966)

An apparatus has been developed for making precise measurements of the absolute thermal expansion of refractory materials at temperatures up to 1600 °C. This apparatus consists of an optical comparator and a controlled gradient vacuum furnace. Special care was taken on the techniques of measuring length and temperature and on the calibration of the microscopes and thermometers. The expansion data obtained with this apparatus on specimens of platinum and sapphire have a standard deviation of less than 30 ppm and are estimated to be accurate to within 50 ppm.

Key Words: Controlled-gradient vacuum furnace, elevated temperatures, optical comparator, thermal expansion.

1. Introduction

Accurate data on the thermal expansion of solids at temperatures above 1000 °C are needed for several reasons. (1) They are needed on at least one reproducible material so that engineering data on other materials can be obtained with relatively simple apparatus by a comparison method [1].[1] (2) The material on which the data is obtained can be used to measure temperatures in high-temperature x-ray diffraction cameras and diffractometers [2, 3]. (3) Accurate high-temperature data can be useful in the study of lattice defect formation [4], phase transitions [5], and the theory of thermal expansion [4, 6]. The apparatus described in this paper was constructed primarily to furnish accurate thermal expansion data up to 1600 °C on a reference material that could be used by others in measuring thermal expansion. Because of this, special care was taken on the techniques of measuring length and temperature and on the construction of the furnace.

An optical comparator method was chosen because it can be used to make accurate and precise measurements of the expansion of solid material at elevated temperatures. The present method makes use of a pair of microscopes mounted on an invar bar and each measurement of the length of the specimen is compared to the length of a reference bar kept at room temperature. This procedure gives a correction that compensates for any apparent change in distance between the microscopes caused by the expansion of the invar bar or the tilting of the microscopes. The nominal length of the specimen between the fiducial marks is 10 cm. The specimen, hung vertically in the furnace, is free of all restraint so that measurements of expansion will be accurate as long as the specimen does not creep significantly under its own weight. The vacuum furnace is specially designed to correct for end heat losses. In addition the temperature profile over the length of the specimen was measured with a calibrated probe thermocouple. A detailed description of the apparatus and techniques is given in the following sections.

[1] Figures in brackets indicate the literature references at the end of this paper.

2. Apparatus

2.1. Furnace

To make accurate length versus temperature measurements the furnace must be designed and constructed to produce a uniform temperature along the length of the specimen or the temperature gradient along the specimen length must be known at each temperature to determine the effective or average temperature of the specimen [7]. To obtain a uniform temperature over the specimen length a controlled-gradient furnace was constructed that has five individually controlled heating sections obtained by tapping an evenly wound resistance heater at 5 cm intervals. By the use of isolation transformers the power in any one section can be controlled with only a negligible change in power in the remaining sections. This design, as shown in figure 1, makes it possible to adjust the power input at any temperature to com-

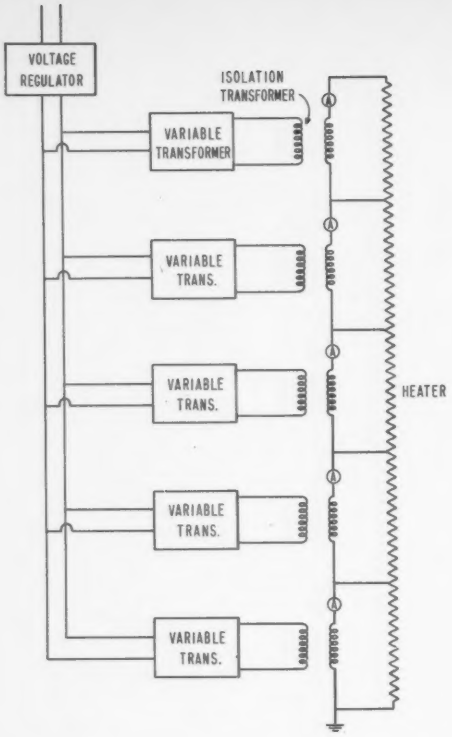

FIGURE 1. *Schematic diagram of heater control circuit.*

pensate for end heat losses. A voltage regulator was used to compensate for line voltage variations as it was felt that this would be the main cause of temperature variations. The power required to obtain 1600 °C was 2.6 kW.

The heater wire, having a diameter of about 1 mm, is wound about a core in a 1.6 mm deep continuous groove, 6 revolutions per 25.4 mm. Tantalum, tungsten, and rhenium wire have been used. Although each have desirable resistivity and high temperature properties, rhenium proved to be the best because of its high-temperature inertness and greater ability to be worked.

The high-purity alumina (99% Al_2O_3) core on which the heater is wound is 30.5 cm long and has a 1.91 cm I.D. and a 2.54 cm O.D. Sight holes, 6.3 mm in diameter, in the core, see figure 2, are alined with holes in the heat shields and the windows in the outer shell. Two windows on one side, with centers 10 cm apart, allow viewing of the specimen for length measurements. A third window on the opposite side permits temperature measurements with an optical pyrometer.

The specimen, a 12 to 14-cm rod having a diameter of about 5 mm, is hung from the top of the furnace by two loops of tungsten wire. The small lower loop runs through a small hole in the top of the specimen and is connected to the larger upper loop by a tungsten joint which allows the specimen to hang freely in a vertical position. Vertical, lateral, and rotational movement can be achieved through a bellows and vacuum seal.

The control and measuring thermocouples are positioned in 0.76 mm holes in the wall of a high-purity alumina tube. This tube, 1.11 cm I.D. by 1.75 cm O.D., is 35.6 cm in length. The thermocouples are shielded by a grounded rhenium foil placed between the heating core and thermocouple protection tube. A small a-c pickup can be detected but did not affect the thermocouple emf output as read by either the potentiometer or recorder.

The outer stainless steel shell of the furnace is water-cooled and vacuum sealed. The vacuum system consists of a fore pump, oil diffusion pump, water-cooled baffle, and vacuum gages. The vacuum gage indicator, power supply and controls, and temperature indicators are mounted in a relay rack.

2.2. Comparator and Reference Scale

The comparator shown in figure 3, consisting of two microscopes mounted on an invar bar, was obtained commercially. The microscopes have filar micrometer eyepieces, 50× magnification, and relay lenses which allow a working distance of 16 cm. They can be raised or lowered and rotated about a vertical axis. The comparator, however, was modified to allow for precise alinement after being rotated between the specimen and scale positions.

The reference scale, mounted outside the furnace, is made by wrapping a 0.020 mm tungsten wire about a vitreous-silica rectangular bar 2.54 cm × 1.91 cm × 15.2 cm. The wires are spaced 1 mm apart by grooves at the edges of the silica bar and held in position by epoxy. The back surface of the clear bar was ground so that when illuminated from the back the wires stood out sharply against an evenly illuminated field. The scale was calibrated accurately to within ±0.2 micrometers by using a line standard, Decimeter No. 43, provided by the Length Section of the National Bureau of Standards. The position of the scale can be adjusted in the vertical and horizontal directions.

The scale eliminates any apparent or real shift in the measurement of length caused by expansion of the invar bar or tilting of the microscopes and establishes the absolute length of the specimen. In preliminary tests on the microscopes, measurements were made on the reference scale while changing the ambient room temperature. These tests disclosed that one of the microscopes was tilting in its mount and might have contributed an error in length measurements of about 100 micrometers/meter. The mount was remachined and provided no further difficulty. This experience emphasizes the usefulness of a reference scale for if the defective mount had not been detected the use of the scale would have automatically corrected the length measurements.

The microscopes were alined and calibrated by first adjusting the invar bar on which the microscopes are mounted to the vertical position. Next, the micro-

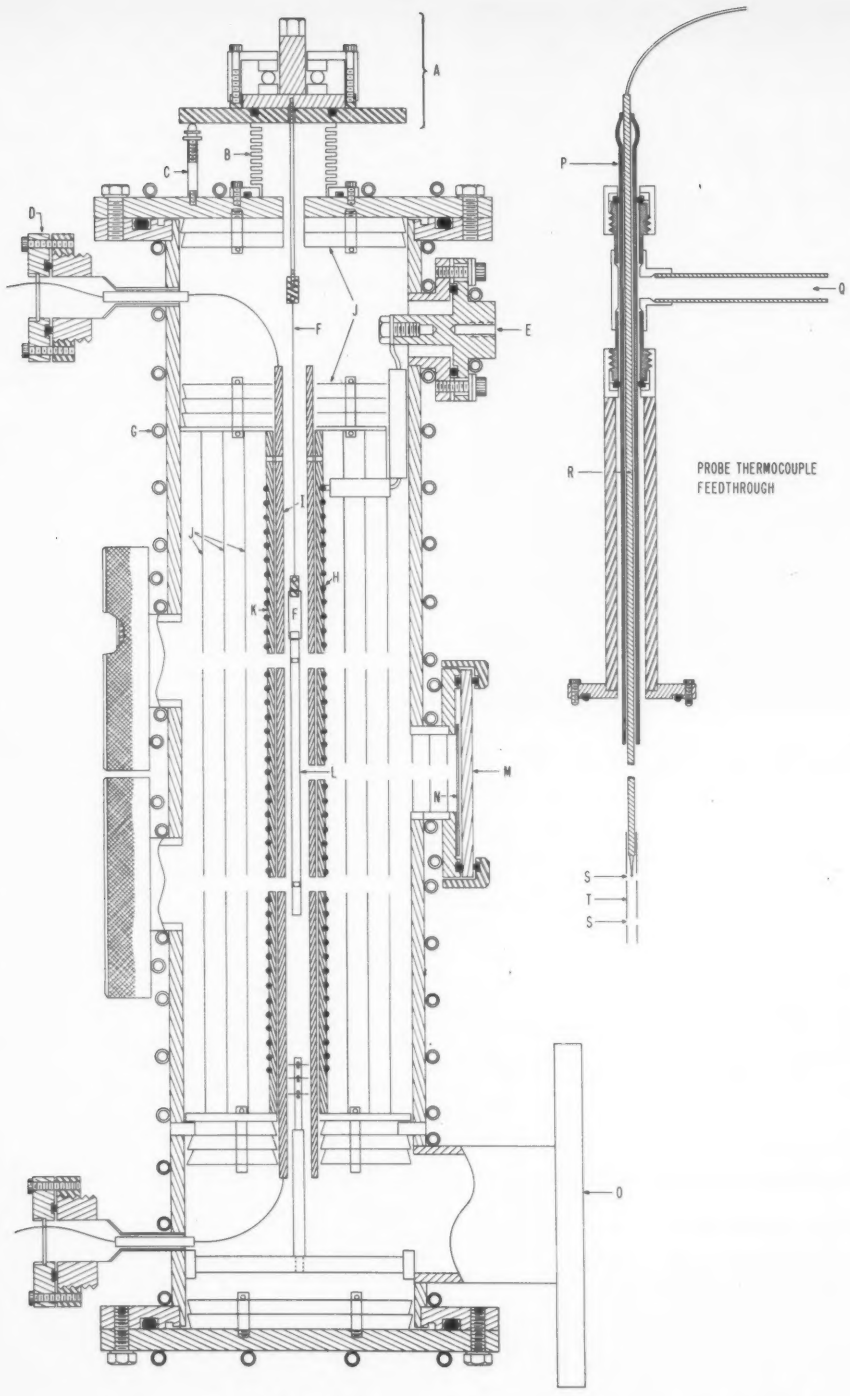

FIGURE 2. *Controlled gradient vacuum furnace and probe thermocouple feedthrough.*

A. Specimen support
B. Bellows
C. Position adjusting screw, one of three
D. Thermocouple feedthrough
E. Electrical feedthrough, one of ten
F. Tungsten wire loop
G. Water cooling coil
H. Resistance heating wire
I. Thermocouple protection tube
J. Radiation heat shields
K. Alumina core
L. Specimen
M. Window
N. Shutter
O. Vacuum port
P. Vicor tube
Q. Vacuum
R. Thermocouple protection tube
S. Pyrometer viewing hole
T. Tantalum tube.

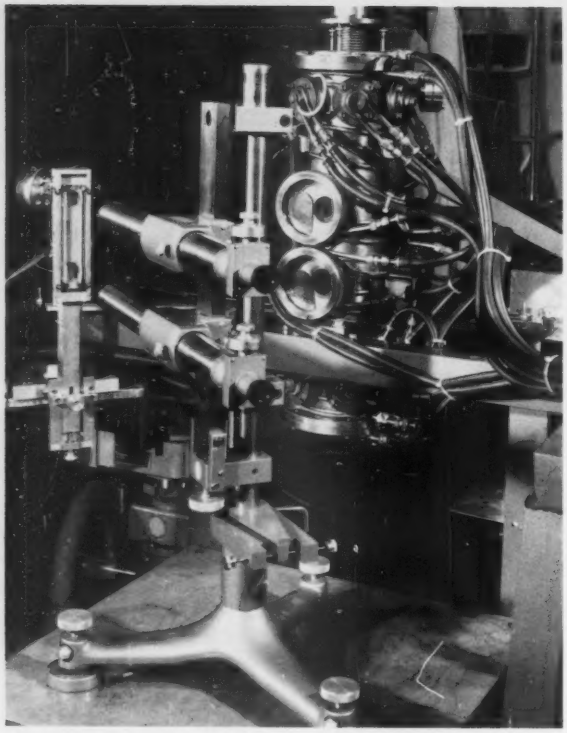

FIGURE 3. *Photograph showing relative position of comparator, furnace and reference scale.*

scope tubes were adjusted until they were horizontal and parallel. The microscopes were then moved in their individual mounts until they were both focused on a freely hanging 0.38 mm wire. The paired microscopes were turned toward the reference scale and the position of the scale was adjusted until it was focused in each microscope. With the microscopes focused on the scale each eyepiece was calibrated by measuring the separation of two wires. After many repeated measurements the values for the eyepieces were determined to be 1.128 and 1.095 micrometers per division.

3. Control and Measurement Techniques

3.1. Temperature

To control the temperature gradient in the furnace four differential W-Re thermocouples were placed in the thermocouple protection tube. One of the junctions of each of the thermocouples was placed at the center of the furnace and the other junction was placed at the center of one of the other four heating sections. This provides a comparison of temperature at the center of each heating section with the temperature at the center of the furnace.

A multipoint strip chart recorder is used to record the output of the differential thermocouples. The recorder scale is zero centered with a full scale deflection of ± 300 μV (10 μV per scale division). The plot can be read to better than 1 scale division and hence the differential temperature to better than 1 °C. The 24-second printing cycle of the recorder is about the response time of the furnace to a power change. Using this system it is not difficult to maintain a gradient within ± 2 °C as indicated by the recorder. In the time it takes to make a set of readings the average temperature usually did not vary more than ± 1 °C.

To test the actual temperature profile at the position occupied by the specimen an arrangement was made for measuring the temperature with a single absolute thermocouple. This probe thermocouple was inserted into the furnace through the top plate by means of a sliding vacuum seal, see figure 2. The wires were insulated with a two-hole high-purity alumina protection tube. The junction was about 5 mm below the end of the alumina tube but was shielded by a thin-walled 4-mm O.D. tantalum tube. The tantalum tube extended about 3 cm above and below the junction and had two small holes in it to allow the optical pyrometer to "see" the junction when it was located at the center of the furnace and to use the tube as a blackbody when the junction was located slightly above the center of the furnace.

The probe thermocouple measured the temperature profile along the axis of the furnace at several different temperatures. At each temperature the current in each heating section was adjusted until the print out on the strip chart recorder indicated that all four differential thermocouples were at the same temperature. The probe thermocouple was then raised and lowered and readings taken at 1 cm intervals. As shown in figure 4, the actual temperature profile has an overall slope with dips at the viewing windows. This same slope was found when the probe thermocouple was inserted into the furnace through the bottom plate. The temperature profile that is obtained when each heating section has the same current flowing through its heating element is also shown in figure 4.

Temperature measurements are made at the center of the furnace with a W-Re thermocouple and a Pt-Rh 30–6 thermocouple placed in the thermocouple protection tube. These thermocouples and the optical pyrometer were calibrated by comparison with a probe thermocouple that had been calibrated by the Temperature Physics Section of the National Bureau of Standards. During this calibration the probe thermocouple was at a point 2 cm above the center of the furnace where the slope of the temperature profile was nearly zero. The value of the average temperature and its position was determined from the temperature profile over the specimen length. A correction was made to the indication of the probe thermocouple corresponding to the difference between the average temperature and the temperature at the 2 cm position as taken from the temperature profile.

Because the thermocouples were calibrated with the probe thermocouple occupying the same space that the specimen occupies during an expansion test,

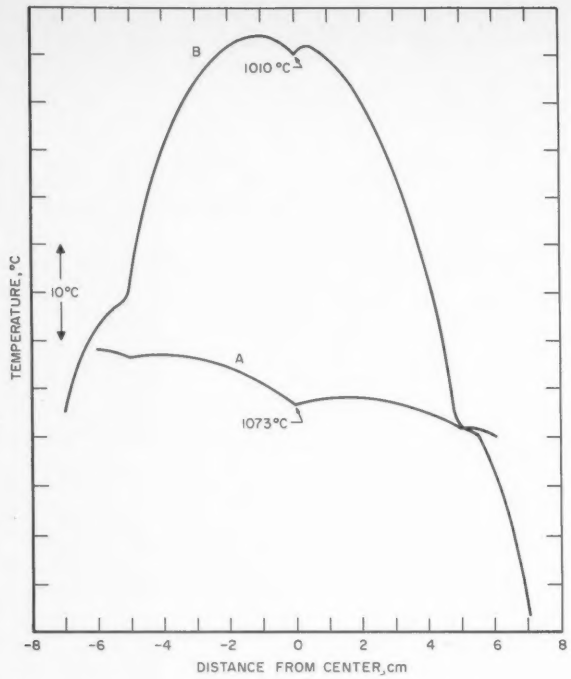

FIGURE 4. *Temperature profile along the axis of the furnace (top of furnace to right): A, current adjusted in each heating section until all four differential thermocouples were at the same temperature; B, same current flowing through each heating section.*

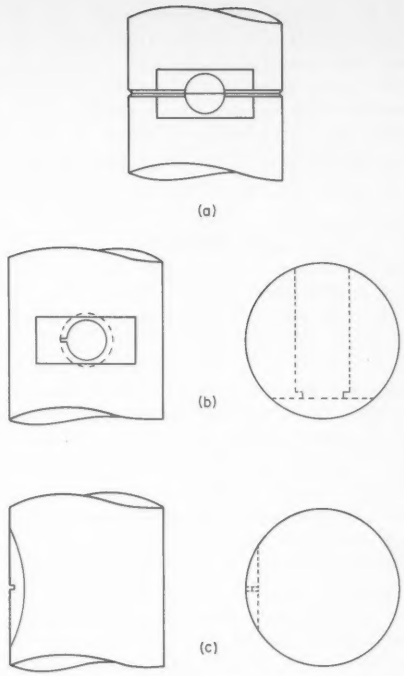

FIGURE 5. *Fiducial marks: (a) 0.020 mm tungsten wire tied taut around the specimen; (b) platinum specimen; (c) sapphire specimen.*

it is assumed that the temperature measurements accurately represent the temperature within the specimen.

While the temperature measurements made with the optical pyrometer and the thermocouples were usually in reasonable agreement, within ±3 °C, the measurements made with the pyrometer were only used as an additional check on the thermoucouples. After the furnace had been heated above 1500 °C, slight deposits could be seen on the windows and the temperature measurements made with the pyrometer would be as much as 50 °C lower than those made with the thermocouples.

3.2. Length

In order to obtain reliable measurements of length the fiducial marks should be an integral part of the specimen or not subject to arbitrary shifts. In order to obtain measurements of high precision the fiducial marks should be small (of the order of 0.025 mm when using a magnification of 50×), symmetrical, and capable of forming an image with sharp focus. Several experimenters [8, 9, 10] have used fiducial marks made by peening small wires into holes drilled into the specimen, clipping the wires off close to the specimen and placing nicks in the resulting sharp edge. Other investigators have used marks scribed or indented into the surface of the specimen [4] or sighted on the ends of the specimen [11, 12].

A promising method of tying two 0.020 mm tungsten wires taut around the specimen was tried, see figure 5 (a). Each wire crossed in front of a 1.5 mm diam hole drilled in the specimen and was held in position by running through grooves on either side of the hole. When the furnace became hot enough that the wires were self illuminating they stood out sharply against the dark background and precise settings, within ±0.7 micrometers, with the filar eyepiece could be made. At temperatures above 1500 °C, however, probably because of recrystallization, the wires grew in length and warped. Because they were no longer straight any further readings could not be relied upon.

It has been found that small holes (of the order of 0.25 mm) drilled through a specimen [13] or small nicks or grooves [14] will serve as reliable fiducial marks. It is sometimes difficult, however, to obtain a round hole that is small enough for high precision measurements.

Satisfactory fiducial marks were finally made by placing a small symmetrical nick at the edge of the specimen. This was done for the platinum specimen, see figure 5 (b), by drilling a 1.73 mm hole radially into the rod to within about 0.25 mm of penetrating a milled flat on the opposite surface. A second hole of 1.57 mm diam, concentric with the first hole, was drilled in the flat, penetrating through to the larger diameter hole. This left a thin ring around the inside of the hole and a small nick was placed in the ring with a hardened steel ruling edge to serve as a fiducial mark. In the case of the sapphire specimen, see

figure 5 (c), a local area on one side was ground with a diamond wheel until a thin ridge was left, the faces of which were parallel to the axis of the specimen. A small nick was then placed in the ridge with a 0.25 mm carbide disk as a fiducial mark. The precision of setting the cross hairs on these marks was found to be comparable to that of setting on the tungsten wires.

4. Procedure

With the specimen in the furnace and the furnace sealed the vacuum pumps were turned on and the pressure reduced to about 1×10^{-5} torr. Power was applied slowly to heat the specimen. When the desired temperature was reached the optimum temperature gradient was obtained by adjusting the power supplied to the two heating sections at either end. This condition was held for 10 min to allow the specimen to stabilize. A longer stabilizing period was not necessary since it was found that no change in length of the specimen could be detected after a 5 min wait. The microscopes were focused on the specimen by adjusting the position of the comparator and on the reference scale by adjusting its position. The emf of the two absolute thermocouples was determined with a potentiometer to the nearest microvolt and the brightness temperature of the specimen was measured using the disappearing filament optical pyrometer. Five settings with each microscope were made in turn on the specimen, the reference scale, and again on the specimen. Finally, the temperature measurements were repeated.

5. Discussion

Although care has been exercised in measurement of temperature and length, errors inherent in any system operating at these temperatures restrict the accuracy in the measurement of these values and the determination of the coefficient of expansion. An error in temperature measurement of 1 °C in a specimen having a coefficient of 10×10^{-6}/°C is equivalent to an error in length measurement of 10 micrometers/meter. Also, an error in temperature measurement of 1 °C, or in length measurement of one micrometer in a specimen 10 cm long having a coefficient of 10×10^{-6}/°C and heated over a temperature range of 100 °C, will result in an error of less than $\pm 0.1 \times 10^{-6}$/°C in the determination of the coefficient.

Uncertainties in temperature measurements may arise from a shift in calibration of the thermocouples through contamination and aging. Although high-purity alumina (99% Al_2O_3) has been used for thermocouple insulation the trace impurities can affectively change the output of the thermocouples. To reduce the effect of this and other possible sources of error the following procedure was used: (1) The probe thermocouple was calibrated by the Temperature Physics Section of the National Bureau of Standards, (2) the absolute thermocouples were calibrated by comparison with the probe thermocouple, (3) the expansion tests were conducted, (4) the absolute thermocouples were again calibrated, and (5) the probe thermocouple was again calibrated. This procedure demonstrated that the uncertainties in temperature measured during the thermal expansion tests did not exceed 2 deg at 800 °C and 4 deg at 1600 °C. The standard deviation of the differences between the temperatures indicated by the two absolute thermocouples was 1.5 °C, and that of the average of the two readings is 0.7 °C.

Preliminary results [2] have been obtained on specimens of platinum and sapphire. Figure 6 indicates the difference (residuals) between observed expansion of these materials and the expansion calculated from quadratic equations fitted to the data by the method of least squares. For the platinum and sapphire specimens the standard deviations computed from the residuals are 23 and 27 micrometers/meter respectively.

From these estimates of the precision of the temperature measurements, ±0.7 °C, and of the expansion measurements, ±23 and ±27 micrometers/meter, the precision of the length measurements expressed as standard deviations are 2.1 and 2.6 micrometers, respectively.

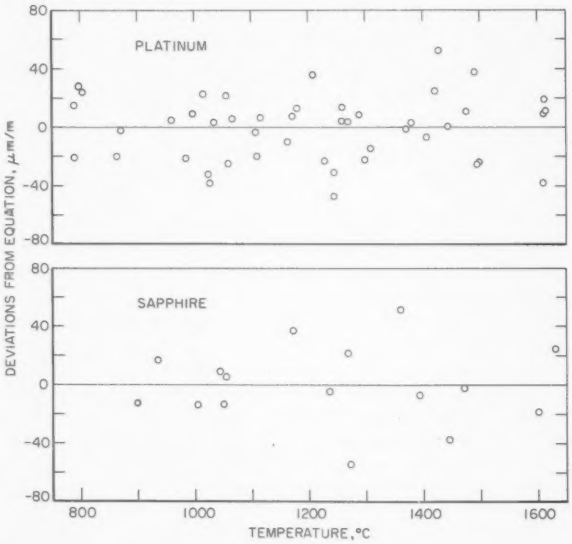

FIGURE 6. *A plot of the differences between observed expansion and the expansion calculated from an equation fitted to the data by the method of least squares.*

Assuming that the accuracy and precision of the length measurements are comparable and the uncertainties in the temperature measurements are as previously stated, thermal expansion measurements made with this equipment can be estimated to be

[2] A complete report on these measurements will be made after the investigation has been completed.

accurate within ±30 micrometers/meter at 800 °C and within ±50 micrometers/meter at 1600 °C.

It was discovered that a small wedge (6 min) between the faces of each vitreous silica window contributed an error in the measurement of expansion from room temperature. Since the measurement of initial length is made with the specimen outside the furnace there is no precise measurement of the change in length of the specimen from room temperature to 900 °C where the specimen is self illuminating. This error was virtually constant for a fixed position of the window, however, and did not significantly affect the determination of the coefficient of expansion at the operating temperature. To eliminate this and other possible errors two higher quality windows are being made that will have surfaces flat to 1 wavelength of visible light and parallel to 1 sec.

Light sources are also being placed in the furnace so that the length of the specimen can be determined inside the furnace at ambient and intermediate temperatures.

With the improvements discussed in the previous paragraphs and the preliminary results obtained on platinum and sapphire it is believed that the apparatus and the procedure described in this paper will yield important and useful thermal expansion data on high temperature materials.

The authors thank L. Frenkel for contributions made in the design of the apparatus and to T. A. Hahn for helpful discussions.

6. References

[1] S. D. Mark, Jr. and R. C. Emannelson, A thermal expansion apparatus with a silicon carbide dilatometer for temperatures to 1500 °C, Bull. Am. Ceram. Soc. **37,** 193 (1958).

[2] W. J. Campbell, Platinum expansion values for thermal calibration of high-temperature x-ray diffraction cameras and diffractometers, U.S. Bureau of Mines Information Circular 8107 (1962).

[3] R. G. Merryman and C. P. Kempter, Precise temperature measurements in Debye-Scherrer specimens at elevated temperatures, J. Am. Ceram. Soc. **48,** 202 (1965).

[4] R. D. Fouchaux and R. O. Simmons, Measurements of thermal expansion and thermal equilibrium defects in silver chloride, Phys. Rev. **136,** 1664 (1964).

[5] Z. S. Basinski, W. Hume-Rothery, and A. L. Sutton, The lattice expansion of iron, Proc. Roy. Soc. London **A229,** 459 (1955).

[6] A. Schauer, Thermal expansion, Grueneisen parameter, and temperature dependence of lattice vibration frequencies of aluminum oxide, Can. J. Phys. **43,** 523 (1965).

[7] J. Otto and W. Thomas, Die Thermische Ausdehnung von Quarzglas im Temperaturbereich von 0 bis 1060 °C, Z. Physik **175,** 337 (1963).

[8] N. S. Rasor and J. D. McClelland, Thermal property measurements at very high temperatures, Rev. Sci. Instr. **31,** 595 (1960).

[9] I. B. Fieldhouse, J. C. Hedge, and J. I. Lang, Measurements of thermal properties, Wright Air Development Center Technical Report 58–274, ASTIA Document No. 206892 (1958).

[10] H. W. Deem, W. D. Wood, and C. F. Lucks, Thermal properties of materials at elevated temperatures, Wright Air Development Center Technical Report 59–215, ASTIA Document No. 233182 (1959).

[11] B. R. Micciole and P. T. B. Shaffer, High-temperature thermal expansion behavior of refractory materials: 1. Selected monocarbides and binary carbides, J. Am. Ceram. Soc. **47,** 351 (1964).

[12] O. J. Whittemore, Jr. and N. N. Ault, Thermal expansion of various ceramic materials to 1500 °C, J. Am. Ceram. Soc. **39,** 443 (1956).

[13] J. B. Conway, Properties of some refractory metals, GEMP–375 General Electric, June 29, 1965.

[14] C. J. Engberg and E. H. Zehms, Thermal expansion of Al_2O_3, BeO, MgO, B_4C, SiC, and TiC above 1000 °C, J. Am. Ceram. Soc. **42,** 300 (1959).

(Paper 71C2–247)

JOURNAL OF RESEARCH of the National Bureau of Standards—C. Engineering and Instrumentation
Vol. 71C, No. 2, April–June 1967

Determination and Smoothing of Fourier Coefficients Representing Piecewise Continuous Functions

B. A. Peavy

Institute for Applied Technology, National Bureau of Standards, Washington, D.C. 20234

(February 7, 1967)

This paper presents a method of solving for Fourier coefficients where the dependent variable can be expressed as a piecewise continuous function, when various conditions of continuity and smoothing are assumed. An example is included to show the effect of smoothing in the region of a discontinuity for a system composed of two materials that exhibit a discontinuity at their interface and surrounded by a third material which does not have a discontinuity. An advantage to be gained from smoothing is an increase in the convergence of a finite Fourier series representation of a piecewise continuous function in the region of the discontinuities.

Key Words: Continuous function, Fourier series, piecewise, smoothing.

1. Introduction

Many time-independent problems of a practical nature involve the solution to the partial differential equation

$$\frac{\partial^2 v}{\partial x^2}+\frac{\partial^2 v}{\partial y^2}+\frac{\partial^2 v}{\partial z^2}=0$$

in rectangular coordinates, or

$$\frac{\partial^2 v}{\partial r^2}+\frac{1}{r}\frac{\partial v}{\partial r}+\frac{1}{r^2}\frac{\partial^2 v}{\partial \phi^2}+\frac{\partial^2 v}{\partial z^2}=0 \tag{1}$$

in cylindrical coordinates. From the general solution, one particular solution is in the form

$$v=B+Cz+\sum_n A_n \sin\frac{n\pi z}{\omega}, \tag{2}$$

where the Fourier coefficients, $A_n=A_n(x, y)$ for rectangular coordinates, or $A_n=A_n(r, \varphi)$ for cylindrical coordinates, are determined from boundary conditions in the region $0\leq z\leq \omega$, and fixed coordinate positions for x and y, or r and φ, with the condition that other necessary solutions of (1) disappear on this boundary. Also, $B+Cz$ must satisfy v at the end points, $z=0$ and $z=\omega$.

From an experimental point of view, the dependent variable, v, can be approximated from measured values at several z positions on the boundary by a relationship, $v=g(z)$. The Fourier coefficients are usually simply determined if the function $g(z)$ and its derivatives are continuous over the region $0\leq z\leq \omega$. For various applications, the variable v must be expressed as piecewise continuous functions in this region, with apparent discontinuities at discrete points. If it is known that the discontinuities do not exist, then an appropriate smoothing function can be employed.

The purpose of this paper is to solve for Fourier coefficients, when it is assumed that the dependent variable v can be expressed by polynomials representing discrete portions of the region $0\leq z\leq \omega$, and that conditions of continuity and smoothing exist. An application of functions developed to a hypothetical problem is also presented.

2. Analysis

On a fixed surface lying in the region $0 \leq z \leq \omega$, the dependent variable v is defined

$$v = g_i(z); \qquad z_{i-1} < z < z_i,$$

where $i = 1, 2, 3, \ldots m$, $z_0 = 0$, and $z_m = \omega$. The functions $g_i(z)$ and their derivatives may have discontinuities at the points z_i, $i = 1, 2, \ldots m-1$. Substituting in (2), multiplying through by $\sin k\pi z/\omega$, and integrating between the specified limits gives the following equations

$$\int_{z_{i-1}}^{z_i} [g_i(z) - B - Cz] \sin \frac{k\pi z}{\omega} dz = \sum_n A_n \int_{z_{i-1}}^{z_i} \sin \frac{n\pi z}{\omega} \sin \frac{k\pi z}{\omega} dz.$$

Adding the above equations

$$\sum_n A_n \int_0^{\omega} \sin \frac{n\pi z}{\omega} \sin \frac{k\pi z}{\omega} dz = -\int_0^{\omega} (B + Cz) \sin \frac{k\pi z}{\omega} dz + \sum_{i=1}^{m} \int_{z_{i-1}}^{z_i} g_i(z) \sin \frac{k\pi z}{\omega} dz,$$

from which

$$A_n = \frac{2}{n\pi} \{C\omega(-1)^n - B[1 - (-1)^n]\} + \frac{2}{\omega} \sum_{i=1}^{m} \int_{z_{i-1}}^{z_i} g_i(z) \sin \frac{n\pi z}{\omega} dz.$$

Repeated integration by parts yields

$$\int g_i(z) \sin \frac{n\pi z}{\omega} dz = \frac{\sin \dfrac{n\pi z}{\omega}}{\left(\dfrac{n\pi}{\omega}\right)^2} \left\{ g_i'(z) - \frac{g_i'''(z)}{\left(\dfrac{n\pi}{\omega}\right)^2} + \frac{g_i^{v}(z)}{\left(\dfrac{n\pi}{\omega}\right)^4} - \ldots \right\}$$

$$- \frac{\cos \dfrac{n\pi z}{\omega}}{\dfrac{n\pi}{\omega}} \left\{ g_i(z) - \frac{g_i''(z)}{\left(\dfrac{n\pi}{\omega}\right)^2} + \frac{g_i^{iv}(z)}{\left(\dfrac{n\pi}{\omega}\right)^4} - \ldots \right\},$$

where superscripts $'$, $''$, $'''$, represent the first, second, third, etc., derivative with respect to z. Letting

$$G_i = \frac{\sin \dfrac{n\pi z_i}{\omega}}{\left(\dfrac{n\pi}{\omega}\right)^2} \left\{ g_i'(z_i) - g_{i+1}'(z_i) - \frac{[g_i'''(z_i) - g_{i+1}'''(z_i)]}{\left(\dfrac{n\pi}{\omega}\right)^2} + \ldots \ldots \right\}$$

$$- \frac{\cos \dfrac{n\pi z_i}{\omega}}{\dfrac{n\pi}{\omega}} \left\{ g_i(z_i) - g_{i+1}(z_i) - \frac{[g_i''(z_i) - g_{i+1}''(z_i)]}{\left(\dfrac{n\pi}{\omega}\right)^2} + \ldots \ldots \right\},$$

$$H = \frac{g_1''(0)}{\left(\dfrac{n\pi}{\omega}\right)^2} - \frac{g_1^{iv}(0)}{\left(\dfrac{n\pi}{\omega}\right)^4} + \ldots \ldots,$$

$$K = \frac{g_m''(\omega)}{\left(\dfrac{n\pi}{\omega}\right)^2} - \frac{g_m^{iv}(\omega)}{\left(\dfrac{n\pi}{\omega}\right)^4} + \ldots \ldots,$$

then

$$A_n=\frac{2}{n\pi}\{g_i(0)-B+(-1)^n[C\omega+B-g_m(\omega)]-H+(-1)^nK\}+\frac{2}{\omega}\sum_{i=1}^{m-1}G_i.$$

For the condition that $B=g_1(0)$ and $C\omega+B=g_m(\omega)$, the Fourier coefficients are

$$A_n=\frac{2}{n\pi}\{(-1)^nK-H\}+\frac{2}{\omega}\sum_{i=1}^{m-1}G_i. \tag{3}$$

Assume for the region, $0\leq z\leq\omega$, that v as a function of z behaves as shown in figure 1, where g_1, g_2, g_3, and g_4 are known functions of v, (perhaps as determined from experiment) and f_1, f_2, and f_3 encompass regions of uncertainty or regions which cannot be defined by experiment. If it is known that there are no discontinuities within the regions of the uncertainties, it is possible to smooth or bridge between the known functions with a cubic polynomial which gives continuity to two adjacent g functions and their first derivatives. Examining the first region that includes an uncertainty, the cubic polynomial, $f_1(z)=M_0+M_1z+M_2z^2+M_3z^3$ is solved for the coefficients, M, such that $g_1(z_1)=f_1(z_1)$, $g_1'(z_1)=f_1'(z_1)$, $g_2(z_2)=f_1(z_2)$ and $g_2'(z_2)=f_1'(z_2)$, from which the necessary coefficients are

$$M_2=\frac{3[g_2(z_2)-g_1(z_1)]\bar{z}-\epsilon[(3\bar{z}+\epsilon)g_1'(z_1)+(3\bar{z}-\epsilon)g_2'(z_2)]}{4\epsilon^3}$$

$$M_3=\frac{\epsilon[g_1'(z_1)+g_2'(z_2)]+g_1(z_1)-g_2(z_2)}{4\epsilon^3},$$

where $\bar{z}=z_1+\epsilon=z_2-\epsilon$ is the midpoint between z_1 and z_2. Assuming bridging between g_1 and g_2, then

$$G_1=F_1+F_2 \tag{4}$$

where

$$F_1=\frac{1}{\left(\frac{n\pi}{\omega}\right)^4}\left[\left\{g_2'''(z_2)-\frac{g_2^{V}(z_2)}{\left(\frac{n\pi}{\omega}\right)^2}+\cdots\right\}\sin\frac{n\pi z_2}{\omega}-\left\{g_1'''(z_1)-\frac{g_1^{V}(z_1)}{\left(\frac{n\pi}{\omega}\right)^2}+\cdots\right\}\sin\frac{n\pi z_1}{\omega}\right]$$

$$+\frac{1}{\left(\frac{n\pi}{\omega}\right)^3}\left[g_1''(z_1)-\frac{g_1^{IV}(z_1)}{\left(\frac{n\pi}{\omega}\right)^2}+\cdots\right\}\cos\frac{n\pi z_1}{\omega}-\left\{g_2''(z_2)-\frac{g_2^{IV}(z_2)}{\left(\frac{n\pi}{\omega}\right)^2}+\cdots\right\}\cos\frac{n\pi z_2}{\omega}\Bigg] \tag{4a}$$

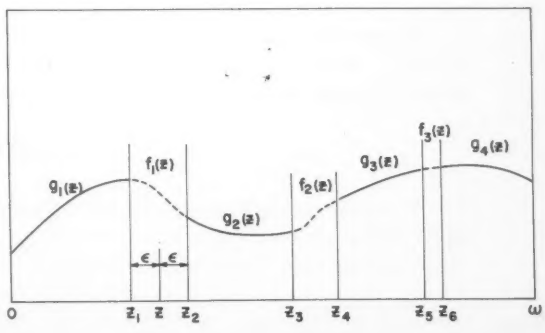

FIGURE 1. *Variation of* v *with respect to* z *showing the defined functions* g_1, g_2, g_3, *and* g_4 *connected by functions* f_1, f_2, *and* f_3 *through regions of uncertainty.*

and

$$F_2=\frac{1}{\left(\frac{n\pi}{\omega}\right)^4}\left[f_1'''(z_1)\ \sin\frac{n\pi z_1}{\omega}-f_1'''(z_2)\ \sin\frac{n\pi z_2}{\omega}\right]$$

$$+\frac{1}{\left(\frac{n\pi}{\omega}\right)^3}\left[f_1''(z_2)\ \cos\frac{n\pi z_2}{\omega}-f_1(z_1)\ \cos\frac{n\pi z_1}{\omega}\right].$$

Making the substitutions $z_1=\bar{z}-\epsilon$, $z_2=\bar{z}+\epsilon$, $f_1''(z)=2M_2+6M_3z$, and $f_1'''(z)=6M_3$ in F_2, yields

$$F_2=[g_1'(z_1)-g_2'(z_2)]\frac{U\left(\frac{n\pi\epsilon}{\omega}\right)\sin\frac{n\pi\bar{z}}{\omega}}{\left(\frac{n\pi}{\omega}\right)^2}$$

$$-[g_1(z_1)-g_2(z_2)+\epsilon\{g_1'(z_1)+g_2'(z_2)\}]\frac{T\left(\frac{n\pi\epsilon}{\omega}\right)\cos\frac{n\pi\bar{z}}{\omega}}{\frac{n\pi}{\omega}} \qquad (4b)$$

where

$$U(\beta)=\frac{\sin\beta}{\beta}=1-\frac{\beta^2}{3!}+\frac{\beta^4}{5!}-\ \cdots$$

$$T(\beta)=\frac{3}{\beta^3}(\sin\beta-\beta\cos\beta)$$

$$=3\left(\frac{1}{3\cdot 1!}-\frac{\beta^2}{5\cdot 3!}+\frac{\beta^4}{7\cdot 5!}-\ \cdots\right).$$

Plots of $U(\beta)$ and $T(\beta)$ are given in figure 2.

For the interval $z_1\leq z\leq z_2$, (4b) is the bridging or smoothing function that gives continuity to $g_1(z)$ and $g_2(z)$ and their first derivatives at z_1 and z_2, respectively. This function also eliminates computation of the cubic polynomial $f_1(z)$, where the values of M_2 and M_3 sometimes give inordinately large values with subsequent loss of significance. The same analysis can be applied to the regions encompassed by $f_2(z)$ and $f_3(z)$ so that G_2 and G_3 can be found.

3. Specific Cases

Where successive differentiation terminates, the functions $g_i(z)$ may be represented by polynomials. There are many variations of $g_i(z)$ possible, but probably the best example is to examine a set of straight lines as given in the following specific cases.

3.1. Functions as Straight Lines

The functions $g_i(z)$ are represented by a set of straight lines. Here $g_i''(z)=H=K=0$, so that (3) becomes

$$A_n=\frac{2}{\omega}\sum G_i. \qquad (5)$$

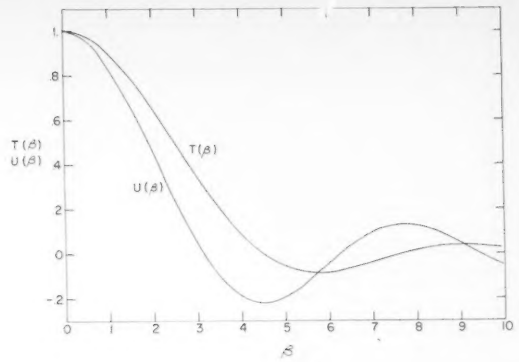

FIGURE 2. *Variation of* U(β) *and* T(β) *with* β.

FIGURE 2. *Variation of* U(β) *and* T(β) *with* β.

If a set of straight lines which do not intersect at critical positions z_i, as shown in figure 3 are assumed, then

$$G_i=\left(\frac{\omega}{n\pi}\right)^2[g_i'(z_i)-g_{i+1}'(z_i)]\sin\frac{n\pi z_i}{\omega}-\frac{\omega}{n\pi}[g_i(z_i)-g_{i+1}(z_i)]\cos\frac{n\pi z_i}{\omega}, \tag{6}$$

where the functions and derivatives are evaluated at z_i. For the cases where the lines do intersect at z_i, i.e., $g_i=g_{i+1}$, the second term on the right side of (6) is zero.

3.2. Straight Line Functions Smoothed Near Intersections

The convergence of (6) when substituted in (5) and (2) is not very satisfactory, and it is possible to increase the convergence by joining the straight lines with smoothing curves that give continuity to the lines and their first derivatives at points $z_i-\gamma_i$ and $z_i+\epsilon_i$, as shown in figure 4.

Proceeding as in the derivation of (4), where $F_1=0$, yields

$$G_i=[(\epsilon_i-\gamma_i)(g_{i+1}'(z_i)-g_i'(z_i))+2(g_{i+1}(z_i)-g_i(z_i))]\frac{T(n\lambda_i)\cos\alpha_i}{2\left(\frac{n\pi}{\omega}\right)}$$

$$-\{g_{i+1}'(z_i)-g_i'(z_i)\}\frac{U(n\lambda_i)\sin\alpha_i}{\left(\frac{n\pi}{\omega}\right)^2}, \tag{7}$$

where

$$\alpha_i=\frac{n\pi}{2\omega}(2z_i+\epsilon_i-\gamma_i)$$

$$\lambda_i=\frac{\pi}{2\omega}(\epsilon_i+\gamma_i).$$

As $\epsilon_i=\gamma_i\to 0$, (7) becomes (6). There are many possible specific cases for (7), i.e., $\epsilon_i=0$, $\gamma_i=0$, $\epsilon_i=\gamma_i$, etc. Essentially, smoothing increases convergence by introducing the factors $T(\beta)$ and $U(\beta)$, $\beta=n\lambda_i$, to the terms on the right side of (6). The plots $T(\beta)$ and $U(\beta)$ (fig. 2) indicate that the advantage of the increase in convergence is not realized until $\beta\gg 0$.

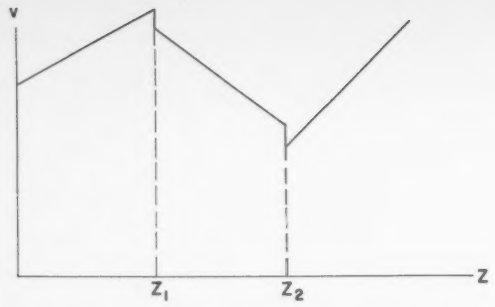

FIGURE 3. *Variation of* v *as a set of straight lines with function discontinuities at* z_1 *and* z_2.

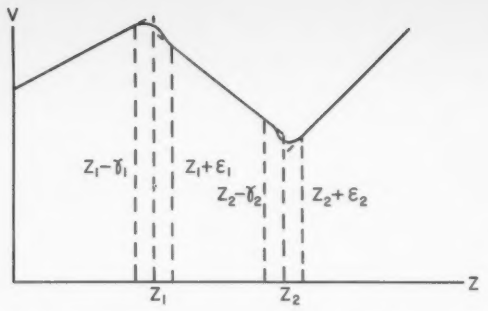

FIGURE 4. *Variation of* v *as a set of straight lines with smoothing in the regions of* z_1 *and* z_2.

3.3. Example of Smoothing

Figure 5 is used as an example of the variation of the dependent variable v with the dimension z in order to show the need for smoothing in the region of a discontinuity. For a hypothetical process, consider the potential on the surface of a system of two materials which is surrounded by a third material (not a perfect insulator), and where, on the surface of the system, the region $0 \leq z \leq 0.5$ represents the potential in a perfect conductor, the region $0.5 \leq z \leq 1.0$ represents that in a material of finite conductivity, and the discontinuity represents the contact resistance between the two materials. Usually, experimental processes allow measurement of potential in the two regions, but measurements at or near the discontinuity are not always possible or desirable. Assuming homogeneous isotropic materials, measurements taken in the two separate regions give linear relations which, when extrapolated to the point of contact ($z=0.5$), do not meet in a common point and give an apparent discontinuity. When it is known that the process must be continuous, i.e., the surrounding material is continuous at $z=0.5$, then a smoothing function may be applied.

Numerical values for substitution in (7) are $z_1=0.5$, $g_1=1.0$, $g_1'=0$, $g_2=0.95$, $g_2'=1.9$, and $\epsilon=\gamma$, where $\alpha=n\pi/2$, $\lambda=\pi\epsilon$. Substitution in (7), (5) and (2) gives

$$v=1-z-\sum_n (-1)^n \left\{\frac{T(2n\lambda)\,\sin 2\pi nz}{20n\pi}+\frac{3.8U[(2n-1)\lambda]\,\sin (2n-1)\pi z}{(2n-1)^2\pi^2}\right\}. \tag{8}$$

Figure 6 is a plot of v in the region of the discontinuity shown in figure 5 for the summation of 200 terms of the above series and values of $\epsilon=0.0$, 0.002, 0.003, and 0.004, and their respective smoothing curves. Figure 6 shows the influence of the increased convergence of the series toward its

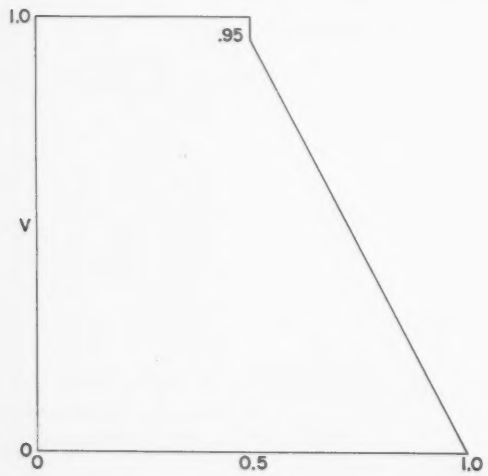

FIGURE 5. *Variation of* v *with* z *for the problem of section 3.3.*

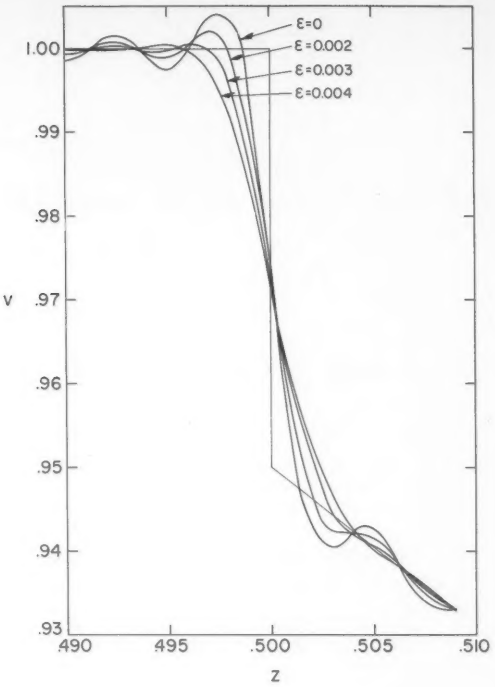

FIGURE 6. *Numerical values of* v *from* (8) *in the region of the discontinuity of figure 5 for a summation of 200 terms and values of* $\epsilon = 0, 0.002, 0.003$ *and* 0.004.

intended values with increase in the value of ϵ. For this case, fairly good convergence of the series is attained for $n > 1/2\epsilon$. For the summation of 300 terms, the fluctuations shown on figure 6 are virtually eliminated, except for $\epsilon = 0$.

4. Discussion

The example of section 3.3 as shown in figure 5 was chosen because it illustrates an extreme condition that a physical process may undergo; that is, the dependent variable has a zero slope up to the discontinuity at the point $z = 0.5$. It is then to be expected that actual physical processes where apparent discontinuities occur would give better convergence when smoothing conditions are employed.

Generally, the Fourier sine series (2) can be used to represent a piecewise continuous function over an interval, $0 \leq z \leq \omega$, by the use of (3). Numerical evaluation will, of course, present problems of convergence in the regions where discontinuities occur (as shown in fig. 6, $\epsilon = 0$). The lack of sufficient convergence in (2) can cause serious problems when (2) is used in the solution of (1). It is therefore expedient to employ the bridging or smoothing relationship (4) (or (7) for the special case of a set of straight lines) for which adequate convergence can be assured for a reasonable number of terms in the series of (2).

A fairly simple heat transfer system that may be analyzed employing the method presented in this paper is shown in figure 7a by a cross section through a composite cylinder. The inner cylinder (regions 1 and 2) $0 \leq r \leq a$ is composed of two materials of different thermal conductivities, usually with values greater than that for the material of the outer cylinder (region 3). For the determination of thermal conductivity, region 1 may comprise a material of known thermal conductivity and region 2 a material of thermal conductivity to be determined. It is necessary to determine the heat transfer characteristics in the material of region 3 in order to evaluate the radial heat loss or gain of the inner cylinder, $0 \leq r \leq a$.

The temperature distribution at $r = a$ will vary according to the thermal conductivities of the materials of regions 1 and 2, and the distribution may have an infinite number of variations. One

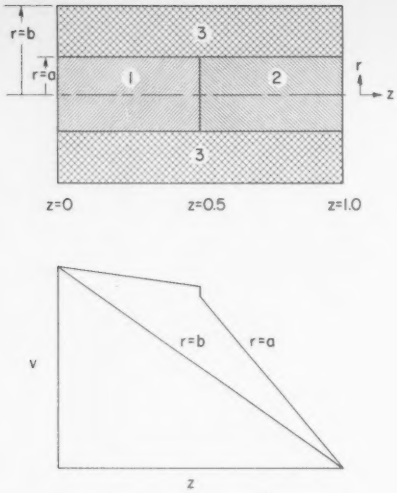

FIGURE 7. *Heat transfer system.*
(a) Cross-section through composite cylinder.
(b) A possible variation in temperature potential, v at $r=a$ and $r=b$.

such distribution for $r=a$ with a thermal contact resistance at $z=0.5$ is shown in figure 7b, where the intended heat flow is in the positive z-direction with a unit temperature potential at $z=0$ and a zero value at $z=1$. On $r=b$ the temperature is assumed to decrease linearly in the above limits. considering region 3 only, a solution of (1)(assuming no ϕ dependence) is

$$v=1-z+\sum \frac{A_n F_0(n\pi r,\ n\pi b)\ \sin\ n\pi z}{F_0(n\pi a,\ n\pi b)} \tag{9}$$

where $F_0(x,\ y)=I_0(x)K_0(y)-I_0(y)K_0(x)$ and I_0 and K_0 are modified Bessel functions of zero order and first and second kind, respectively. The substitution of $r=a$ in (9) gives a form similar to (2), for which a solution for A_n can be found from (7), the temperature distribution shown in figure 7b and a reasonable value of ϵ that insures convergence of the resulting series.

Two of the objectives of the NBS Heat Transfer Laboratory are to develop and analyze methods for the determination of thermal conductivity of materials which vary widely in thermal properties and to make measurements of thermal conductivity for government agencies. For both analysis and experiment, the smoothing or bridging relationships described are applicable.

(Paper 71C2–248)

JOURNAL OF RESEARCH of the National Bureau of Standards—C. Engineering and Instrumentation
Vol. 71C, No. 2, April–June 1967

A 2:1 Ratio Inductive Voltage Divider With Less Than 0.1 PPM Error to 1 MHz

Cletus A. Hoer* and Walter L. Smith*

Institute for Basic Standards, National Bureau of Standards, Boulder, Colo. 80302

(October 25, 1966)

A simple ratio transformer having a 2:1 ratio of input voltage to output voltage can be made with a ratio error less than 0.1 ppm from 1 kHz to above 1 MHz. Applications and sources of error are discussed. Experimental results leading to an optimum transformer design are given. A bridge to measure the ratio error to 0.025 ppm from 1 kHz to 1 MHz is also described.

Key Words: Attenuator, bridge, high frequency, inductive voltage divider, ratio transformer.

1. Introduction

Techniques for winding inductive voltage dividers with adjustable ratios have been improved during the last few years to where dividers having errors less than 0.1 ppm at frequencies around 1 kHz are not too difficult to make. Unfortunately, as the frequency increases, the ratio error increases rapidly so that this accuracy cannot be maintained above about 10 kHz. At frequencies above 10 kHz the most accurate ratio device is an inductive voltage divider which has a fixed voltage ratio of 2:1; that is, one dividing an input voltage into two equal parts such as is shown in figure 1. Such dividers have recently been made with errors less than 0.1 ppm from 1 kHz to above 1 MHz. This paper summarizes the research that was done to develop this accurate high frequency divider.

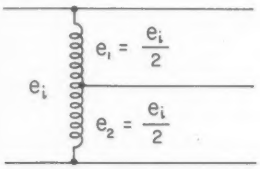

FIGURE 1. *A 2:1 ratio inductive voltage divider.*

2. Applications

A few of the many possible applications for this type of divider are shown in figure 2. Figure 2a is a bridge for comparing two impedances, z_1 and z_2. Figure 2b shows n basic 2:1 ratio dividers connected to give a voltage ratio

$$\frac{V_{out}}{V_{in}} = \frac{1}{2^n}.$$

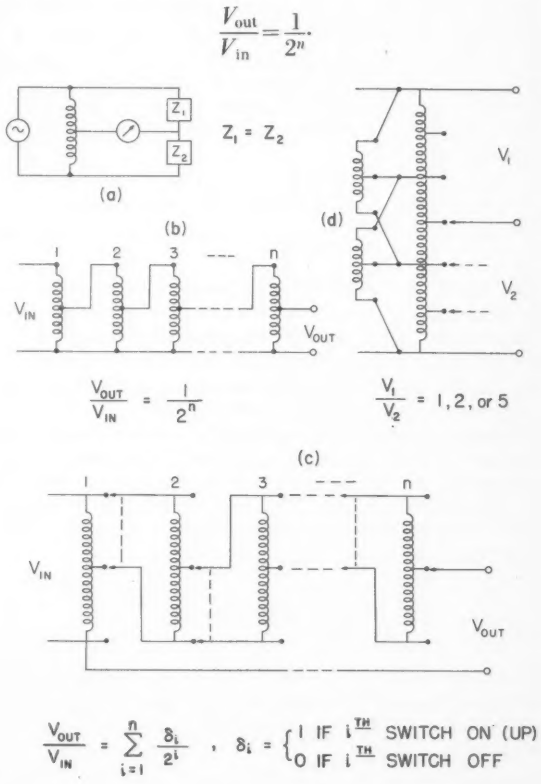

FIGURE 2. *Some possible applications for 2:1 ratio dividers.*

*Radio Standards Engineering Division, NBS Laboratories, Boulder, Colo. 80302.

247-602 O-67—2

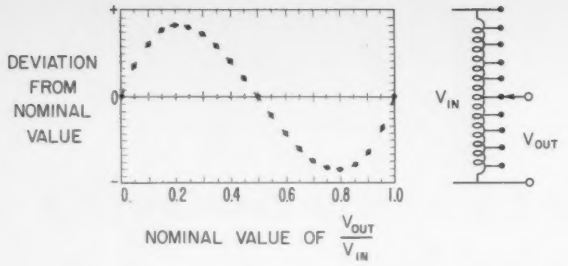

FIGURE 3. *Typical error curve for one decade of a low-frequency decade voltage divider.*

Each section of this divider accurately divides its input voltage in half to give an attenuation of 6 dB.[1] An attenuator made with n sections will have approximately $6n$dB.

Figure 2c shows an adjustable ratio "binary" inductive voltage divider. The principle of operation is the same as for low frequency decade voltage dividers except that each section divides its input voltage into only two equal parts instead of 10 equal parts. T. L. Zapf et al., have shown that the error curve for any one isolated decade of a low frequency decade voltage divider has an "S" shape such as shown in figure 3 [1].[2] As the frequency increases, the magnitude of the error increases but the curve still tends to go through zero at a ratio of 0.5. It is this error curve that suggested that 2 : 1 ratio dividers would be accurate at high frequencies as well as low frequencies. If n of these 2 : 1 ratio dividers are connected as shown in figure 2c the voltage ratio is

$$\frac{V_{out}}{V_{in}}=\sum_{i=1}^{n}\frac{\delta_i}{2^i},\quad \delta_i=\begin{cases}1 \text{ if the } i\text{th switch is up}\\ 0 \text{ if the } i\text{th switch is down.}\end{cases}$$

The input of each section is connected either across the top half or across the bottom half of the preceeding section. To obtain the same resolution with a binary divider as with a decade divider requires that the binary divider have approximately 3 times as many sections as the decade divider has.

Figure 2d shows three basic 2 : 1 ratio dividers connected in series with two more 2 : 1 ratio dividers connected so as to assure that the same voltage is applied to each of the three in series. Any number could be connected in series, however the combination shown gives the very useful ratios

$$\frac{V_1}{V_2}=1,\ 2,\ \text{and}\ 5.$$

This type of divider could be used in a bridge such as shown in figure 2a to compare standards of impedance which are often built to have nominal values in a 1-2-5 sequence.

[1] More accurately 20 log 2 = 6.020600 dB.

[2] Figures in brackets indicate the literature references at the end of this paper.

3. The 2 : 1 Ratio Divider

The 2 : 1 ratio divider is a center-tapped transformer that divides a voltage into two equal parts. It is convenient to define the complex ratio error, $\rho=\rho_r+j\rho_i$, as the error in the ratio of the output voltage to the input voltage. The output voltages e_1 and e_2 shown in figure 1 then become

$$e_1=\frac{e_i}{2}(1+\rho),\qquad e_2=\frac{e_i}{2}(1-\rho).$$

If $|\rho|\ll 1$, the ratio e_1/e_2 is approximately

$$\frac{e_1}{e_2}=1+2\rho. \tag{1}$$

To get an expression for the ratio error, consider the divider as two impedances in series which differ by a small amount ΔZ as shown in figure 4. If no current is drawn from the center tap, the voltage ratio e_1/e_2 is

$$\frac{e_1}{e_2}=\frac{Z+\Delta Z}{Z}=1+\frac{\Delta Z}{Z}. \tag{2}$$

From (1) and (2) we get

$$\rho=\frac{\Delta Z}{2Z}=\frac{\Delta R+j\omega\Delta L}{R+j\omega L} \tag{3}$$

where $R+j\omega L$ is the open circuit input impedance, Z_{in}, of the transformer. The real and imaginary components of ρ obtained from (3) are

$$\rho_r=\frac{R\Delta R+\omega^2L\Delta L}{R^2+\omega^2L^2} \tag{4}$$

$$\rho_i=\frac{\omega R\Delta L-\omega L\Delta R}{R^2+\omega^2L^2}. \tag{5}$$

If $Q^2\gg 1$ as is often the case, where $Q\equiv\omega L/R$, (4) and (5) reduce to

$$\rho_r=\frac{\Delta L}{L}+\frac{\Delta R}{\omega LQ} \tag{6}$$

$$\rho_i=-\frac{\Delta R}{\omega L}+\frac{\Delta L}{LQ}. \tag{7}$$

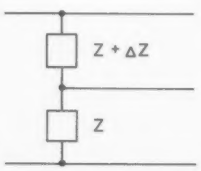

FIGURE 4. *Simplified circuit of a 2:1 ratio divider.*

These equations show the importance of winding the transformer so that it has a large inductance. The value of $\Delta L/L$ is made small by winding the transformer on a high permeability core to increase L, and by twisting the wires to minimize ΔL. A twisted cable is made by folding one wire in half and twisting the pair fairly tightly with a hand drill as shown in figure 5a. This cable is wound on the magnetic core and connected as shown in figure 5b. The wires are connected so that the current path from the upper tap to the center tap is the same as the current path from the center tap to the bottom tap. Thus, both windings link very nearly the same magnetic flux and have a small difference in inductance ΔL. Twisting the wires helps assure that both windings link the same flux.

Figure 6 shows the variation of ρ with frequency for a transformer having 42 turns of twisted No. 26 magnet wire wound on a ferrite torodial core. Note that ρ_r is essentially constant with frequency up to 2 MHz which is the upper frequency limit of our bridge. To see how high in frequency ρ_r will remain constant, we need to look at the equivalent circuit of the divider.

Figure 7 shows one of two exact equivalent circuits for an autotransformer [2] which is what the 2:1 ratio divider is. The Y_{oc} is the open-circuit admittance measured across the input terminals and Z_{sc} is the short-circuit "leakage" impedance measured across either output with the input terminals short-circuited. It can be seen from figure 7 that the voltage ratio V_1/V_2 at the output terminals will be equal to e_1/e_2 only if no current flows through Z_{sc}. If within the transformer housing the admittance from A to B differs from that from B to D by an amount ΔY_t, and if $|Z_{sc}\Delta Y_t| \ll 1$, then

$$\frac{V_1}{V_2} = \frac{e_1}{e_2} - 2Z_{sc}\Delta Y_t. \tag{8}$$

If ΔY_t is mainly a difference in capacitance, ΔC_t,

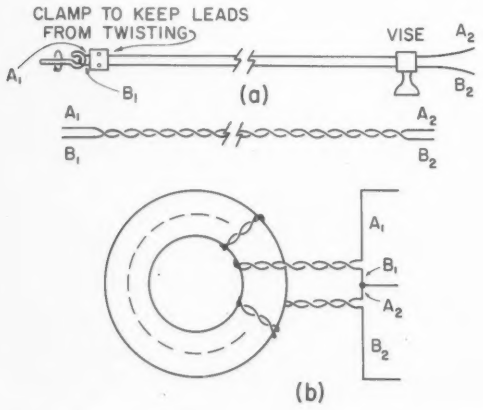

FIGURE 5. *The wires are twisted, wound on the core and connected as shown here to make a 2:1 ratio divider.*

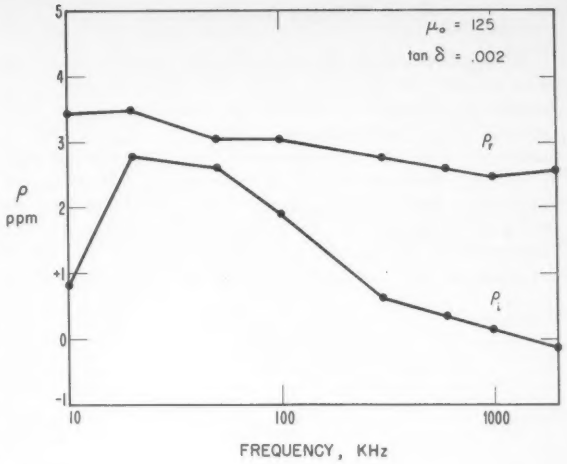

FIGURE 6. *Error curve for one of the first experimental dividers showing how ρ_r and ρ_i are relatively constant with frequency.*

$$\frac{V_1}{V_2} = 1 + 2\rho + 2\omega^2 L_{sc}\Delta C_t - j2R_{sc}\omega\Delta C_t \tag{9}$$

where L_{sc} is the leakage inductance defined by $Z_{sc} \equiv R_{sc} + j\omega L_{sc}$. A typical value of L_{sc}, such as for the transformer whose ratio error is shown in figure 6, is $L_{sc} = 0.1$ μH. By using trimmer capacitors from A to B and B to D, ΔC_t can be made less than 0.01 pF giving, in ppm,

$$2\omega^2 L_{sc}\Delta C_t < 0.1\, f_{MHz}^2$$

and

$$2R_{sc}\omega\Delta C_t < 0.01\, f_{MHz}$$

where f_{MHz} is the frequency in MHz. Since this loading error is proportional to the frequency squared, it will be the predominant error term at frequencies much above 1 MHz. The transformer whose characteristic is shown in figure 6 has trimmer capacitors across the output leads to adjust ΔC_t to a minimum. Without adjusting ΔC_t to a minimum the ρ_r curve increases to a value of about 5 ppm at 2 MHz.

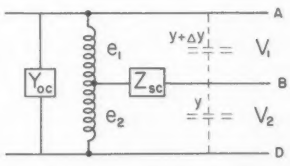

FIGURE 7. *An "exact" equivalent circuit for an autotransformer with lead admittances Y and Y + ΔY added.*

4. A Bridge to Measure ρ

A simplified diagram of the bridge used to measure ρ is shown in figure 8. The two arms of the transformer are balanced against two capacitors C', each having a nominal value of 1000 pF. The bridge is balanced with the capacitance C and the conductance G. The transformer is then removed from the bridge, rotated so that D is at the top and A is at the bottom, and then replaced on the bridge. The bridge is again balanced as before, changing C an amount ΔC and G an amount ΔG. Solving the bridge equations gives

$$\rho_r = \frac{\Delta C}{4C'} \tag{10}$$

$$\rho_i = \frac{-\Delta G}{4\omega C'} \tag{11}$$

where it has been assumed that $|\rho| \ll 1$, $C'' \ll C'$, and $G''^2 \ll \omega^2 C'^2$.

A more detailed diagram of the bridge is shown in figure 9a. The capacitors C and C' are three-terminal capacitors having admittances to ground shown as dotted lines. If these admittances are unequal they will load the transformer causing currents to flow through Z_{sc} and, thereby, change the apparent voltage ratio of the transformer. To measure the true voltage ratio e_1/e_2 of the transformer, a second detector, D_2, is placed between the center tap of the transformer and ground in order to balance the admittances to ground with Y. With both detectors nulled for both positions of the transformer, the bridge equations yield (10) and (11) as before.

To measure the small changes in conductance, ΔG, the T-network shown in figure 9b was used for G. Changing C_s an amount ΔC_s gives a change in conductance

$$\Delta G = \omega^2 C_g R \Delta C_s \tag{12}$$

and a change in capacitance which is negligible compared to ΔC. Putting (12) into (11) gives

$$\rho_i = -\frac{RC_g}{4C'} \omega \Delta C_s. \tag{13}$$

The resolution for ρ_r and ρ_i is 0.025 ppm from 1 kHz to 1 MHz and 0.25 ppm to about 3 MHz. A photograph of the bridge is shown in figure 10. Bridges of similar design are described in references [3] and [4].

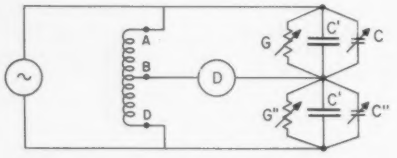

FIGURE 8. *Simplified circuit of a bridge to measure the ratio error of a 2:1 ratio divider.*

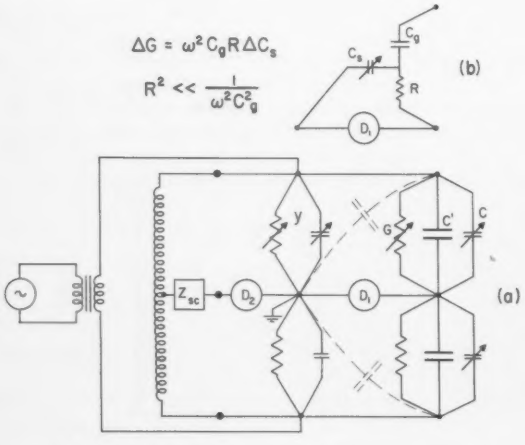

FIGURE 9. *A more detailed drawing of the circuit shown in figure 8.*

5. Optimum Transformer Design

Using the bridge shown in figure 10, a number of experiments were made to determine the optimum coil geometry, core material, type of wire, wire sizes, and amount of twist of the wire.

5.1. Coil Geometry

Theoretically the best coil geometry would be that which gives a maximum inductance for a minimum

FIGURE 10. *Photograph of bridge components, showing a divider, with its shield removed, connected at the top of the bridge.*

length of cable. Large inductance is needed to decrease ρ_r, and minimum cable length is needed to make L_{sc} small. The leakage inductance per unit length of cable is given approximately by

$$\frac{L_{sc}}{l}=0.2\,\frac{P}{d}\tan^{-1}\frac{d}{P}\ \mu\text{H/m} \tag{14}$$

where

$P=2t+\delta$

$t=$ wire insulation thickness

$d=$ wire diameter

$\delta=$ skin depth $\left(\leq\frac{d}{2}\right)$

$l=$ cable length.

If $\delta > d/2$, use $d/2$ in place of δ. Equation (14) is actually the inductance per unit length of two long parallel thin tapes of width d spaced a distance P apart. By defining P and d as stated under (14), the results from (14) agree with measured data to within 10 percent which is sufficiently accurate for most applications. Note that L_{sc} is independent of the core permeability. To decrease L_{sc} it is necessary to decrease the cable length. Changing the wire diameter or insulation thickness has only a secondary affect on L_{sc}. Measured values of L_{sc} and R_{sc} from 100 kHz to 2 MHz are shown in figure 11 for No. 24 wire. The leakage inductance decreases slightly due to skin effect. The resistance R_{sc} increases slightly faster than the square root of frequency primarily due to skin effect.

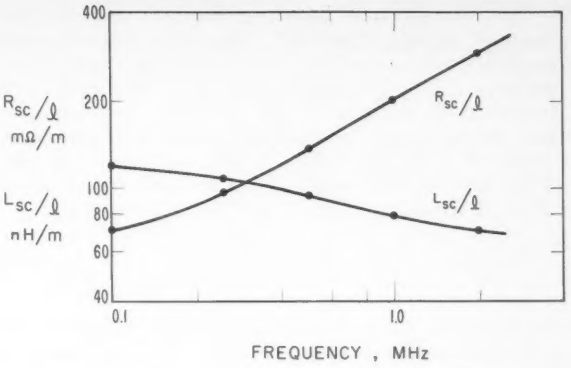

FIGURE 11. *Variation of the leakage inductance and resistance with frequency.*

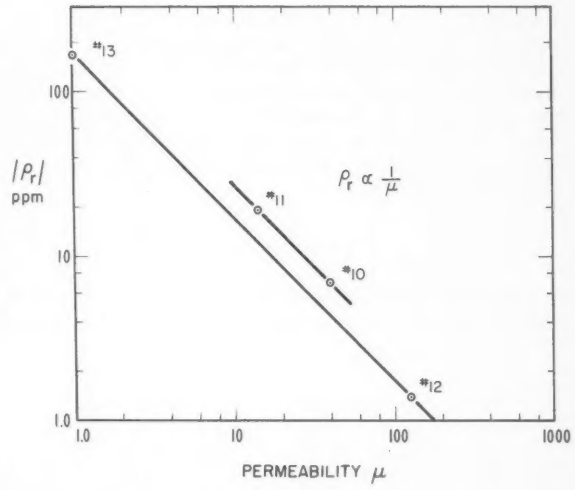

FIGURE 12. *Ratio error versus core permeability for four transformers made identical except for core permeability.*

5.2. Core Material

Figure 12 shows how ρ_r is decreased by increasing the permeability μ. These four transformers were identical except for the type of core material used. One long twisted cable was made and cut in half. One half was used to wind No. 10 and the other half to wind No. 11. Transformers Nos. 12 and 13 were, likewise, made from one cable cut in half. The results show that ρ_r is inversely proportional to μ. The cores were all very low-loss ferrite toroids with loss tangents of about 0.002. Cores which are very lossy do not give the same results. The Q for transformers with lossy cores is so low that the second term on the right of (6) may become larger than the first. The second term is a function of the core loss as well as the permeability. The core material, therefore, should have a high μ but not be too lossy. The core material can be fairly lossy if ΔR is small enough to make the second term on the right of (6) negligible.

5.3. Type of Wire

A number of experiments with different types of wire led to the conclusion that wire which has a very uniform resistivity and diameter gives the lowest ΔR values. Figure 13 shows the errors for four transformers which are identical except for the type of wire used. These transformers have air cores to eliminate the effect of magnetic core properties. Another reason for using air core transformers is that the errors are larger and easier to measure. The shape of the single layer solenoid type winding is shown in figure 14. The different types of wire used were formvar coated magnet wire (C), TEFLON® coated magnet wire (A1 & A3), and copper thermocouple wire (T). Note that the thermocouple wire ρ_r curve is constant with frequency and quite small for an air core. This means that the second term in (6) is negligible even though the Q is fairly low. Using thermocouple wire we were consistently able to wind transformers with low errors which are constant with frequency.

The thermocouple wire transformers are true "inductive" voltage dividers. The other transformers are more nearly "resistive" dividers than "inductive" dividers. The inductance of each of these four transformers is about 15 μH. Since $\rho_r \doteq 10$ ppm for the thermocouple wire transformer, (6) gives $\Delta L \doteq 150$ *pH*. Typical values of ΔL are 100 to 500 *pH*. They are constant with frequency and independent of μ. Expressing L as $L = \mu N^2 L_a$, (6) becomes

$$\rho_r \doteq \frac{\Delta L}{\mu N^2 L_a}$$

where N = number of turns on the core and L_a is the geometric inductance of the core. Typical values of ΔR are 50 to 500 $\mu\Omega$ for thermocouple wire and 10 times that for the other wire we tried. These figures are all for No. 24 wire.

It should be noted that any wire, including thermocouple wire, generally gives larger errors if the wire is stretched. A number of transformers were made with wire that was stretched approximately 1 percent to remove slight kinks in the wire. The errors were significantly larger than for transformers made from the same spool of wire with the slight kinks left in the wire. It is best to purchase wire wound on large spools so that it is relatively free of kinks when removed from the spool.

5.4. Wire Size

The experiment described above was repeated with No. 20 wire and also with No. 30 wire. The larger wire transformers gave slightly lower ρ_i errors than the corresponding No. 24 wire transformers gave. There was no significant decrease in the ρ_r errors. The results are shown in figure 15. Transformers made with No. 30 wire had considerably higher errors than those made with No. 24 or No. 20 wire.

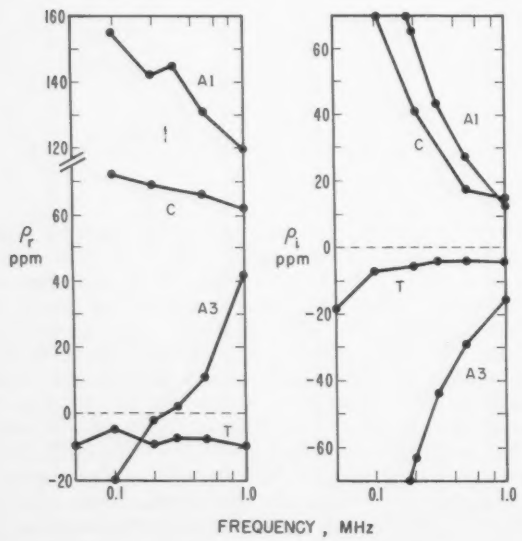

FIGURE 13. *Comparing results from four different types of No. 24 wire, where A1 and A3 are TEFLON ® coated magnet wire with single (0.0006 in) and triple (0.0015 in) insulation thickness; C is formvar coated magnet wire, and T is enamel coated copper thermocouple wire.*

5.5. Cable Twist

To determine how much the wires should be twisted, a number of transformers were made identical except for the amount the wires were twisted. Figure 16a shows ρ_r and ρ_i plotted against the number of turns per unit length of the cable. The length, l_T of one turn is defined in figure 16b. These are all air core transformers wound with No. 24 thermocouple wire. The dots are single layer solenoid windings whereas the X's are multilayer coils wound on nylon bobbins. The inductance, L, of each transformer is approximately 15 μH. As can be seen from figure 16, any twist from four to ten turns/inch (160 to 400 turns/meter) gives about the same results. Below four turns/inch the error increases. At about 12 turns/inch (500 turns/meter) the wire breaks. In terms of the twist length, l_T, and wire diameter, d, satisfactory results were obtained in the range

$$0.08 < \frac{d}{l_T} < 0.2.$$

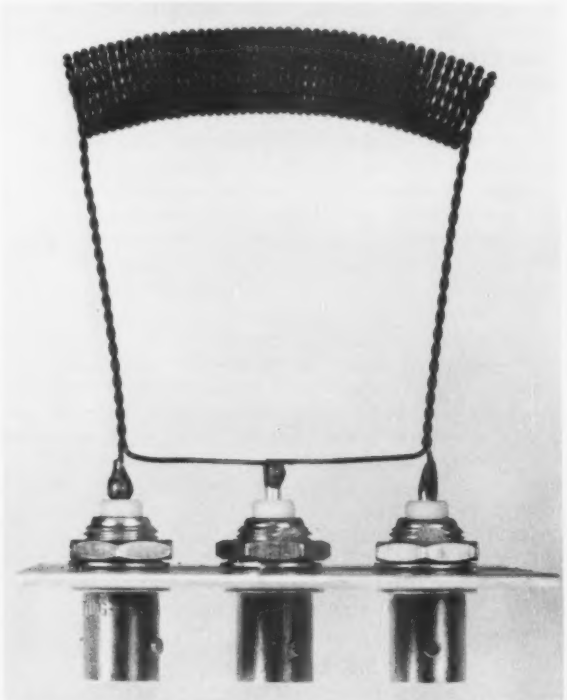

FIGURE 14. *An air core, solenoid type winding.*

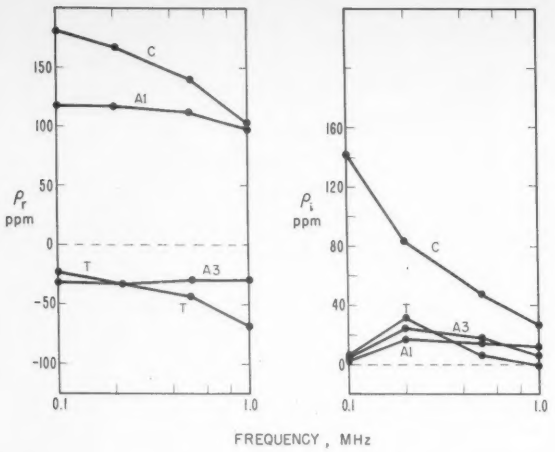

FIGURE 15. *Comparing results from four different types of No. 20 wire where A1, A3, C, and T are as defined in figure 13.*

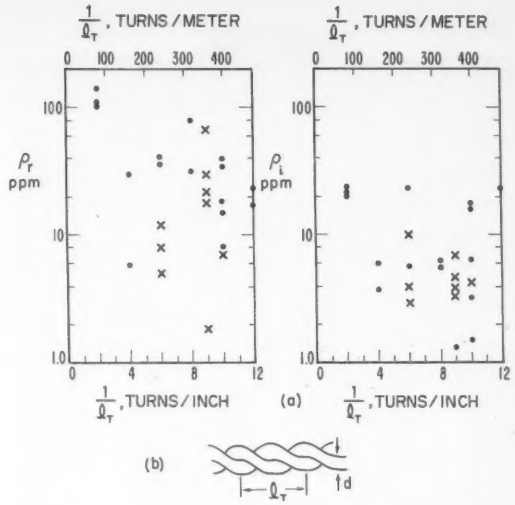

FIGURE 16. *Results of air core solenoid type (dots) and bobbin type (X's) transformers wound with cables twisted a different number of turns per inch.*

This equation should also be a reasonable guide for twisting wires other than size No. 24.

5.6. Lead Connections

One more important consideration in winding the transformers is how the leads are connected. The first transformers that we wound were connected as shown in figure 17a. The ratio errors were quite unstable and very sensitive to slight movement of the leads. To find a better way of connecting the leads, a number of air core transformers were made identical except for the lead connections. Figure 17 shows the three different ways the leads were connected. Of these three ways, the one shown in figure 17c was most stable and gave the smallest errors. The improvement in stability is probably due to the smaller mutual inductance and capacitance between leads. The lower error is probably a result of the ease with which the corresponding leads can be cut to the same length. It is important that in any arrangement of the leads that the leads on one side of the center tap be the same length as the corresponding leads on the other side. A difference in lead length of 0.001 in will give a ΔL of about 40 pH for No. 24 wire.

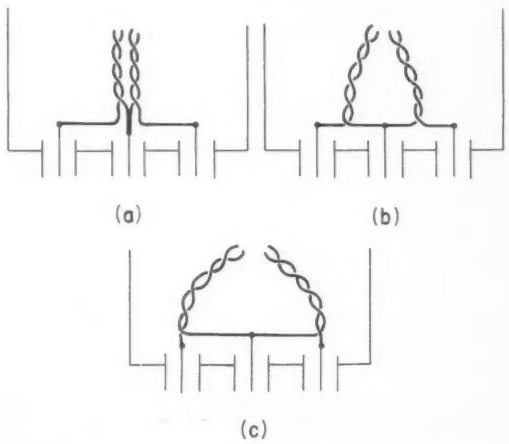

FIGURE 17. *Three different arrangements of the transformer leads.*

5.7. Cup-Core Design

One of the easiest ways of constructing a transformer with magnetic cores is to wind the cable on a bobbin and then clamp magnetic cup cores to the bobbin such as shown in figure 18. Figures 19 and 20 show the errors for three cup core transformers constructed like the one shown in figure 18. These transformers were made with all the optimum parameters that were found. The cables were made with No. 24 thermocouple wire twisted to six turns/inch (240 turns/meter). The cores are high permeability, fairly low-loss ferrite cores. The increase in ρ_r and ρ_i at frequencies above 100 kHz is due to the capacitance between leads not being equal. If these capacitances were balanced as discussed in part 3, the errors would be less than 1 ppm to above 1 MHz.

With care, the error can be made less than 0.1 ppm. A fourth cup core transformer was adjusted to have a ρ_r error less than 0.1 ppm at 100 kHz by changing the length of one lead slightly. Then ρ_r was adjusted to less than 0.1 ppm at 1 MHz by adjusting small trimmer capacitors placed between the leads. As figure 21 shows, the resulting ρ_r error is less than 0.1 ppm from 30 kHz to above 1 MHz.

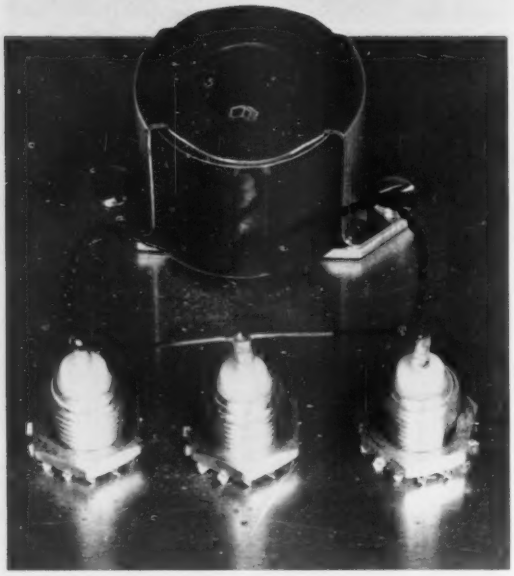

FIGURE 18. *A cup-core transformer having very low ratio errors like that shown in figures 19 and 20.*
The cover of the shield is not shown.

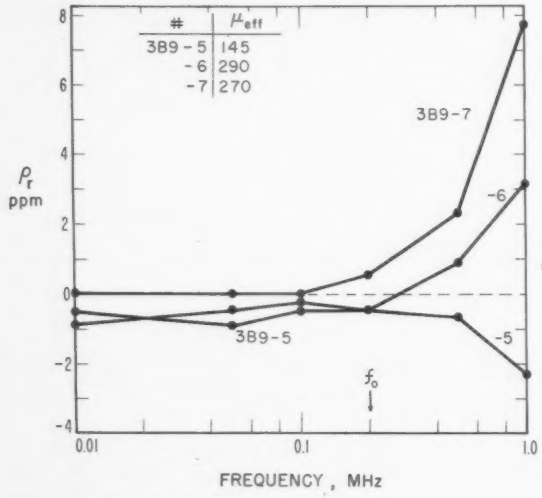

FIGURE 19. *Results from three cup-core transformers wound with No. 24 copper thermocouple wire twisted to six turns/inch.*

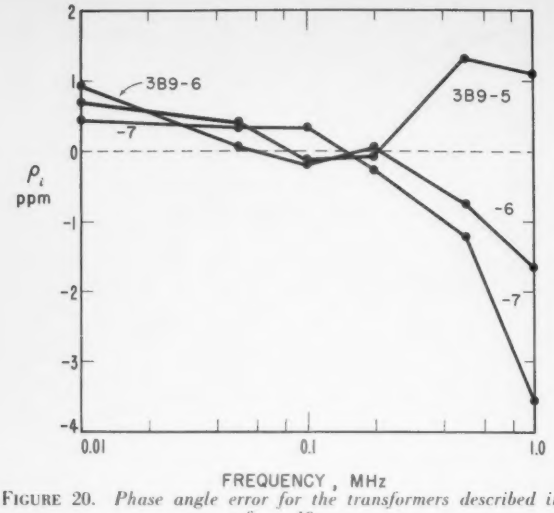

FIGURE 20. *Phase angle error for the transformers described in figure 19.*

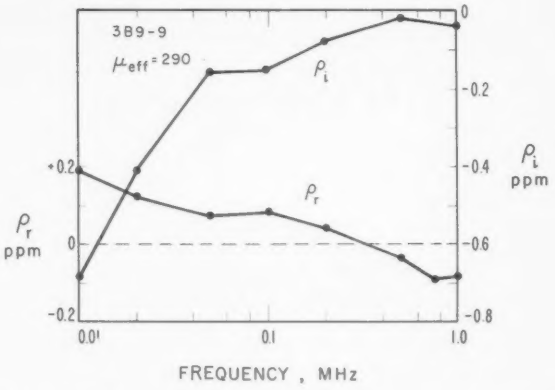

FIGURE 21. *Ratio error of a cup core transformer which has been adjusted to have a minimum ρ_r by adjusting lead length and by balancing the capacitance between leads.*

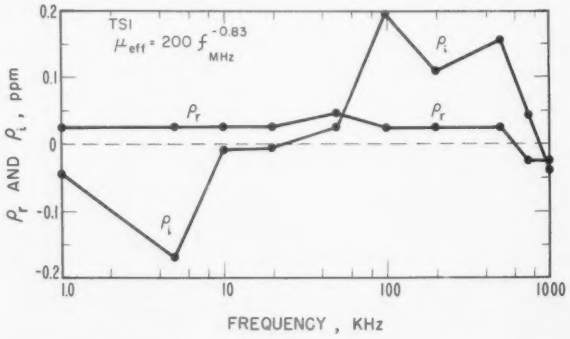

FIGURE 22. *Ratio error of a transformer wound on a supermalloy 1 mil tape core having dimensions OD=1.150, ID=0.650 and H=0.375 in.*

5.8. Tape-Core Transformers

Very broad band 2:1 ratio dividers can be made with high permeability magnetic tape cores. Figure 22 shows the ratio error of a divider wound on a supermalloy tape core having a tape thickness of 1 mil. The

core has 64 turns of No. 24 copper thermocouple wire twisted to about 8 turns/inch (320 turns/meter). The capacitance between leads has been adjusted to be equal. The ρ_r error is less than 5 parts in 10^8 from 1 kHz to 1 MHz.

6. Conclusion

The 2:1 ratio transformer is a simple, yet accurate, divider which is easy to construct. Using the optimum parameters discussed in part 5, it is easy to keep the ratio error less than 1 ppm from 1 kHz to 1 MHz. Air core transformers having no magnetic cores can be made with errors less than 10 ppm over a reduced frequency range. With extra care, ρ_r can be made less than 0.1 ppm to above 1 MHz. The ratio errors are quite insensitive to temperature, time, shock, and most any change in the environment since both windings of the transformer are influenced equally by any change in the environment.

Five cup-core transformers such as described in part 5.7 have been combined as shown in figure 2b to make an accurate 30 dB attenuator at 1 MHz. Details of this type of attenuator together with a complete error analysis will be given in a future publication.

7. References

[1] Zapf, T. L., C. H. Chinburg, and N. K. Wolf (September 1963), Inductive voltage dividers with calculable relative corrections, IEEE Trans. on Instrumentation and Measurement **IM-12,** 80–85.

[2] EE Staff, MIT (1943), Magnetic circuits and transformers (John Wiley & Sons, Inc., New York, N.Y.), 400.

[3] McGregor, M. C., J. F. Hersh, R. D. Cutkosky, F. K. Harris, and F. R. Kotter (Dec. 1958). New apparatus at the National Bureau of Standards for absolute capacitance measurement, IRE Trans. on Instrumentation **I-7,** No. 3 and 4, 253–261.

[4] Cutkosky, R. D., and J. Q. Shields (September 1960), The precision measurement of transformer ratios, IRE Trans. on Instrumentation **I-9,** No. 2, 243–250.

(Paper 71C2–249)

JOURNAL OF RESEARCH of the National Bureau of Standards—C. Engineering and Instrumentation
Vol. 71C, No. 2, April–June 1967

A Dual-Load Flow Calorimeter for RF Power Measurement to 4 GHz

M. L. Crawford* and P. A. Hudson*

Institute for Basic Standards, National Bureau of Standards, Boulder, Colo. 80301

(December 6, 1966)

A new dual-load flow coaxial calorimeter power meter has been constructed at the National Bureau of Standards, Boulder Laboratories. Designed for use as a reference standard, the frequency range of the calorimeter extends up to 4 GHz and beyond. The power range extends from 2 W to 100 W with an error limit of 0.38 percent.

Design details, error analysis, and results of intercomparison with other standards are given.

Key Words: Coaxial, flow calorimeter, radio frequency power.

1. Introduction

The increasing complexity and higher performance characteristics of radio frequency and other electronic equipment in recent years has resulted in the need for more accurate measurement of the rf quantities. In rf power measurements, for example, 1 percent uncertainty for measurements in industrial standards laboratories is often required. Formerly, uncertainties of 5 percent were tolerable. Because uncertainties are accumulated in a chain of calibrations, the uncertainties in reference standards maintained by the National Bureau of Standards must be less than 1 percent.

The dual-load flow calorimeter described here is essentially a refinement of earlier calorimeters of this type [1][1] and was developed to meet the need for greater accuracy, and extend the range of NBS reference power standards up to 100 W. This development made possible the intercomparison between this standard and the NBS dry-load calorimeter [2] (50 mW to 5 W), thereby increasing the confidence in each.

2. Theory of Operation

The calorimetric principle has been considered the most accurate method for the measurement of rf power. This principle is based upon the first Law of Thermodynamics, or the conservation of energy. The measurement of electrical power using this principle depends upon the complete conversion of the electrical energy as delivered by a generator into thermal energy in a resistive load. The heat generated in the load results in a temperature rise in the load and its surroundings. This temperature rise is a monotonic function of the input power level and may be detected, for example, with a thermopile located between the load and a reference body whose temperature is stable with time.

Two types of calorimeters could be constructed to measure power at the levels of interest. They are the absolute flow calorimeter and the substitution flow calorimeter. (The use of dry-load calorimeters at these power levels, 5–100 W, is not practical because of the large physical size of loads required and the long measurement time constant.) An example of a "true" or "absolute" calorimetric system is shown in figure 1. In this system, power is measured in terms of mass, time, and temperature by the equation $P=Fc\Delta T$. In this equation F is the mass flow rate of the calorimeter fluid, c is its specific heat, and ΔT is the equilibrium temperature rise of the fluid. A conservative measure of the uncertainty with which such a measurement can be made is the sum of the uncertainties with which F, c, and ΔT can be determined. The value of c is known very accurately for the common fluids. The value of ΔT, however, is difficult to determine accurately for low input power levels, and F can be measured with an uncertainty no better than 0.5 percent at usual values of flow rate. In addition great care must be taken to prevent heat exchange with surroundings, and a correction must be made for heating due to friction flow of the fluid. Therefore, the uncertainty in power measurement using an absolute flow calorimeter is usually 1 percent or more.

Many of the above difficulties can be overcome by use of the dual-load calorimeter employing d-c substi-

*High Frequency Electrical Standards Laboratory, National Bureau of Standards Laboratories, Boulder, Colo. 80301.

[1] Figures in brackets indicate the literature references on page 116.

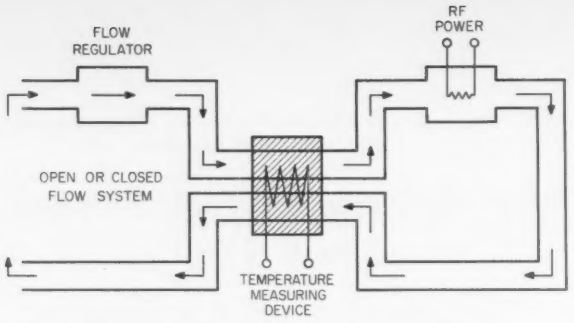

FIGURE 1. *Flow type "absolute" calorimeter.*

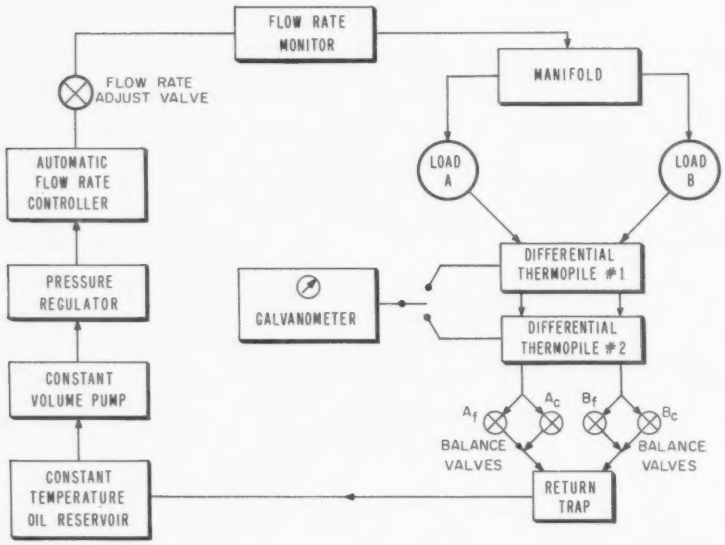

FIGURE 2. *Block diagram of dual-load flow calorimeter power meter 2–100 W, dc to 4 GHz.*

tution. A block diagram showing the system is given in figure 2. As the name implies, the dual-load calorimeter consists of two nearly identical loads connected in series or parallel to the fluid flow supply. Radio frequency power is applied to one load while d-c power is applied to the other. A differential thermopile, or other temperature sensing device, detects the temperature difference between the two streams on the downstream side of the loads when the system has reached thermal equilibrium. The d-c power level is adjusted to make the temperature difference zero, and the rf power is equated to the d-c power. Prior to the above measurement, it is necessary that the system be balanced by applying equal d-c power to each load at or near the rf power level to be measured. If the loads are in parallel to the fluid flow, then the flow rate through either one or the other may be adjusted for a null at the differential thermopile output.

Thus, in the dual-load substitution calorimetric technique, accurate knowledge of flow rate and temperature is not required for accurate measurement results. In addition heat exchange with surroundings due to external sources is not a problem as long as it remains constant during the measurement period. The substitution principle is based upon the assumption that heat generated by d-c or low frequency power absorbed by a load will have the same effect on the device used to sense the temperature rise of the load or a fluid surrounding it as heat generated by an equal amount of rf power. However, in general, equal quantities of rf and d-c power will not produce exactly the same calorimeter sensor response. Thus, an error, commonly known as the rf-dc substitution error, may exist. This error arises primarily because the rf current distribution in the load resistor is not identical to the d-c current distribution. This results in a difference

in the distribution of heat sources in the load in the two cases. In flow calorimeters, this error is minimized since the load resistor and mount structure are in intimate contact with a moving fluid, and the heat generated by the load tends to be transferred to the liquid regardless of the distribution of heat sources.

The main problems associated with measuring power by the substitution calorimetric method are the relatively long measurement time constants and the difficulty in maintaining thermal environmental and flow stability over this time period. The dual-load flow calorimeter was designed with emphasis on reducing some of these problems. For example, by reducing the time constant of the system to a minimum, the need for extremely stable rf sources and temperature control devices was reduced.

3. Description of Calorimeter and Operating Procedure

3.1. Loads

The loads (see fig. 3) were designed for rapid transfer of heat and low VSWR (≤ 1.03 referenced to 50 Ω at frequencies up to 4 GHz). The load resistor is a thin metal film deposited by vacuum evaporation onto a truncated conical substrate. The load is mounted inside a cylindrical outer conductor. This type of design was proposed by D. Woods [3]. The sheet resistivity, ρ, of the film is uniform over the area of the cone and the resistance is given by

$$R=\frac{\rho}{2\pi \sin \theta} \ln b/a \qquad (1)$$

where θ is the cone semiangle, and b/a is the ratio of outer to inner diameter of the coaxial line. The temperature coefficient of the resistive film is less than 10 ppm/°C thus insuring a nearly constant value of R at all power levels. The characteristic impedance of the section of coaxial line containing the conical resistor is

$$Z_0=\frac{Z_m}{2\pi} \ln b/a \qquad (2)$$

where $Z_m=\sqrt{\mu/\epsilon}$ is the wave impedance of the medium. By making $\rho/\sin\theta$ equal to Z_m, $Z_0=R$ at any point along the length of the load. This condition tends to assure the same current distribution along the resistor for both rf and dc. Measurements using a time domain reflectometer indicated that small discontinuities of the order of 0.1 Ω did exist along the length of the load. Thus, it appeared probable that a small substitution error could exist. The upper limit of the error was evaluated and is discussed in the following section.

The resistors are capable of absorbing up to 100 W of power with no significant change in their impedance characteristics. The physical dimensions of the loads were made small to reduce the measurement time. In order to absorb 100 W without damage to the film, the oil had to be circulated rapidly around and through the resistor body. At low levels of input power (2–5 W) the minimum oil flow rate was such that the temperature rise of the oil was approximately 5 deg. This flow rate per watt was about $\frac{15 \text{ cm}^3/\text{min}}{\text{watt}}$. At higher levels of input power, the flow rate per watt was reduced to about $\frac{7.5 \text{ cm}^3/\text{min}}{\text{watt}}$ so that the temperature rise was 10 deg centigrade.

3.2. Temperature Detection System

This system consists of two differential thermopiles (T.P. #1 and T.P. #2), of 10 junctions each, and a sensitive galvanometer. A selector switch allows either thermopile to be connected separately or both in series, to the galvanometer. The junctions of the thermopiles are located in the path of the moving oil as shown in figure 2. The oil is mixed thoroughly in a chamber downstream from the loads and then

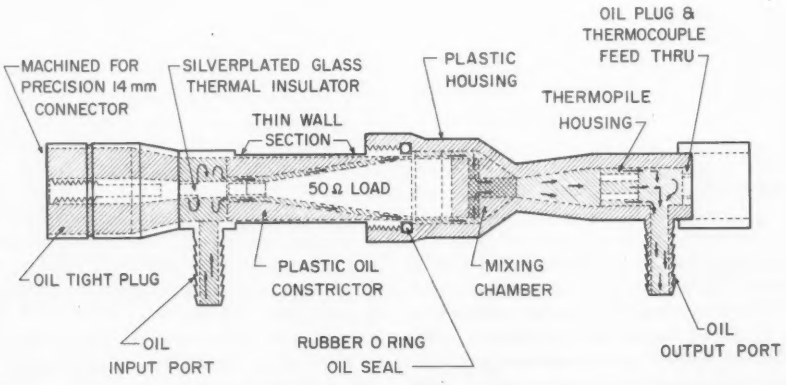

FIGURE 3. *Oil flow calorimeter load.*

passes around and through a plastic block in which the junctions of T.P. #1 are located. The close proximity of the thermojunctions of T.P. #1 to the load resistors results in rapid temperature detection and reduces the possibility of heat leakage before detection. Thermopile #2 was installed as a cross check against thermopile #1. Its junctions are mounted symmetrically inside plastic holders located farther downstream from T.P. #1. Any differences in the temperature of the oil flowing in channel A as compared to channel B will result in an emf generated by both T.P. #1 and T.P. #2. Either one or the sum of these emf's is detected by the galvanometer and within the limits of ± 0.02 percent, it is possible to detect any balance in the calorimeter system.

3.3. Flow System and Reservoir Temperature Control

The flow system of the dual-load flow calorimeter employs precision needle valves, a flow controller and meter, pressure regulator, constant volume pump, and reservoir, all incorporated into a closed circulation system (see fig. 2). Oil pumped from the reservoir passes through the pressure regulator which is set at 15 psi. It is then filtered and flows on to the flow rate meter and controller which is adjusted for the desired flow rate. Following the flow meter, the oil flow is divided into two channels, A and B, by means of the manifold. The flow path through each load is indicated by the arrows in figure 3. Oil leaving the loads passes through the mixing chamber, across thermopile #1, and across thermopile #2, on through the balance valves, to the return trap, and thence to the reservoir. The flow division between the two channels is regulated by means of the balance valves $A_F - A_C$ and B_F–B_C. These valves were placed downstream from the loads because this arrangement causes a back-pressure which resulted in better stability and control and insured that the load bodies were completely filled with oil at all times. Each valve has an adjustment range of 350:1 and by properly setting the ratio of flow between the fine and course valves, very small adjustments can be made in the flow division between channels.

The temperature of the oil in the reservoir is controlled at 28 ± 0.02 °C by a conventional automatic control circuit-cooling coil combination. This provides a nearly infinite heat sink for the system and helps to reduce the measurement time constant.

4. Estimation of Uncertainties

Uncertainties in measurement of power with the dual-load flow calorimeter were minimized by careful design and precision flow control and adjustment. The uncertainty of measurement is the difference between the true value and the measured value. This difference is usually expressed as a percentage of the true value. Sources of significant error and a brief explanation of each are given below.

4.1. Flow Division Instability and Thermal Effects

The instability in the flow division through each channel and the thermal drift are both reflected as a null shift or unbalance in the outputs of the thermopiles between loads A and B. As mentioned earlier, the effect of heat exchange with surroundings is much reduced in the dual-load configuration as compared to the single-load "absolute" calorimeter. Efforts were, nevertheless, made to minimize and equalize heat exchange between the two loads and their surroundings. Unequal heat exchange is not critical because the effect can be cancelled by proper adjustment of the flow rate through the individual loads during the d-c balancing operation. It is required, however, that the heat exchange be constant during the time a measurement is being made. After initial null (zero temperature difference between the oil leaving loads A and B) was achieved, the emf output of the thermopiles was recorded over a time period much greater than the measurement time constant which was approximately 5 min. Tests at several power levels indicated that for periods of up to 30 min the maximum drift was no greater than 6 μV. Since an oil temperature rise of 10 deg centrigrade produces a net thermopile output of 4000 μV, a maximum emf unbalance of ± 6 μV, corresponds to 0.15 percent shift in the thermal balance between the loads.

4.2. Detection System

The degree to which the two channels are balanced is a function of the overall resolution of the system. The sensitivity of the complete system is limited by the temperature fluctuations in the oil and not by the detection system which consists of the galvanometer and differential thermopile. These fluctuations limited the resolution to 0.02 percent.

4.3. RF–D-C Substitution Error

As mentioned earlier, the calorimeter loads and temperature detecting system were designed to minimize the rf–d-c substitution error. The loads were designed to provide matched terminations and thus insure, as nearly as possible, identical rf and d-c current distributions. In addition, the oil flowing over the resistor surfaces tends to absorb all the heat generated in the load regardless of the distribution of heat sources in the load. A small portion of heat may be conducted away at the points where electrical connection is made between the load resistor and the mount. Negligible heat conduction to the mount occurs at the input end where the center conductor is immersed in the moving oil stream for a distance of 1½ cm. At the grounded end of the resistor, where it contacts the outer conductor, some heat conduction is possible. In order to check for a temperature difference in this area a 10-junction thermopile was cemented to the outer conductor of one of the loads and referenced to an ice bath. "Equal" levels of d-c or rf power were then applied alternately to the load.

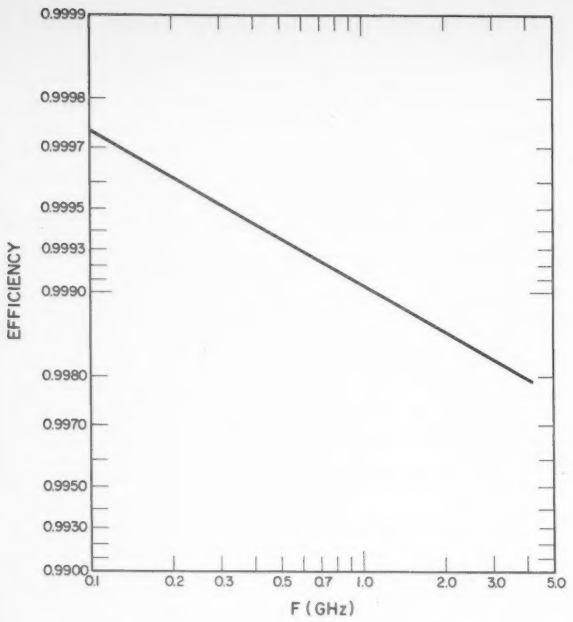

FIGURE 4. *DLFC input line efficiency versus frequency.*

At a frequency of 4 GHz, a difference in temperature of 0.035 °C was observed while at 2 GHz no measurable difference was discernible. Calculations were made (appendix) which show that at 4.0 GHz, with a temperature difference of 0.035 °C, an error less than 0.1 percent exists.

On the basis of the above tests the rf–d-c substitution uncertainty was estimated to be 0.1 percent at frequencies of 1 GHz and above and 0.05 percent at frequencies below 1 GHz. The resolution of the measurement, due to noise and ambient temperature variations, was approximately 0.05 percent.

4.4. Uncertainty in Input Lines and Mismatch Losses

In the load bodies as described in the preceding section, the only portion of input transmission line not immersed in the oil stream is a length of approximately 3.7 cm. The portion immersed in oil can be considered as a part of the load since the I^2R loss will be absorbed by the oil. The loss in the remaining 3.7 cm of input line was calculated using the following equation: [4]

$$\alpha_T = 8.686l\left[\alpha_0\sqrt{f}\,\frac{1/a+1/b}{\ln b/a}+\frac{\omega}{2}\sqrt{\mu\epsilon}\,\tan\delta\right]\ dB \quad (3)$$

where $\alpha_0=\frac{1}{2}\sqrt{\frac{\pi\epsilon}{\sigma}}$ and $\omega=2\pi f$,

ϵ = dielectric constant,
μ = permeability,
σ = conductivity of metal used for inner and outer conductors,
a = inner conductor radius,
b = outer conductor inside radius,
f = frequency,
l = input line length, and
$\tan\delta$ = loss tangent of dielectric.

The results of this calculation as a function of frequency are plotted in figure 4. The uncertainty in the calculations of the loss factor is due to the combined uncertainty in measuring a, b, l (length = 3.7 cm), and in the assumed values of ϵ, μ, σ, and $\tan\delta$. The combined uncertainty of these factors could be as great as ±35 percent at 4 GHz. This was primarily due to the uncertainty in the thickness of the silver plating on the inner and outer conductors of the line, hence an uncertainty in the value of σ. For example, at 4 GHz the following data were obtained from calculations for the loss of the input line:

Loss in input connectors	0.0026 ± 0.0005 dB
Loss in straight region	.0030 ± .0009 dB
Loss in taper region	.0028 ± .0019 dB
Total loss	.0084 ± .0033 dB

The loss is then 0.2 ± 0.07 percent or an efficiency of 99.8 ± 0.07 percent. Thus the power at the input connector was higher than that measured by the calorimeter by the factor 1.002 ± 0.0007. The rf efficiency factor versus frequency is shown in figure 4. At lower frequencies the loss in the input line decreases and below 10 MHz the efficiency is assumed equal to unity.

Due to the fact that the calorimeter loads are not perfectly matched to Z_0, part of the incident power will be reflected. Because a measurement of the incident power is usually desired, reflections cause the calorimeter to read low with respect to the incident power. The impedance of both loads was matched to Z_0 (50 Ω) using a time domain reflectometer so that VSWR < 1.03 ±0.01 at frequencies from 1.0 to 4.0 GHz and < 1.015 ±0.005 at frequencies below 1.0 GHz. A plot of VSWR versus frequency for each load is shown in figure 5.

At the maximum VSWR of 1.03, 0.02 percent of the incident power will be reflected resulting in a 0.02 percent error in the power measurement if the reflection loss is neglected. For a VSWR of 1.015, the reflected power is only 0.01 percent of the incident source. Combining the maximum expected uncertainty in the correction factor for rf efficiency with the maximum mismatch error gives 0.09 percent above 1 GHz and 0.04 percent below 1 GHz.

4.5. D-C Power Measurement Error

The d-c power substituted in the loads is calculated from measured values of current and voltage. The voltage drop across a 1 Ω standard resistor in series with the termination is measured with a potentiometer

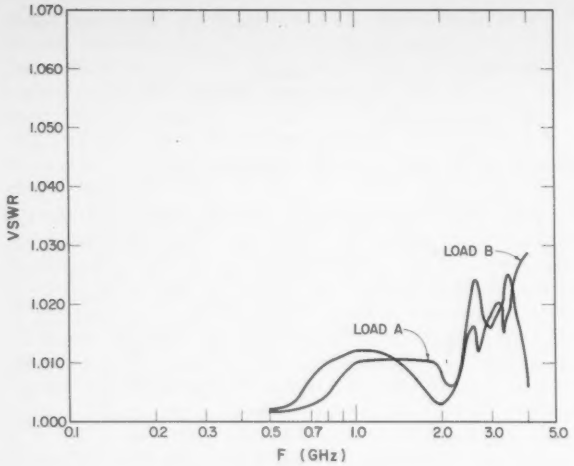

FIGURE 5. *VSWR versus frequency of DLFC loads.*

to obtain the current flowing into the loads, and the voltage drop across the loads is measured directly with a digital voltmeter. The power is then found by the simple equation $P=VI$. Both V and I can be determined accurately to 0.01 percent giving a maximum d-c measurement error of 0.02 percent.

The errors discussed are believed to be the only significant ones in the calorimeter and measuring system described herein. The overall limit of error can be found by adding the maximum values:

	0–1 GHz	1–4 GHz
1. Flow division stability	0.15	0.15
2. Detection system	.02	.02
3. RF–D-C substitution	.05	.10
4. Line loss and rf reflection (mismatch errors)	.04	.09
5. D-C measurement error	.02	.02
Limit of error	0.28%	0.38%

5. Conclusions

The dual-load flow calorimeter was designed and constructed to provide a reference standard for cw power measurements in the range 2 to 100 W at frequencies up to 4.0 GHz. A maximum uncertainty or error limit of 0.38 percent was achieved. This is a significant improvement over prior capabilities at these power levels. Also the frequency range of the NBS reference standards was extended from 1.0 GHz up to 4.0 GHz in the power range of 5 to 100 W.

Intercomparisons at 1, 3, and 4 GHz have been made between this calorimeter and the reference standard dry-load calorimeter which has a total estimated uncertainty of 0.35 percent. The intercomparisons included measurements at power levels of 2 W and 4 W and the disagreement was no greater than 0.2 percent.

6. References

[1] J. P. Vinding, An accurate calorimeter for high microwave power, The Microwave Journal **4,** No. 1, 41–46 (Jan. 1961).

[2] P. A. Hudson, A calorimetric reference standard power meter for the frequency range 0–4000 MHz. Paper in process.

[3] D. Woods, Improvements in precision coaxial resistor design, IRE Trans. on Instr. **I–II,** Nos. 3–4 305–309 (Dec. 1962).

[4] S. Ramo and J. R. Whinney, Fields and waves in modern radio, (John Wiley & Sons, Inc., New York, 2d edition, fifth printing, Nov. 1960). See Table 9.01 between pages 364–365. Equation (3) was derived using equations in this table.

7. Appendix

7.1. Analysis of RF–D-C Substitution Error

In the following analysis of the rf–d-c substitution error, an upper bound is arrived at which, though derived from approximate considerations, is felt to have significance.

The total input power to the calorimeter, P_t, is related to the power absorbed by the oil, P_a, and the power P_c absorbed elsewhere, by

$$P_t=P_a+P_c. \tag{1A}$$

Using additional subscripts, rf and d-c, to indicate when the input power is respectively rf and d-c (1A) becomes

$$P_{t\mathrm{dc}}=P_{a\mathrm{dc}}+P_{c\mathrm{dc}} \tag{2A}$$

and

$$P_{t\mathrm{rf}}=P_{a\mathrm{rf}}+P_{c\mathrm{rf}}. \tag{3A}$$

The measuring technique used with the calorimeter results in

$$P_{a\mathrm{dc}}=P_{a\mathrm{rf}}. \tag{4A}$$

Using (2A), (3A), and (4A), one can obtain the relation

$$\frac{P_{t\mathrm{rf}}}{P_{t\mathrm{dc}}}=1+\frac{P_{c\mathrm{dc}}}{P_{t\mathrm{dc}}}\left[\frac{P_{c\mathrm{rf}}}{P_{c\mathrm{dc}}}-1\right]. \tag{5A}$$

Thus, if $P_{c\mathrm{rf}}=P_{c\mathrm{dc}}$, there would be no substitution error. However, this condition may not hold for all frequencies and a measure of the ratio of $P_{c\mathrm{rf}}$ to $P_{c\mathrm{dc}}$ is obtained from the following considerations.

As noted in the text, there is little chance for heat losses to the external environment except possibly at the junction of the load resistor with the outer conductor. A thermopile connected externally between this area and an ice bath indicated that there was no

difference in the temperature for frequencies up to 2 GHz when equal rf and d-c power were alternately applied to the calorimeter. However, at 4.0 GHz a temperature difference of 0.035 °C was measured. Because of the construction and nature of operation of the calorimeter, the principle mode of heat transfer to the external environment is by conduction. Since the rate at which heat flows by conduction is proportional to the temperature difference between the source and sink,

$$\frac{P_{crf}}{P_{cdc}}=\frac{T_{rf}-T_{amb}}{T_{dc}-T_{amb}}, \tag{6A}$$

where T_{rf} and T_{dc} are the respective temperatures at the junction of the load resistor and outer conductor when rf and d-c power are alternately applied to the calorimeter. The ambient temperature is noted by T_{amb}. From experimental data at 4 GHz,

$$\frac{P_{crf}}{P_{cdc}}=1.023. \tag{7A}$$

An upper bound for the ratio of P_{cdc}/P_{tdc}, obtained from using the dual-load calorimeter as an absolute flow calorimeter, is

$$\frac{P_{cdc}}{P_{tdc}}=0.03. \tag{8A}$$

Substituting (7A) and (8A) into (5A), the upper limit for the substitution error is 0.07 percent which was increased to 0.1 percent because of the approximations used.

(Paper 71C2–250)

247-602 O-67—3

JOURNAL OF RESEARCH of the National Bureau of Standards—C. Engineering and Instrumentation
Vol. 71C, No. 2, April–June 1967

Polymeric Materials for Dielectric Reference Specimens

Arnold H. Scott* and Joseph R. Kinard, Jr.

Institute for Basic Standards, National Bureau of Standards, Washington, D.C. 20234

(December 1, 1966)

The results from a study of the effects of aging and humidity change on certain polymer specimens indicate it is possible to establish stable dielectric reference specimens. Specimens of polyethylene, polystyrene, polycarbonate, poly(tetrafluoroethylene) (PTFE), fluorinated ethylene-propylene polymer (FEP), and poly(1,4-cyclohexylenedimethylene terephthalate) were used in the investigation. Slow changes in the dielectric properties were observed on some specimens over a period as long as three years. Very long timed humidity runs indicate PTFE, and FEP to only a slightly less degree, are best suited for dielectric reference specimen preparation.

Key Words: Dielectric constant, dissipation factor, frequency, fluorinated ethylene-propylene, humidity, polycarbonate, polyethylene, poly(1,4-cyclohexylenedimethylene terephthalate), polystyrene, poly(tetrafluoroethylene), time, reference specimens.

1. Introduction

A long term study of certain polymer specimens under consideration as dielectric reference specimens has been conducted. Such reference specimens may be used to compare the measurement accuracy of various other laboratories, so these specimens must have accurately determined and stable dielectric properties. Specimens from several polymers were found to exhibit sufficient stability to permit their use. The materials investigated were polyethylene (PE), polystyrene (PS), polycarbonate (PC), poly(tetrafluoroethylene) (PTFE), fluorinated ethylene-propylene polymer (FEP), and poly(1,4-cyclohexylenedimethylene terephthalate) (T–16). All data were taken on flat disk specimens, and the conditions under which the measurements were made were carefully controlled. The humidity of the surrounding atmosphere as well as the specimen temperature was controlled because the properties of most specimens were functions of humidity.

2. Measuring Equipment

A low-voltage conjugate Schering bridge similar to one described in a paper by Scott and Harris [1][1] was used to measure dielectric constant and dissipation factor from 10^2 Hz to 10^5 Hz. The cell used with the Schering bridge was of the guard-ring micrometer-electrode type [2, 3, 4] and was mounted in a chamber whose temperature was controlled by pumping liquid from a temperature bath through coils around the chamber, and whose humidity was maintained by exposing inside the box either P_2O_5 for < 1.5 percent relative humidity (rh) or a saturated $Mg(NO_3)_2$ solution for about 52 percent relative humidity. The humidity in the chamber was measured with an electric hygrometer.

In the frequency range from 1 MHz to 10 MHz a Q-meter was used for dielectric constant and dissipation factor measurements. The cell used was a two-terminal micrometer-electrode cell mounted in a box whose temperature and humidity were controlled in a manner similar to that used for the three-terminal cell. A two-terminal Schering bridge was used to coordinate the Q-meter measurements with the more accurate three-terminal data.

3. Specimens

3.1. Contact Electrodes

Many of the measurements were made without contact electrodes using the air-gap technique [5] with 8.5 cm diam disks from 2 mm to 5 mm thick. Disks with 3.8 cm diam were prepared with contact electrodes so that specimens might be measured at higher frequency with the Q-meter and used to calibrate two-terminal equipment. Heavy gold electrodes, about 1500 Å thick, were evaporated on the faces of these similar specimens to form the contact electrodes. Care was always taken to see that the resistance across the electrode surface was never more than a few tenths of an ohm.

*Present address: 4220 Franklin Street, Kensington, Md. 20795.

[1] Figures in brackets indicate the literature references at the end of this paper.

3.2. Surfacing Specimens

At the beginning of this study a modified Schiefer abrasion machine was used to surface the specimens [6]. Even though this method produced specimens with thicknesses uniform to within 5 μ, we later used a technique which produced more uniform thicknesses. The second method made use of a vacuum chuck and a fly cutter on a milling machine. The vacuum chuck consisted of a metal vacuum chamber with holes drilled in one side for holding the specimen in place and could be positioned on a milling machine for successive passes made with the cutter. The specimen was turned over or rotated with each pass until the faces became quite parallel. With careful preparation of the cutting tool and proper adjustment of the cutting rate, this technique could produce specimens with thicknesses uniform to within 3 μ over an 8.5 cm diam.

3.3. Measuring Thicknesses

The specimen thicknesses were measured with an indicating micrometer having a reference point set by gage blocks. Measurements were made at points around concentric circles as determined by a pattern. These numbers were averaged to determine the measured thickness. Comparisons indicate agreement to 0.05 percent between the micrometer thickness and that determined with the two-fluid electrical technique [7].

3.4. Storage

Between measurements and for initial conditioning, specimens were stored in glass vessels with humidity controlled in the same manner as in the measuring chamber.

3.5. General Properties

The suppliers indicated the following general properties for the various materials. The polyethylene was the high molecular weight, low pressure type. It had a linear structure with no detectable branching and a crystallinity of from 90 to 95 percent. The T–16 polyester was a linear, thermoplastic, crystallizable polymer about 36 repeating units long. It had a crystal melting point of around 265 °C and a glass transition at about 87 °C. The polycarbonate material contained no plasticizers and had a molecular weight ranging around 30,000 to 35,000. The polystyrene material was reported to be of high purity. PTFE and FEP specimens were from laboratory grade stock.

The polyethylene specimens and certain of the polystyrene specimens were compression molded in our laboratory. The polycarbonate specimens were impact molded, the T–16 specimens were injection molded, and the FEP and PTFE specimens were compression molded, all by the supplier.

3.6. Density

The density of most specimens was measured in order to characterize the materials better and to provide a rough measure of the uniformity of specimens from the same material. Two methods were used for determining density. In the first method the volume of the specimen was determined by liquid displacement. The second method was based on dimensional volume measurements. Since our specimens were very carefully machined disks, they were, in fact, good approximations of right circular cylinders. By measuring the diameter with a traveling microscope and using the thickness, we could calculate a dimensionally determined volume. The same mass data was used with each volume to calculate two different densities. Based on repeated measurements and calibration of the traveling microscope, we estimate the dimensional volume measurement to be accurate within about 0.1 percent; however, the liquid displacement densities were consistently larger than the dimensional densities by 0.1 percent to 0.5 percent, even though care was taken to reduce errors caused by insufficient surface wetting of the specimen and by surface tension acting on the suspension wire. Since the dimensional measurements also produced much more reasonable relationships between the dielectric constant and density, it was concluded that our liquid displacement measurements were less accurate, so all the density data presented were determined from mass and dimensional measurements.

4. Measurement Procedure

The following procedure was used to obtain the dielectric properties of individual specimens as functions of time after humidity change. Each specimen was stored in a chamber with the desired relative humidity until it reached equilibrium, i.e., until its dielectric properties no longer changed with time. A timed humidity run was then begun by transferring the specimen to another chamber at the new humidity. Periodic measurements were made with careful note being taken of the elapsed time since the humidity change. All timed humidity run data as well as frequency sweep data were taken at 23 °C.

It was observed for some of the electrodeless specimens that slightly different values of dielectric constant and dissipation factor were obtained when the specimen was turned over. The amount of this effect varied from specimen to specimen, and for some disks only the dielectric constant differed significantly. Differences as large as 0.2 percent in the dielectric constant were observed. This behavior was caused by the specimens being slightly curved instead of flat although they were of uniform thickness. In some cases it was possible to partially flatten out the warped specimens, and this reduced the difference. Whenever possible, the same face was kept turned up throughout the timed humidity runs; however, for some of the older data, taken before the effect was discovered, this was not done.

5. Results

5.1. Timed Humidity Runs

Figures 1 through 7 show timed humidity runs measured at 1000 Hz for certain specimens of the various

materials. For all of these figures, time from humidity change is plotted on the horizontal axis using a logarithmic scale, and those points marked with arrow heads on the left-hand margin of some of the plots indicate zero time starting values, which are measurements made at the storage humidity shortly before the beginning of the timed humidity run. Even though there are usually curves from only one or two specimens for a given material, the trends are generally representative for several of our specimens. All the dielectric properties given here were measured using the air-gap technique except when contact electrodes are indicated.

Figure 1 shows a plot for a T–16 specimen going from < 1.5 percent rh to 52 percent rh after being exposed to the low humidity for 455 days. This material does not show long term stability as indicated by the negative slope of the curves after about 100 days. We suggest that this aging process may be due to very slow crystallization of this material. We offer this as a possible explanation, even though the specimens were kept well below the glass transition temperature, because the material was not completely amorphous and the trend is indeed in the direction of higher crystallinity. Other specimens of this material in both humidities also showed this downward trend with time.

Figure 2 is a plot for two contact electrode specimens of polystyrene going from 52 percent rh to < 1.5 percent rh. The specimen for curve A had been in 52 percent rh for 1600 days, and the specimen for curve B had been in 52 percent rh for 74 days.

In figure 3 are curves for two specimens of polycarbonate. The specimen producing curve A was in 52 percent rh for 992 days before the humidity change and likewise the specimen for curve B was in < 1.5 percent rh for 1096 days before the change. These curves show the reversibility of the process, but the long time data seem to indicate an aging process again. Figure 4 shows curves for a polycarbonate specimen differently prepared by the manufacturer; this specimen had been in 52 percent rh for 174 days. Aside from

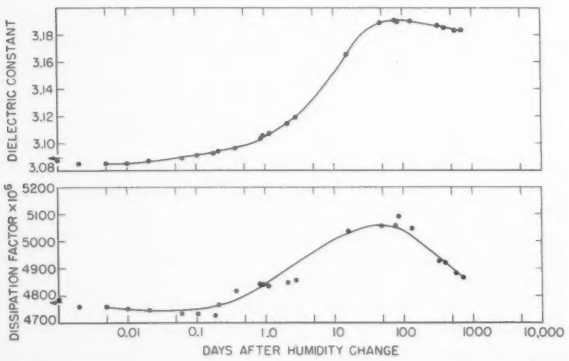

FIGURE 1. *Timed humidity run for a specimen of T–16 going from < 1.5 percent rh to 52 percent rh.*

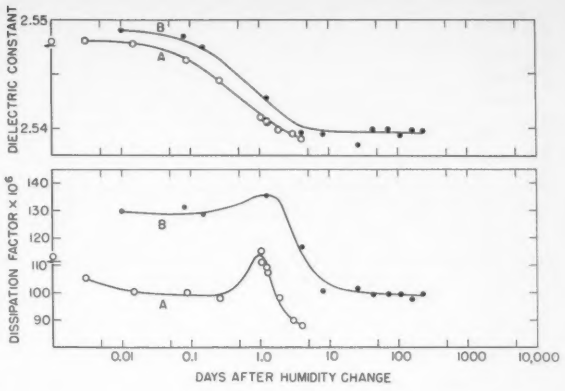

FIGURE 2. *Timed humidity runs for two contact electrode specimens of PS going from 52 percent rh to < 1.5 percent rh.*

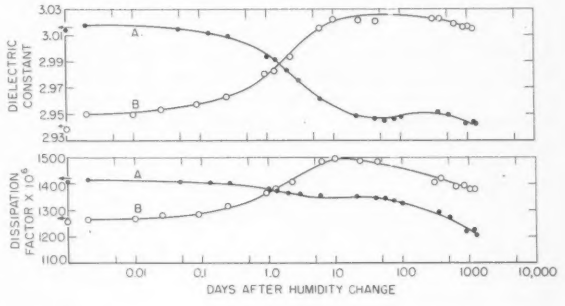

FIGURE 3. *Timed humidity runs for two specimens of PC.* Specimen A going from 52 percent rh to < 1.5 percent rh, and specimen B going from < 1.5 percent rh to 52 percent rh.

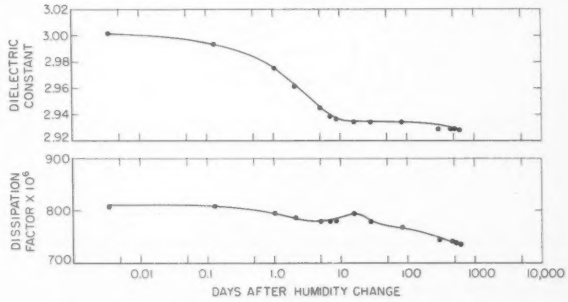

FIGURE 4. *Timed humidity run for a specimen of differently prepared PC going from 52 percent rh to* < 1.5 percent rh.

a lower dielectric constant and dissipation factor, the behavior indicated is about the same.

The data in figure 5 are for a specimen of FEP which was in < 1.5 percent rh for 448 days before the change; these curves show a slight upward trend going from < 1.5 percent rh to 52 percent rh. However, within the

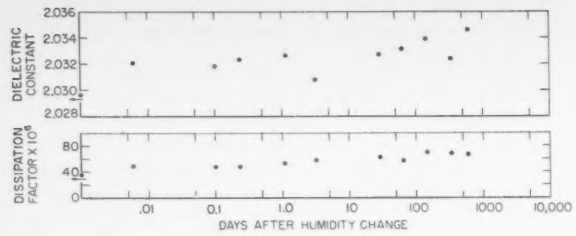

FIGURE 5. *Timed humidity run for a specimen of FEP going from < 1.5 percent rh to 52 percent rh.*

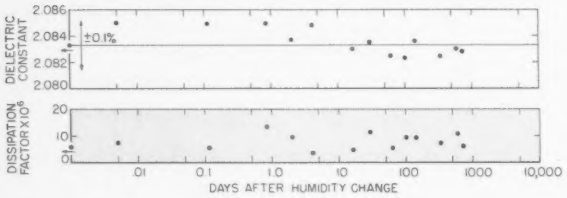

FIGURE 6. *Timed humidity run for a specimen of PTFE going from < 1.5 percent rh to 52 percent rh.*

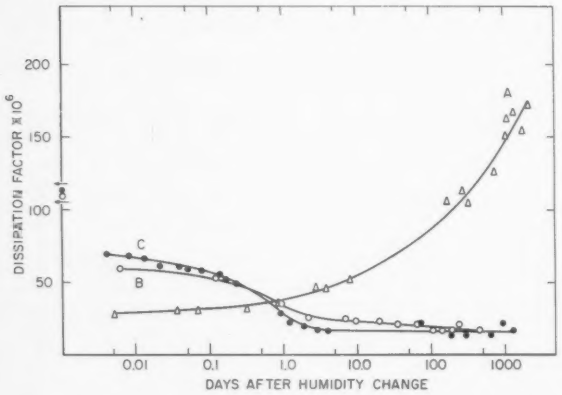

FIGURE 7. *Timed humidity runs for three specimens of PE.*
Specimen A going from < 1.5 percent rh to 52 percent rh, and specimens B and C going from 52 percent rh to < 1.5 percent rh.

limit of our estimated accuracy, no change is indicated by the curves for the PTFE specimen in figure 6. This specimen was in < 1.5 percent rh for 453 days before the change to 52 percent rh. In fact, no change was observed for any specimen of PTFE.

Figure 7 contains curves for specimens of polyethylene. Curve A shows the very slow rise in dissipation factor going from < 1.5 percent rh to 52 percent rh for a contact electrode specimen which had been in < 1.5 percent rh for 199 days. No change in dielectric constant has been observed for any polyethylene specimen. The specimen producing curve B was in 52 percent rh for 700 days before the change while the

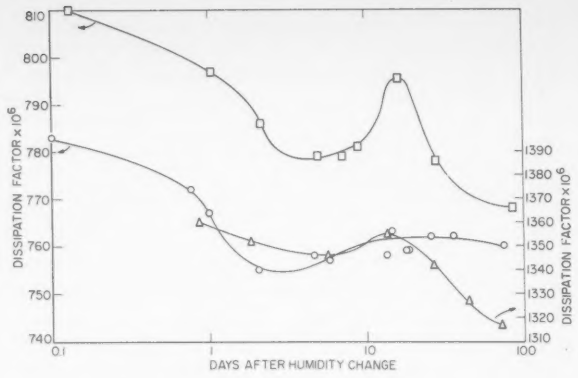

FIGURE 8. *An expansion of timed humidity runs for three specimens of PC going from 52 percent rh to < 1.5 percent rh.*

contact electrode specimen associated with the curve C was in 52 percent rh for 123 days. Taken together these data would seem to indicate that, even though water is sorbed into polyethylene slowly, some of the water is released very quickly.

In figure 2 there are peaks in the PS dissipation factor curves after one day. Figure 8 shows similar peaks for three specimens of PC on an expanded time scale, but for this material the peak is in the region of 10 to 30 days. This strange behavior was observed only on PS and PC specimens. Moreover, it has been observed for specimens measured with contact electrodes as well as with the air-gap method. No explanation has been found for this unusual data.

5.2. Frequency Sweeps

Figure 9 contains the dielectric constant and dissipation factor plotted against frequency for a contact electrode specimen of PC; these data were measured at < 1.5 percent rh equilibrium. Figure 10 likewise shows the dissipation factor and dielectric constant for contact electrode specimens of PS at both < 1.5 percent rh and 52 percent rh equilibrium. Figure 11 contains similar plots for two T–16 specimens.

From the other materials – PE, PTFE, and FEP – no specimens showed a significant change in dielectric constant over our frequency range. Dissipation factor data for FEP specimens at both the low and high humidity appear in curves A and B in figure 12. The dissipation factors for PE specimens at < 1.5 percent rh measured less than the limit of our accuracy so were not plotted, but 52 percent rh data appear as curve C in figure 12.

Results differed slightly from specimen to specimen for most measurements; this was especially true at 52 percent rh. We were ultimately concerned more with the careful recording of the behavior of a particular specimen or group of specimens than with the general material, so none of the data presented here should be taken to represent the whole material in a detailed way.

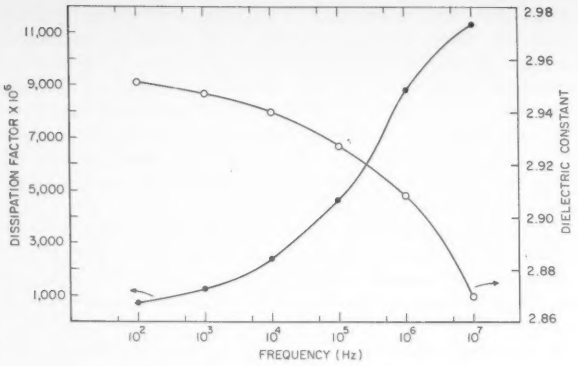

FIGURE 9. *Dielectric constant and dissipation factor versus frequency for a contact electrode specimen of PC at < 1.5 percent rh equilibrium.*

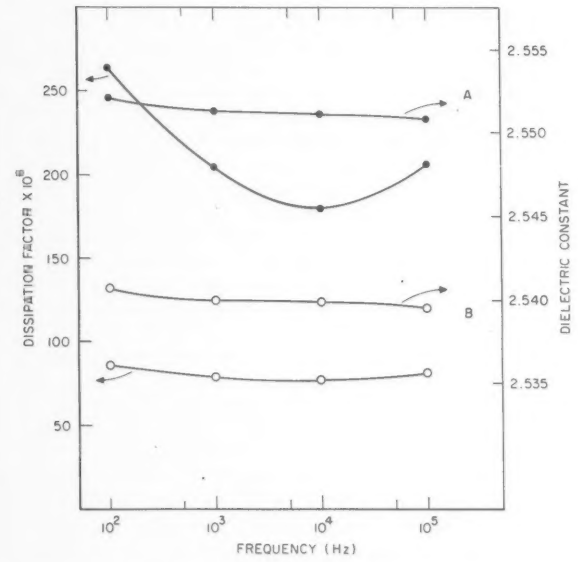

FIGURE 10. *Dielectric constant and dissipation factor versus frequency for two contact electrode specimens of PS.*

Specimen A is in 52 percent rh equilibrium and specimen B is in < 1.5 percent rh equilibrium.

5.3. Density and Water Absorption

A linear relationship between the dielectric constant and density is a good approximation over a restricted density range for polyethylene. The common form for this relation is the Clausius-Mossotti equation,

$$\frac{\epsilon'-1}{\epsilon'+2}=K\rho,$$

where ρ is the density, ϵ' is the dielectric constant, and K is a constant for the material which depends on the molecular weight and the total polarizability per mole-

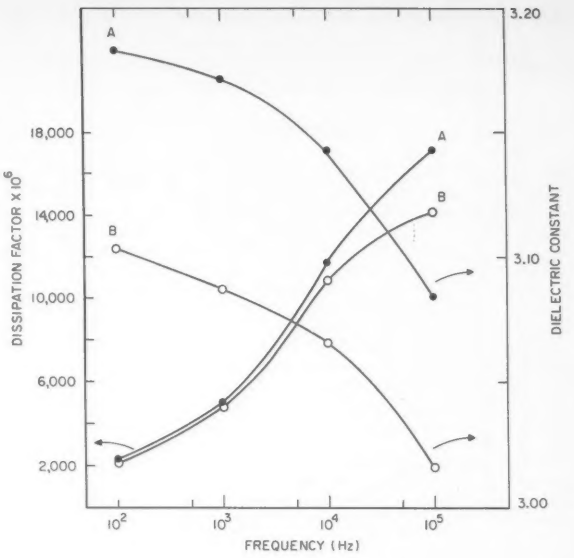

FIGURE 11. *Dielectric constant and dissipation factor versus frequency for two specimens of T–16.*

Specimen A is in 52 percent rh equilibrium and specimen B is in < 1.5 percent rh equilibrium.

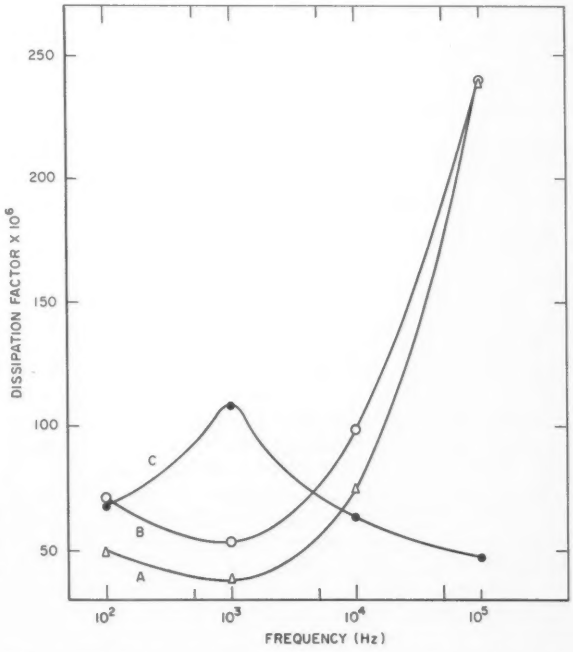

FIGURE 12. *Dissipation factor versus frequency for specimens of FEP and PE.*

Specimen A is FEP at < 1.5 percent rh equilibrium; specimen B is FEP at 52 percent rh equilibrium; and specimen C is PE at 52 percent rh equilibrium.

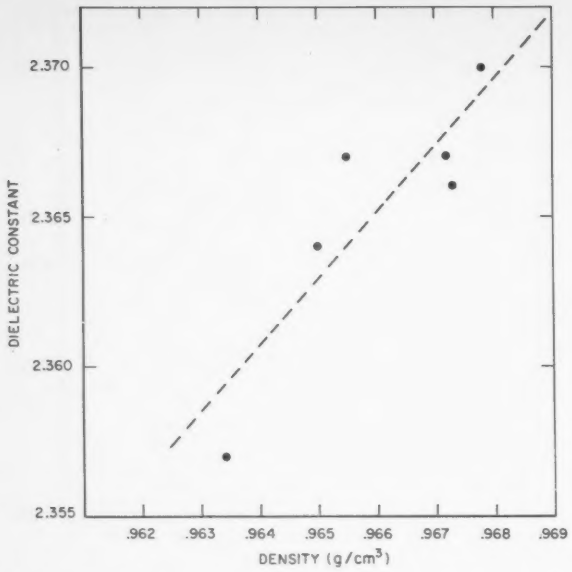

FIGURE 13. *Dielectric constant versus density for specimens of polyethylene.*

cule. The dielectric constant of six PE specimens is plotted versus density in figure 13. A straight line was fitted to the data by a method, useful when the errors in the variables are unknown, as given by Bartlett [8], and this line is also shown. These differences in density were probably caused by the slightly different thermal and mechanical treatment received during molding and machining.

Some effort was made to determine the amount of water absorbed by certain specimens by taking the difference between the equilibrium weight at < 1.5 percent rh and weight at room humidity which was generally 20 percent rh to 40 percent rh and never above 50 percent rh. A difference in weight of 0.03 percent was obtained from the average change of two PS specimens. This roughly agrees with the value observed by von Hippel and Wesson [9] of 0.048 percent for 60 percent rh at 25 °C. Likewise, for PC we observed a 0.13 percent change in weight which compares with the 0.15 percent observed by Thompson and Goldblum [10] for 50 percent rh. These can not be exact comparisons since the materials were, at best, only similar in composition, but they do show order of magnitude agreement. We were unable to detect a difference in weight for FEP, PTFE or PE even though the dissipation factor of PE showed a quite definite change going to 52 percent. The amount of water absorbed by PE has been shown to be quite small (on the order of 0.03 or 0.06 mg/cm³) [11, 12], and beyond the sensitivity of our weighing system.

6. Estimated Error Limits

From the use of this low-voltage conjugate Schering bridge over a long period of time, it is estimated that repeated measurements of capacitance over the frequency range 100 Hz to 100 kHz could be expected to agree to within ±0.001 pF for measured capacitances above 10 pF and 0.0001 pF for 10 pF and below. Based on this estimate and comparisons with the two-fluid technique as well as repeated determinations, we estimate our dielectric constant measurements using this bridge and the air-gap technique to be accurate within ±0.1 percent.

Previous papers by Scott and Harris [2, 13] discuss some of the important problems involved in the measurement of small dissipation factors. Significant errors can arise if both the high and low sides of the circuit have some finite common impedance to ground. In general, this is the case with a three-terminal cell or capacitor. It is possible, in principle, to completely analyze the circuits involved for a given cell and bridge to allow the most accurate dissipation factor determination; however, that study has not yet been completed for our equipment. Heating by the measuring field can also be a problem with higher loss specimens, since the properties may change rapidly with temperature and frequency, so we have included large percentage limits with the estimated accuracies for the dissipation factor.

From the use of this Schering bridge over a long period of time, in the same manner as capacitance, it is estimated that repeated measurements of the dissipation factor of a stable specimen could be expected to agree within 2×10^{-6}, and based on this and comparisons with carefully constructed low loss capacitors, we estimate the absolute and relative dissipation factor measurements using this bridge to be accurate within the greater of the two limits given in their respective columns in table 1.

The dissipation factor measurements made using the *Q*-meter with an extra-high-*Q* coil at 1 MHz are estimated to be accurate within ±0.0002. At 10 MHz, this accuracy was reduced somewhat due to the uncertainty of corrections for lead inductance. The dielectric constant measurements made with this *Q*-meter are believed to be accurate within ±0.2 percent. These estimates were derived from measurements made on specimens whose properties at 1 MHz and 10 MHz were believed to be essentially the same as at lower frequencies, where they could be determined more accurately.

TABLE 1. *Estimated error limits for absolute and relative dissipation factor measurements made with the low-voltage conjugate Schering bridge are given by greater of the two values*

Frequency	Absolute error limits	Relative error limits
10^2	$\pm30\times10^{-6}$ or ±2%	$\pm20\times10^{-6}$ or ±2%
10^3	$\pm20\times10^{-6}$ or ±1%	$\pm10\times10^{-6}$ or ±1%
10^4	$\pm20\times10^{-6}$ or ±1%	$\pm10\times10^{-6}$ or ±1%
10^5	$\pm40\times10^{-6}$ or ±3%	$\pm30\times10^{-6}$ or ±3%

7. Discussion

The PC and T–16 timed humidity runs show large rapid changes as well as the long term drift. If these

materials were to be used for making dielectric reference specimens, it would be necessary to carefully control the humidity, and obviously their usefulness would be limited at best. The PC data does give a clear indication of the reversibility of this process for the same or a similar specimen, and therefore, if a copy of the timed humidity run were sent along with a specimen, a somewhat more accurate characterization could be obtained under a large variety of conditions.

For the PS specimens, the change was not nearly so great; however, it would still be necessary to take the humidity into account to obtain an accuracy better than about 1 percent for dielectric constant and about 1×10^{-4} for dissipation factor.

The PE data show a very rapid initial change in the dissipation factor when the relative humidity is changed from 52 percent rh to < 1.5 percent rh, but quite a slow drift upward on the return to 52 percent rh. This behavior coupled with the lack of a change in the dielectric constant means that it would be possible to predict a specimen's properties quite well if it were stored in low humidity before and after a measurement even if the measurement were made at a higher humidity.

PTFE, and FEP to possibly a slightly less degree, are materials well suited for dielectric reference specimen preparation. Although the FEP dielectric constant and dissipation factor data seem to show an upward trend going from < 1.5 percent rh to 52 percent rh, lines fitted by the least squares method versus the logarithm of time after humidity change do not have slopes statistically different from zero. For PTFE, no change in dielectric constant or dissipation factor is indicated within our error limits for the 100 Hz to 10 MHz frequency range or for a change in humidity.

The authors thank the following manufacturers for their assistance by supplying the materials used in this study. Allied Chemical Corp., Dow Chemical Co., E. I. du Pont de Nemours and Co., General Electric Co., Phillips Chemical Co., and Tennessee Eastman Co.

We also thank M. G. Broadhurst and W. P. Harris for their very valuable assistance and advice.

8. References

[1] A. H. Scott and W. P. Harris, Residual losses in a guard-ring micrometer-electrode holder for solid-disk dielectric specimens, J. Res. NBS **65C** (Phys. and Chem.) No. 2, 101 (1961).

[2] A. H. Scott and W. P. Harris, Long-time effects of humidity changes on the dielectric properties of certain polymers, 1962 Annual Report, Conference on Electrical Insulation, Nat. Acad. Sci.—Nat. Research Council, Publ. **1080,** p. 41.

[3] J. I. Lauritzen, Jr., The effective area of a guarded electrode, 1963 Annual Report, Conference on Electrical Insulation, Nat. Acad. Sci.—Nat. Research Council, Publ. **1141,** p. 67.

[4] W. P. Harris, Precise determination of the area of guarded electrodes for accurate dielectric measurements on solid disk specimens, 1963 Annual Report, Conference on Electrical Insulation, Nat. Acad. Sci.—Nat. Research Council, Publ. **1141,** p. 71.

[5] A. H. Scott, Techniques for using the air-gap method for the precise determination of the dielectric constant and loss angle of solid disk specimens, 1963 Annual Report, Conference on Electrical Insulation, Nat. Acad. Sci.—Nat. Research Council, Publ. **1141,** p. 74.

[6] H. F. Schiefer, L. E. Crean, and J. F. Krasny, J. Res. NBS **42,** 481 (1949), RP1988.

[7] W. P. Harris and A. H. Scott, Precise measurement of dielectric constant by the two-fluid technique, 1962 Annual Report, Conference on Electrical Insulation, Nat. Acad. Sci.—Nat. Research Council, Publ. **1080,** p.51.

[8] M. S. Bartlett, Fitting a straight line when both variables are subject to error, Biometrics **5** (Sept. 1949), No. 3, p. 207.

[9] A. von Hippel and L. G. Wesson, Polystyrene plastics as high frequency dielectrics, Industrial and Engineering Chemistry **38,** No. 11, p. 1121 (1946).

[10] R. J. Thompson and K. R. Goldblum, Polycarbonate resin, Modern Plastics **35** (April 1958), p. 131.

[11] C. H. Klute, Diffusion of small molecules in semicrystalline polymers: water in polyethylene, J. of Applied Polymer Science **1,** No. 3, p. 340 (1959).

[12] D. W. McCall, J. F. Ambrose, and V. L. Lanza, J. of Polymer Science **26,** 165 (1957).

[13] W. P. Harris, Apparent negative impedances and their effect on three-terminal dielectric loss measurements, 1965 Annual Report, Conference on Electrical Insulation, Nat. Acad. Sci.—Nat. Research Council, Publ. **1356,** p. 83.

(Paper 71C2–251)

JOURNAL OF RESEARCH of the National Bureau of Standards—C. Engineering and Instrumentation
Vol. 71C, No. 2, April–June 1967

The Sensitivity of the Dicke Radiometer*

David F. Wait**

Institute for Basic Standards, National Bureau of Standards, Boulder, Colo. 80302

(January 25, 1967)

The literature is reviewed concerning the sensitivity of the Dicke radiometer, excluding gain fluctuations. Discrepancies are pointed out and a new derivation of sensitivity using a Fourier transform method is used to resolve these discrepancies and to extend the results to radiometers with lossy switches.

Experimentally it is shown that radiometers using a half-wave square-law, linear-law, intermediate-law, or envelope detectors all have a sensitivity equal to the theoretical full-wave square-law detector (within the ±20 percent uncertainty of the experiment).

Key Words: Dicke, microwave, radiometer, sensitivity, switching.

1. Introduction

At the National Bureau of Standards a switching radiometer is used to compare microwave noise sources with a standard hot load [1],[1] and a sum-and-difference-correlation radiometer is being developed to compare microwave cryogenic noise sources which uses a switching radiometer as a component [2].

Although there is extensive literature discussing the Dicke radiometer, existing publications are difficult to use. This is partly due to a series of errors and corrections and partly due to divergent assumptions, notation, and forms. The literature as a whole has unresolved differences between various statements of the sensitivity for the Dicke radiometer.

The purpose of this paper is to review the literature (sec. 2), derive the sensitivity of the Dicke radiometer in a form which includes switch noise (sec. 3), and to compare the derived sensitivity with experiment (sec. 4). The sensitivity is rederived, rather than making a further correction, for two reasons. First, a statement of sensitivity is needed in a form general enough to include the prior literature. This facilitates identifying discrepancies. Second, a basically different derivation helps to avoid prior errors and to increase confidence where agreements are obtained.

2. Review of the Literature

To facilitate comparison between the various authors in the literature, a brief discussion of a model switching radiometer is presented. The literature is compared in terms of this model. The symbols of this paper may be converted to the notation of the other authors by means of appendix A. Also contained in appendix A are equivalent statements of predetector bandwidth B, and postdetector integration constant τ.

*Sponsored by Advanced Research Projects Agency, Project DEFENDER; ARPA Order No. 515.

**Microwave Circuit Standards, National Bureau of Standards Laboratories, Boulder, Colo. 80302.

[1] Figures in brackets indicate the literature references at the end of this paper.

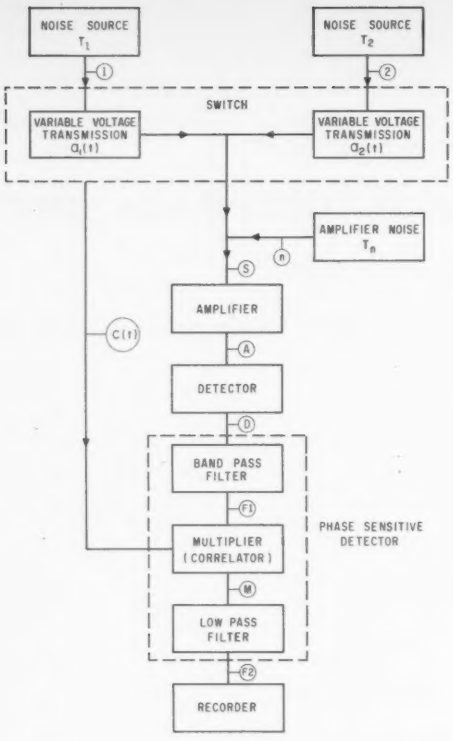

FIGURE 1. *Dicke radiometer.*

2.1. Basic Switching Radiometer

The basic switching radiometer is shown in figure 1. Essentially the power from a noise source at the effective temperature T_1 is compared with a noise source at effective temperature T_2. It is usually advantageous to operate the radiometer with a known and variable T_2 which is made equal to T_1. The comparison of T_1 to T_2 is effected by switching the input of a receiver from T_1 to T_2 and examining the output of the receiver for a signal correlated with the switching frequency. Uncorrelated terms (for example, the internal noise of the receiver) do not contribute to the dc output of the correlator.

The noise voltage $y_1(t)$ from the noise source at temperature T_1 is connected to the receiver through a variable coupler of voltage transmission coefficient $a_1(t)$. Similarly $y_2(t)$ from noise source T_2 is fed through a variable coupler with voltage transmission coefficient $a_2(t)$. The internal noise of the amplifier referred to the input of the amplifier has effective temperature T_n. The signal $y_s(t)$, the input to an ideal noiseless amplifier, is

$$y_s(t)=a_1(t)y_1(t)+a_2(t)y_2(t)+y_n(t), \tag{1}$$

where $y_n(t)$ is the voltage needed to represent the amplifier noise. Ideally the transmission coefficients $a_1(t)$ and $a_2(t)$ vary from zero to one periodically with period ν_0^{-1}. Typically $a_1(t)$ and $a_2(t)$ are 180° out of phase. The transmission coefficient $a_1(t)$ is referred to as the *voltage modulation*. The power transmission coefficient $p(t) \equiv a^2(t)$ is referred to as the *power modulation*. From the modulation $a_1(t)$ is generated a periodic reference signal $c(t)$ which then goes to the multiplier. The reference signal $c(t)$ is referred to as the *correlation* and usually is sinusoidal or square wave.

2.2. General Comments

Eleven papers (as noted in table 1) are here reviewed which contain statements concerning the sensitivity of a Dicke radiometer. There is an underlying agreement among eight of these and the remaining three retain many of the essential features. In order to recognize this agreement, various definitions must be related (see appendix A) and account taken of the modulation and correlation assumed.

There is an important difference among the various agreeing papers. The nature of this difference is essential to the general understanding of the literature, so it will be discussed before commenting on individual papers.

The radiometer described by Dicke [3] modulates the noise source by means of a variable attenuator which has nearly the same temperature as the noise source of interest. The papers of Goldstein [4, 5], Strom [6, 7], Strum [8], Knight [9], and Johnson [10], collectively referred to as GSSKJ, calculate the sensitivity of a somewhat different radiometer. The GSSKJ version of the Dicke radiometer modulates the noise source of interest by an ideal noiseless device, which could be a variable attenuator at the absolute zero of temperature. This corresponds to $T_2 \equiv 0$ °K in the model introduced in section 2.1. The Dicke radiometer was originally a null device but this concept was extended by Goldstein to include an off-null operation. This introduces many practical differences. For example, a radiometer operated off-null is not immune from receiver gain instabilities. The radiometer described by GSSKJ is a special case of the papers of Kelly, Lyons and Root [11, 12], Colvin [13], and Tiuri [14] collectively referred to as KLRCT. However, GSSKJ and KLRCT differ in detail. For example, GSSKJ's results indicate somewhat greater fluctuations in the radiometer output due to the input noise source (T_1) than the corresponding KLRCT results.

The origin of the discrepancy lies in the different technique of obtaining the output of the square law detector relative to the input. GSSKJ use an autocorrelation method and handle the resulting squared terms by means of a theorem usually attributed to Rice [15]. Rice's theorem for square law devices is rigorous for stationary Gaussian processes. KLRCT essentially apply Rice's theorem directly, neglecting the usually small nonstationary aspect of the signal at the detector input. The errors introduced by this simplifying assumption go to zero as the noise sources being compared approach the same temperature ($T_1 = T_2$), and the receiver is switched between the two sources in such a way that the power to the receiver is constant throughout the switching cycle.

The calculations in this paper are as precise as the GSSKJ calculations. Thus detailed agreement with KLRCT is expected only when $T_1 = T_2$.

In the last column of table 1, which appears later in this paper, prior calculations of the radiometer sensitivity are indicated by modulation and correlation type. Those calculations which differ with this paper are marked with an asterisk. Although Goldstein [4, 5], Strum [8], and Knight [9] are marked with an asterisk, they are considered to be in the group of eight having underlying agreement. More will be said of this in the detailed comments which follow.

2.3. Specific Comments

In 1946, Dicke [3] suggested modulating a noise signal under study as a means of distinguishing the signal of interest from the noise originating in the amplifying system and also to reduce the fluctuations in the radiometer output due to receiver gain instabilities. He derived the sensitivity of a radiometer using a statistical approach for square-wave modulation and sinusoidal correlation. In the analysis Dicke assumed that the detector was square-law, then he generalized to the linear detector. Selove [16] corrects an error in the generalization to the linear detector and Strom [6, pp 37 and 68] challenges an overall factor. For a square-wave modulation and sinusoidal correlation, Dicke obtained a sensitivity which is a factor of 2 greater than the result to be obtained in this paper and thus comparable with the accepted sensitivity of an ideal (no gain fluctuations) total power radiometer [11, 12, 13, or 14]. Because the switching radiometer cannot have comparable sensitivity, Dicke's result must be in error.

In 1955, Goldstein [4] analyzed the switching radiometer using sinusoidal-voltage modulation (or switching), sinusoidal correlation and square-law detection making use of the autocorrelation function and assuming the noise signal had a Gaussian distribution. However, as noted above, he assumed a noiseless modulator which corresponds to assuming $T_2 \equiv 0$ °K. Goldstein's result as corrected by himself [5] and Johnson [10] agrees with a special case of the analysis to be presented.

Also in 1955 Bunkin and Karlov [17] analyzed the switching radiometer using the autocorrelation method. Their analysis assumes a Gaussian noise distribution, square-wave modulation and sinusoidal correlation. In addition, the effects of amplifier gain fluctuations are considered. This paper depends to some extent on other papers in the Russian literature which are not readily available. It was not established for certain if the paper agrees in all details, but no obvious discrepancies occur.

Strom [6, 7] shows that the sensitivity of the switching radiometer is unaltered if a biased diode is used as the detector instead of a square-law detector. He obtains a sensitivity that is less by a factor $\sqrt{2}$ than the expected value because the out-of-phase rejection of noise by the correlator was not taken into account.

Strum [8] discusses the effect of fluctuations in various components of a radiometer system and discusses various types of linear detectors. He comments on the use of an IF amplifier in an analysis. Strum defines a generalized bandwidth which reduces to the usual one for rectangular bandpass but is not equivalent in general to that used by Dicke; Kelly, Lyons, and Root; Ward and Richardson; Tiuri; and in this paper.

Kelly, Lyons, and Root [11, 12] analyzed a general comparison radiometer (T_1 and T_2 arbitrary) for arbitrary modulation and correlation. They treated gain fluctuations and optimized the modulation wave form depending on the rms amplitude of the gain fluctuations. They also presented a proof that a square-law detector is superior to any other detector law for Gaussian noise (ignoring gain fluctuation of the amplifier). Except for the differences off-null already noted, there is no disagreement with this paper.

Colvin [13] discusses the switching radiometer under rather general conditions as part of an extensive survey of various radiometers. Again, except for the off-null differences discussed, there is no disagreement with this paper.

Knight [9] considers a radiometer with asymmetrical rectangular modulation and correlation. The calculation is of the Goldstein type. In his paper, eqs (3) and (4) lack the factor 2π on the right-hand side which occurred in his prior equations. Knight's corrected equations are a special case of the analysis to be presented. However, his extension to the balanced radiometer operation did not take into account the fluctuation of the output due to the noise sources.

Ward and Richardson [18] consider a power sinusoidal modulated radiometer with IF amplifiers of different image and signal responses. The sensitivity obtained is that expected for a total power radiometer, and for the same reason as noted for Dicke's paper, this must be in error.

Johnson [10] corrected Goldstein's results and extended the calculation to include various combinations of sinusoidal and square-wave modulations and correlations. However, in Johnson's extension to square-wave modulation his (1/4) $\sigma_s^2\sigma_n^2$ term should be replaced by $\sigma_s^2\sigma_n^2$.[2]

Tiuri [14] states the radiometer sensitivity for several modulations and correlations. The results are the expected ones within the approximations already discussed.

3. Analysis

The sensitivity of the switching radiometer depicted in figure 1 is determined by calculating the ratio of the dc output of the radiometer $\overline{y_{F2}}$ and the rms fluctuations at the output, σ_{F2}. The time dependent noise voltages will be denoted by $y(t)$ with a subscript denoting the point in the circuit shown in the circles in figure 1. An IF amplifier is not used in figure 1 but is treated in appendix C.

[2] This has been acknowledged by Johnson in a private communication.

3.1. The Fourier Transform

The Fourier transform preserves required phase information. Because the transform of a random function does not converge, all the noise voltages $y(t)$ are defined to be zero except for $-T/2 < t < T/2$. The truncated function of $y(t)$ has identical properties with $y(t)$ in the limit $T \to \infty$. Thus by $y(t)$ it will be understood the truncated function of $y(t)$. The Fourier transform of $y(t)$ is denoted $Y(\nu)$, again with a subscript to denote point in the circuit.

The following form is used for the Fourier transform pair:

$$Y(\nu) = \int_{-\infty}^{\infty} e^{-j2\pi\nu t} y(t)\, dt, \tag{2}$$

$$y(t) = \int_{-\infty}^{\infty} e^{j2\pi\nu t} Y(\nu)\, d\nu. \tag{3}$$

The Fourier transform or inverse transform of a product (in either t or ν space) is the convolution of the transforms of the two factors (convolution theorem). With the choice in (2) and (3), the convolutions (denoted by ★) are defined by

$$y_x(t) \bigstar y_z(t) \equiv \int_{-\infty}^{\infty} y_x(t-t') y_z(t')\, dt', \tag{4}$$

and

$$Y_x(\nu) \bigstar Y_z(\nu) \equiv \int_{-\infty}^{\infty} Y_x(\nu-\nu') Y_z(\nu')\, d\nu'. \tag{5}$$

3.2. The Power Spectral Density and the Wiener-Khintchine Theorem

The power spectral density $W(\nu)$ is related to the Fourier transform of $y(t)$ in the following manner [19],

$$W(\nu) = \operatorname*{Lim}_{T\to\infty} \frac{Y(\nu) Y^*(\nu)}{T}, \tag{6}$$

where the asterisk denotes the complex conjugate. It can be shown that $W(\nu)\, d\nu$ is the power dissipated in a 2-Ω resistor due to the spectral components between ν and $\nu + d\nu$ in the voltage $y(t)$.

The Wiener-Khintchine Theorem is stated [20]

$$W(\nu) = \int_{-\infty}^{\infty} R(t) e^{-j2\pi\nu t}\, dt, \tag{7}$$

so that

$$R(t) = \int_{-\infty}^{\infty} W(\nu) e^{j2\pi\nu t}\, d\nu, \tag{8}$$

where $R(t)$ is the autocorrelation function defined by

$$R(t) \equiv \operatorname*{Lim}_{T\to\infty} \frac{1}{T} \int_{-T/2}^{T/2} y(t') y(t'+t)\, dt'. \tag{9}$$

Using (8) and (9) for $t = 0$,

$$\overline{y^2(t)} = \int_{-\infty}^{\infty} W(\nu)\, d\nu, \tag{10}$$

where the bar indicates the time average in the interval $-T/2$ to $+T/2$.

The analysis is ultimately stated in terms of measurable properties of the input noise signals [21, 22]:

$$W_1(\nu)=\frac{1}{2}kT_1,$$

$$W_2(\nu)=\frac{1}{2}kT_2, \tag{11}$$

$$W_n(\nu)=\frac{1}{2}kT_n,$$

where $k=1.3805\times10^{-23}$ J °K^{-1} is the Boltzmann constant. The factor 1/2 in (11) occurs because the power spectral density is defined for both positive and negative frequencies.

3.3. The Switch

A model for the switch discussed in section 2.1 led to eq (1). For this analysis a more general $y_s(t)$ composed of an arbitrary number of periodically modulated noise signals will be used. The voltage modulation of the ith signal $[a_i(t)]$ is analyzed into its Fourier components:

$$a_i(t)=\sum_m A_{j,\,m}e^{jm2\pi\nu_0 t}, \tag{12}$$

where m takes all integer values between $-\infty$ and $+\infty$. Similarly the correlation signal is decomposed:

$$c(t)=\sum_m C_m e^{jm2\pi\nu_0 t}. \tag{13}$$

The following associated transmission coefficients are also required:

$$p_i(t)\equiv a_i^2(t), \tag{14}$$

$$q_i(t)\equiv p_i^2(t)=a_i^4(t), \tag{15}$$

$$u_{ij}(t)\equiv a_i(t)a_j(t), \tag{16}$$

$$v_{ij}(t)\equiv a_i^2(t)a_j^2(t), \tag{17}$$

which are decomposed into

$$p_i(t)=\sum_m P_{i,\,m}e^{jm2\pi\nu_0 t}, \tag{18}$$

$$q_i(t)=\sum_m Q_{i,\,m}e^{jm2\pi\nu_0 t}, \tag{19}$$

$$u_{ij}(t)=\sum_m U_{ij,\,m}e^{jm2\pi\nu_0 t}, \tag{20}$$

and

$$v_{ij}(t)=\sum_m V_{ij,\,m}e^{jm2\pi\nu_0 t}. \tag{21}$$

3.4. The $y(t)$, $Y(\nu)$, $W(\nu)$ Description

Each element of the radiometer depicted in figure 1 is described by the modification to $y(t)$ before and after the element. Thus,

$$y_S(t)=\sum_i a_i(t)y_i(t) \tag{22}$$

$$y_A(t)= h_A(t)\bigstar y_s(t), \tag{23}$$

$$y_D(t)=y_A^2(t), \tag{24}$$

$$y_{F1}(t)=h_{F1}(t)\bigstar y_D(t), \tag{25}$$

$$y_M(t)=c(t)y_{F1}(t), \tag{26}$$

$$y_{F2}(t)=h_{F2}(t)\bigstar y_M(t), \tag{27}$$

where $h_A(t)$, $h_{F1}(t)$, $h_{F2}(t)$ are the impulse response functions [20] of the amplifier, bandpass filter and low pass filter, respectively, and $c(t)$ is defined in (13).

Taking the Fourier transforms of (22) to (27) and using (12),

$$Y_S(\nu)=\sum_{i,\,m} A_{i,\,-m}Y_i(\nu+m\nu_0), \tag{28}$$

$$Y_A(\nu)=H_A(\nu)Y_S(\nu), \tag{29}$$

$$Y_D(\nu)=Y_A(\nu)\bigstar Y_A(\nu), \tag{30}$$

$$Y_{F1}(\nu)=H_{F1}(\nu)Y_D(\nu), \tag{31}$$

$$Y_M(\nu)=\sum_{m=-\infty}^{\infty} C_{-m}Y_{F1}(\nu+m\nu_0), \tag{32}$$

$$Y_{F2}(\nu)=H_{F2}(\nu)Y_M(\nu). \tag{33}$$

The Fourier transform of the impulse response function is known as the system function, or transfer function, denoted $H(\nu)$,

$$H(\nu)\equiv\int_{-\infty}^{\infty} e^{-j2\pi\nu t}h(t)dt, \tag{34}$$

and will be used to define the power response function $G(\nu)$,

$$G(\nu)\equiv H(\nu)H^*(\nu). \tag{35}$$

247-602 O-67—4

The power spectral density is obtained from (28) to (33) by means of (6) and (B–1) of appendix B. This results in

$$W_S(\nu)=\sum_{i,m} A_{i,\frac{1}{i}m}A^*_{i,-m}W_i(\nu+m\nu_0), \tag{36}$$

$$W_A(\nu)=G_A(\nu)W_S(\nu), \tag{37}$$

$$W_D(\nu)=\operatorname*{Lim}_{T\to\infty} T^{-1}Y_D(\nu)Y^*_D(\nu), \tag{38}$$

$$W_{F1}(\nu)=G_{F1}(\nu)W_D(\nu), \tag{39}$$

$$W_M(\nu)=\sum_{m=-\infty}^{\infty} C_{-m}C^*_{-m}W_{F1}(\nu+m\nu_0), \tag{40}$$

$$W_{F2}(\nu)=G_{F2}(\nu)W_M(\nu), \tag{41}$$

where $G_A(\nu)$ (see eq 35) is the power response of the amplifier, etc. The spectral density of $W_D(\nu)$ will not be deduced from $W_A(\nu)$ due to the complication arising from $W_A(\nu)$ being nonstationary.

3.5. Calculation of $\overline{y_{F2}}$

The calculation of $\overline{y_{F2}}$ (d-c output of the radiometer) is based on the following relationship (see appendix B):

$$\overline{y_{F2}}=\operatorname*{Lim}_{T\to\infty}\frac{Y_{F2}(0)}{T}. \tag{42}$$

Using (31) to (33),

$$Y_{F2}(0)=H_{F2}(0)\sum_{m=-\infty}^{\infty} C_{-m}H_{F1}(m\nu_0)Y_D(m\nu_0). \tag{43}$$

The task now is to obtain $Y_D(m\nu_0)$ in terms of the known power spectral densities of (11). The approach is to cast $Y_D(m\nu_0)$ in a form to utilize the relationship (see appendix B)

$$\operatorname*{Lim}_{T\to\infty}\frac{Y_{xx}(0)}{T}=K_x, \tag{44}$$

where

$$K_x\equiv\int_{-\infty}^{\infty} W_x(\nu)d\nu, \tag{45}$$

and $Y_{xx}(0)$ is the Fourier transform of $y_x^2(t)$ for $\nu=0$, where $y_x(t)$ is a noise function with zero mean.

If we assume a flat amplifier response so that $H_A(\nu+m\nu_0)\simeq H_A(\nu)$, then (29) may be written,

$$Y_A(\nu)\simeq\sum_{i,p} A_{i,-p}Y_{i\bigstar A}(\nu+p\nu_0), \tag{46}$$

where $Y_{1\bigstar A}(\nu)$ is the Fourier transform of $h_A(t)\bigstar y_1(t)$, etc. The approximation for the transfer function of the amplifier, $H_A(\nu)$ might seem unrealistic for large p, but generally $A_{i,p}$ decreases rapidly with increasing $|p|$.

Substituting (46) into (30) will give terms of the form

$$Y_x(\nu+p\nu_0)\bigstar Y_z(\nu+q\nu_0)=Y_{xz}(\nu+p\nu_0+q\nu_0), \tag{47}$$

where $Y_{xz}(\nu)$ is the Fourier transform of $y_x(t)y_z(t)$, x, z are any of the subscripts $1\bigstar A$, $2\bigstar A$ or $n\bigstar A$. Equation (47) is valid even when $x=z$. For a proof of (47) see appendix B.

We are now in a position to use (44) to facilitate the evaluation of (30). Because $Y_{xz}(\nu+p\nu_0+q\nu_0)$ gives no contribution except for $x=z$ and $\nu+p\nu_0+q\nu_0=0$ (see appendix B), then by retaining only nonzero terms and excluding $m=0$ (because $A_{i,0}=0$),

$$\lim_{T\to\infty}\frac{Y_D(m\nu_0)}{T}=\sum_{i,q}A_{i,q}A_{i,-q-m}K_{i\bigstar A}, \tag{48}$$

where from (6), (11), and (45), for $i=1$ or 2,

$$K_{i\bigstar A}=\frac{1}{2}kT_i\int_{-\infty}^{\infty}G_A(\nu)d\nu. \tag{49}$$

Thus, for the usual case that $C_0=0$, (42), (43), (48) and (49) combine to give,

$$\overline{y_{F2}}=\lambda B^{1/2}\left\{\sum_{i,m}C_mH_{F1}(m\nu_0)P_{i,-m}T_i\right\}, \tag{50}$$

where

$$\lambda=\frac{1}{2}\,k\mathrm{H}_{F2}(0)\,[2G_A(0)\bigstar G_A(0)\,]^{1/2}, \tag{51}$$

and

$$B\equiv\frac{\left[\int_{-\infty}^{\infty}G_A(\nu)d\nu\right]^2}{2G_A(0)\bigstar G_A(0)}, \tag{52}$$

or using appendix A,

$$B=\frac{\int_{-\infty}^{\infty}G_A(\nu)\bigstar G_A(\nu)d\nu}{2G_A(0)\bigstar G_A(0)}, \tag{53}$$

and $P_{i,m}$ defined in (18) is introduced by means of (B–7) of appendix B. The term B is the convolution bandwidth of the amplifier. For a rectangular power response, B is the width of the nonzero response in hertz (cycles per second).

3.6. Calculation of σ_{F2}

The rms fluctuation (standard deviation) σ_{F2} is defined by

$$\sigma_{F2}^2=\overline{y_{F2}^2(t)}-\overline{y_{F2}(t)}^2.$$

The bar indicates the time average in the interval $-T/2$ to $T/2$. Using (10) this may be written,

$$\sigma_{F2}^2=\int_{-\infty}^{\infty}W_{F2}(\nu)d\nu-\overline{y_{F2}}^2.$$

If the δ-function term [23] from (38) is separated from $W_{F2}(\nu)$ of (41), denoted by a prime,

$$\sigma_{F2}^2 = \int_{-\infty}^{\infty} W'_{F2}(\nu)\,d\nu. \tag{54}$$

Combining (22), (23), and (24), and assuming the modulation frequency is small compared with the amplifier bandwidth so the modulation factor distortion is negligible, then

$$y_D(t) = \left[\sum_i a_i(t) y_{i\bigstar A}(t)\right]^2, \tag{55}$$

where

$$y_{i\bigstar A}(t) \equiv h_A(t) \bigstar y_i(t). \tag{56}$$

Expanding (55) and using (14) and (16),

$$y_D(t) = \sum_i p_i(t) y^2_{i\bigstar A}(t) + 2\sum_{i<j} u_{ij}(t) y_{i\bigstar A}(t) y_{i\bigstar A}(t). \tag{57}$$

Taking the Fourier transform of (57), then using (6) and (B–2), to obtain the power spectral density,

$$W'_D(\nu) = \sum_{i,\,m} P_{i,\,-m} P^*_{i,\,-m} W'_{i\bigstar A,\,i\bigstar A}(\nu + m\nu_0) + 4 \sum_{i<j,\,m} U_{ij,\,-m} U^*_{ij,\,-m} W'_{i\bigstar A,\,j\bigstar A}(\nu + m\nu_0), \tag{58}$$

where $W_{i\bigstar A,\,j\bigstar A}(\nu)$ is the power spectral density of $y_{i\bigstar A}(t) y_{j\bigstar A}(t)$ and the primes indicate δ-function terms are omitted. It can be shown [15] that

$$W'_{i\bigstar A,\,i\bigstar A}(\nu) = 2[G_A(\nu) W_i(\nu)] \bigstar [G_A(\nu) W_i(\nu)], \tag{59}$$

where $G_A(\nu)$ is introduced in (37). Also for $i \neq j$,

$$W'_{i\bigstar A,\,j\bigstar A}(\nu) = [G_A(\nu) W_i(\nu)] \bigstar [G_A(\nu) W_j(\nu)]. \tag{60}$$

Using (59), (60), (10), (B–8), and (B–9) to simplify (58) and then using (39),

$$W'_{F1}(\nu) = \frac{1}{2} k^2 \left[\sum_i Q_{i,\,0} T_i^2 + 2 \sum_{i<j} V_{ij,\,0} T_i T_j\right] G_{F1}(\nu)[G_A(\nu) \bigstar G_A(\nu)], \tag{61}$$

where $Q_{i,\,0}$ and $V_{ij,\,0}$ are defined via (19) and (21).

For the computation of $W_{F2}(\nu)$ using (41), only $W_M(\nu)$ for $\nu \simeq 0$ will contribute because of the narrow low pass filter $F1$. Consequently in using (40) and (61), $G_{F1}(\nu \pm m\nu_0)[G_A(\nu \pm m\nu_0) \bigstar G_A(\nu \pm m\nu_0)]$ may be replaced by $G_{F1}(m\nu_0)[G_A(m\nu_0) \bigstar G_A(m\nu_0)]$ because the power transfer functions are even in ν. Furthermore, in the case where C_n decreases rapidly with increasing $|n|$, then to a good approximation $G_A(m\nu_0) \bigstar G_A(m\nu_0) \simeq G_A(0) \bigstar G(0)$. Therefore,

$$W'_{F2}(\nu) \simeq \frac{1}{2} \lambda^2 M^2 \left[\sum_i Q_{i,\,0} T_i^2 + 2 \sum_{i<j} V_{ij,\,0} T_i T_j\right] G_{F2}(\nu)/G_{F2}(0), \tag{62}$$

where λ is defined in (51) and

$$M \equiv \left[\sum_m C_{-m} C^*_{-m} G_{F1}(m\nu_0)\right]^{1/2}. \tag{63}$$

Thus using (54),

$$\sigma_{F2} \simeq \lambda M \tau^{-1/2} \left[\sum_i Q_{i,0} T_i^2 + 2 \sum_{i<j} V_{ij,0} T_i T_j \right]^{1/2} \tag{64}$$

where

$$\tau^{-1} \equiv \int_{-\infty}^{\infty} G_{F2}(\nu) d\nu / G_{F2}(0). \tag{65}$$

3.7. Sensitivity

A measure of a radiometer's sensitivity is $\sigma_{\overline{F2}}^{-1}(d\overline{y_{F2}}/dT_1)$. It is customary to specify instead, the minimum resolvable change in T_1, denoted $\Delta T_{\min}$. Using the criterion that a change in $\overline{y_{F2}}$, denoted $\Delta\overline{y_{F2}}$ due to a change in T_1 is resolved when $\Delta\overline{y_{F2}} \geq \sigma_{F2}$, then

$$\Delta T_{\min} = \frac{\sigma_{F2}}{d\overline{y_{F2}}/dT_1}. \tag{66}$$

Using (50) and (64),

$$\Delta T_{\min} = \frac{M \left[\sum_i Q_{i,0} T_i^2 + 2 \sum_{i<j} V_{ij,0} T_i T_j \right]^{1/2}}{\sqrt{B\tau} \left\{ \sum_m C_{-m} H_{F1}(m\nu_0) P_{1,-m} \right\}}, \tag{67}$$

where B, τ, C_{-m}, $H_{F1}(\nu)$, $Q_{i,0}$, $V_{ij,0}$, M are defined in (53), (65), (13), (34), (19), (21), and (63) respectively.

a. Radiometers With Premultiplier Filter

Most radiometers have a narrow (compared with ν_0) bandpass filter (denoted F1 in figure 1) preceding the multiplier. For this type of radiometer the sensitivity is independent of the correlation wave form. This follows from the fact that $H_{F1}(m\nu_0)$ in (50) is zero except for $m = \pm 1$. For this case,

$$\Delta T_{\min} = \frac{\left[\sum_i Q_{i,0} T_i^2 + 2 \sum_{i<j} V_{ij,0} T_i T_j \right]^{1/2}}{\sqrt{2B\tau}\, |P_{1,1}| \cos \psi}, \tag{68}$$

where

$$C_1 H_{F1}(\nu_0) P_{1,-1} \equiv |C_1 H_{F1}(\nu_0) P_{1,-1}| e^{i\psi}.$$

The sensitivity for particular modulation wave forms are shown in table 1.

b. Radiometers With No Premultiplier Filter

To simplify the calculations, assume the transfer function of the bandpass filter is constant in phase and amplitude and equal to $H_{F1}(\nu_0)$. In this case (67) becomes

$$\Delta T_{\min} = \frac{[\overline{c^2(t)}]^{1/2} \left[\sum_i Q_{i,0} T_i^2 + 2 \sum_{i<j} V_{ij,0} T_i T_j \right]^{1/2}}{[\overline{c(t) p_1(t)}] \sqrt{B\tau}}, \tag{69}$$

where $\overline{c(t)p_1(t)}$ is introduced via (B–10) of appendix B and $\overline{c^2(t)}$ is introduced in an analogous manner.

TABLE 1. ΔT_{min} *for special ideal switching radiometers.* The amplifier noise is T_3; $Q_{3,0}=1$ for all radiometers; d is the fraction of the time the transmission coefficient differs from zero.

$$\Delta T_{\min}=F(B\tau)^{-1/2}\left[\sum_i Q_{i,0}T_i^2+2\sum_{i<j} V_{ij,0}T_iT_j\right]^{1/2}$$

Modulation	Correlation	F	$Q_{1,0}$	$Q_{2,0}$	$V_{12,0}$	$V_{13,0}$	$V_{23,0}$	Prior calculations
1. Square wave	sinusoidal	$\pi/\sqrt{2}$	1/2	1/2	0	1/2	1/2	a* c e*† g⁰ j*†‡ k⁰
2. Square wave	square wave	2	1/2	1/2	0	1/2	1/2	e*† f⁰ h*‡ j*†‡ k⁰
3. Voltage sinusoidal	sinusoidal	$2\sqrt{2}$	35/128	35/128	3/128	3/8	3/8	b*†‡ d*†‡ e*† j†‡
4. Voltage sinusoidal	square wave	π	35/128	35/128	3/128	3/8	3/8	
5. Power sinusoidal	sinusoidal	$2\sqrt{2}$	3/8	3/8	1/8	1/2	1/2	g⁰ i* k⁰
6. Power sinusoidal	square wave	π	3/8	3/8	1/8	1/2	1/2	
7. Power sawtooth	sinusoidal	$\sqrt{2}\pi$	1/3	1/3	1/6	1/2	1/2	g⁰
8. Power sawtooth	square wave	4	1/3	1/3	1/6	1/2	1/2	
9. Rectangular	sinusoidal	$\pi/(\sqrt{2}\sin \pi d)$	d	$1-d$	0	d	$1-d$	
10. Rect. ($d\leq\frac{1}{2}$)	square wave	d^{-1}	d	$1-d$	0	d	$1-d$	
11. Rect. ($d\geq\frac{1}{2}$)	square wave	$(1-d)^{-1}$	d	$1-d$	0	d	$1-d$	
12. Rectangular	rectangular	$[d(1-d)]^{-1/2}$	d	$1-d$	0	d	$1-d$	h*‡

*Results of author conflict with this paper as noted in footnote.

°Results of author agrees in detail with this paper only when $T_1=T_2$.

†The calculation made was equivalent to assuming $T_2=0$ °K.

‡A rectangular filter bandpass assumed in calculation.

[a] Dicke [3] obtains a sensitivity greater by a factor 2 (thus $\Delta T_{\min}$ less by factor 2) than this paper.

[b] Goldstein [4, 5], a minor algebraic error corrected in ref. j.

[c] Bunkin, Karlov [17].

[d] Strom [6, 7] obtains a sensitivity less by a factor $\sqrt{2}$ than this paper.

[e] Strum [8]. The bandpass defined does not agree with this paper except for rectangular bandpass.

[f] Kelly, Lyons, Root [11, 12] agree only when radiometer balanced.

[g] Colvin [13] agrees only for balanced, constant power radiometers.

[h] Knight [9]. Equations (3) and (4) of Knight's paper omit a factor 2π. In addition, Knight's results differ from this paper in that the terms in T_1 and T_2 do not occur.

[i] Ward and Richardson [18] obtained a sensitivity greater by a factor $2\sqrt{2}$ than this paper.

[j] Johnson [10] algebraic error for square wave modulation.

[k] Tiuri [14].

4. Special Results

A variety of particular radiometers have been considered in the literature (see sec. 2). These radiometers were listed in table 1. The radiometer types shown in table 1 are ideal in three ways. First, the switching element introduces no noise of its own, second, the maximum transmission coefficient is unity, and last, the relative phases of switching and correlation wave forms $a(t)$, $b(t)$, and $c(t)$ are selected to minimize $\Delta T_{\min}$. The factor F is equal to $2^{-1/2}|P_{1,1}|^{-1}$ for sinusoidal correlation or for radiometers with a narrow band precorrelator filter (and any reasonable correlation). These radiometers are denoted as sinusoidal correlation in table 1. For other radiometers, F is equal to $\overline{[c^2(t)]}^{1/2}\overline{[c(t)p_1(t)]}^{-1}$. Explicitly the power modulation wave forms used are

(i) square wave modulation,

$$p_1(t)=\sum_{m=-\infty}^{\infty}\frac{\sin\dfrac{m\pi}{2}}{m\pi}e^{jm2\pi\nu_0 t}; \tag{70}$$

(ii) voltage sinusoidal modulation,

$$p_1(t)=3/8+1/2\cos 2\pi\,\nu_0 t+1/8\cos 4\pi\,\nu_0 t; \tag{71}$$

(iii) power sinusoidal modulation,

$$p_1(t) = 1/2 + 1/2 \cos 2\pi \nu_0 t; \tag{72}$$

(iv) power sawtooth modulation,

$$p_1(t) = 1/2 + j \sum_{k \neq 0} (2\pi k)^{-1} e^{jk2\pi\nu_0 t}; \tag{73}$$

(v) rectangular modulation,

$$p_1(t) = \sum_k \frac{\sin k\pi d}{k\pi} e^{j2\pi p\nu_0 t}; \tag{74}$$

where d is the fraction of the time that $p_1(t)$ differs from zero. Except for voltage sinusoidal modulation, $p_2(t)$ is chosen such that $p_1(t) + p_2(t) = 1$.

4.1. Nonideal Switch

The theory developed applies to arbitrary switching wave forms. There are two common deviations from the ideal forms used for table 1. First, the nonideal power transmission coefficient, $p_i'(t)$ of the switch varies from zero to $p_{i,\max}$ instead of from zero to one. Thus,

$$p_i'(t) = p_{i,\max} p_i(t),$$

so that

$$Q'_{i,0} = p_{i,\max}^2 Q_{i,0}, \tag{75}$$

and

$$V'_{ij,0} = p_{i,\max} p_{j,\max} V_{ij,0}. \tag{76}$$

Equations (75) and (76) may be used in place of the corresponding ideal parameters, to extend the results of table 1 to the switch with nonideal transmission coefficient.

A second complication is that the nonideal switch radiates thermal energy in direct proportion to its temperature, and the fraction of incident energy absorbed. For a matched three-port device at temperature T_{sw}, the effective temperature of the radiation $p_{sw}(t)T_{sw}$ is [24]

$$p_{sw}(t)T_{sw} = [1 - p_1(t) - p_2(t)]T_{sw}, \tag{77}$$

where the $p_i(t)$ are given by (14). The thermal noise from the switch may be treated formally as a noise source of the temperature of the switch which is power modulated by amplitude $p_{sw}(t)$. Thus for the ideal square-wave modulation, rectangular modulation, power-sinusoidal modulation, and power-sawtooth modulation of table 1,

$$p_{sw}(t) = 0. \tag{78}$$

For ideal voltage sinusoidal modulation,

$$p_{sw}(t) = \frac{1}{4} - \frac{1}{4} \cos 4\pi\nu_0 t. \tag{79}$$

TABLE 2. *Balanced, constant switched power, nonideal radiometer sensitivities.*

The maximum power transmission coefficient through the switch is $p_{1,\max}=p_{2,\max}=\alpha$; $T_1=T_2$; the effective amplifier noise is T_R; and the physical temperature of the switch is T_{sw}.

$$\Delta T_{\min}=F\,\frac{T_1+\alpha^{-1}T_R+(\alpha^{-1}-1)T_{sw}}{\sqrt{B\tau}}$$

A. Narrow band precorrelator filter or sinusoidal correlation

Modulation	F
Square wave	$\pi/\sqrt{2}=2.22$
Power sinusoidal	$2\sqrt{2}=2.83$
Power sawtooth	$\sqrt{2}\pi=4.44$
Rectangular*	$\pi/(\sqrt{2}\sin\pi d)$

B. No precorrelator filter

Modulation	Correlation	F
Square wave	square wave	2
Power sinusoidal	square wave	π
Power sawtooth	square wave	4
Rectangular*	rectangular	$[d(1-d)]^{-1/2}$
Rectangular* ($d\leq\frac{1}{2}$)	square	d^{-1}
Rectangular* ($d\geq\frac{1}{2}$)	square	$(1-d)^{-1}$

*d is the fraction of the time the transmission coefficient is different than zero.

4.2. Balanced Radiometers With Nonideal Switches

The expression for $\Delta T_{\min}$ simplifies when the noise sources being compared have nearly the same effective temperature and when the power to the amplifier is constant [i.e., $p_1(t)+p_2(t)=$constant]. Table 2 lists the results for radiometers having nonideal switches that satisfy these special conditions. The sensitivity indicated is for the correlation phase which minimizes $\Delta T_{\min}$.

The $\Delta T_{\min}$ for the voltage sinusoidally modulated radiometer does not simplify for $T_1=T_2$. However, for a radiometer with a narrow band precorrelator filter (or sinusoidal correlation) and a switch where the maximum power transmission coefficients $p_{1,\max}=p_{2,\max}=\alpha$, $\Delta T_{\min}$ for $T_1=T_2$ is bounded by the following expressions:

$$\Delta T_{\min}>2\sqrt{2}\,\frac{\left[\frac{3}{4}T_1+\alpha^{-1}T_3+\left(\alpha^{-1}-\frac{7}{8}\right)T_{sw}\right]}{\sqrt{B\tau}}, \tag{80}$$

and

$$\Delta T_{\min}<2\sqrt{2}\,\frac{\left[\frac{7}{8}T_1+\alpha^{-1}T_3+\left(\alpha^{-1}-\frac{3}{4}\right)T_{sw}\right]}{\sqrt{B\tau}}. \tag{81}$$

For no precorrelator filter and square wave correlation, $2\sqrt{2}$ is replaced by π.

5. Experimental Procedure

The sensitivity of a Dicke radiometer similar to Wells, Daywitt, and Miller [1] was determined experimentally. A switchable circulator was used for the switch instead of a magic tee and motor driven attenuators. The switchable circulator provided square-wave modulation at 1000 Hz. The 30 MHz output of the IF amplifier was attenuated by various amounts and then fed to a crystal detector. The detector law of this detector is shown in figure 2. The arrows indicate operating points for which the radiometer sensitivity was measured. The numbers near the arrows are the minimum resolvable temperature changes measured for each level.

The mixer-preamplifier-IF amplifier voltage response is shown for one channel in figure 3. The other channel is similar. The markers along the bottom of the figure are synthesized at 2 MHz intervals. The convolution bandwidth was calculated using a computer program based on (53). The system bandwidth is determined from a single channel response as discussed in appendix C.

The time constant for the low pass filter of the lock-in amplifier nominally set at 10 sec integrating time is based on the voltage response measurement shown in figure 4.

The recorded data were plotted on probability paper. The ordinate of this paper is the amplitude (voltage) of the radiometer output, and the abscissa is the percent of the time the recorder trace exceeds the ordinate value. The scale of the paper makes the plot a straight line if the data have normal (Gaussian) distribution. From the plot, the mean of the data is the value of the ordinate for which the abscissa is 50 percent. The standard deviation σ (for normal distribution) is the difference in the ordinate values for abscissa values of 50 percent and 84.1 percent (or 15.9% and 50%). Figure 5 shows two sets of data, one before and one after a change of 0.0087 dB (21.6 °K change from 10,800 °K) of input power is made in one noise source.

The various parameters for the radiometer under test are given in table 3. The theoretical $\Delta T_{\min}$ is based on table 2 for the balanced radiometer using square-wave modulation. The experimental $\Delta T_{\min}$ is the mean result of $\Delta T_1/(\overline{\Delta y_{F2}}/\sigma_{F2})$ taken from four plots similar to figure 5 for a $\Delta T_1 = 21.6$ °K.

A feature common to all data and shown in figure 5 is an increase in σ when the noise power decreases from null. No change in σ is noticeable when the noise power increases (out to 0.2 dB change). The cause of this feature is not known.

The radiometer sensitivity as noted in figure 2 for the radiometer at various operating points are comparable.

6. Conclusions

The areas of agreement within the literature have been ferreted out and the nature of discrepancies determined. A new analysis of the Dicke radiometer was presented which was general enough to include all of the papers reviewed as a special case and to extend the sensitivity calculations to include radiometers with a lossy switch.

The most sensitive radiometer is a square-wave modulated radiometer with wide band (i.e., no premultiplier filter) square-wave correlator. However, the potential 11 percent advantage in sensitivity for wide band square-wave correlation over systems using a narrow premultiplier filter must be weighed against the practical difficulties associated with wide band systems. Also the narrow band correlator insures that the output of the radiometer is proportional to the difference of input powers [i.e., to $T_1 - T_2$; see eq (50)] independent of the asymmetry of the modulation.

The sensitivity of a square-wave modulated radiometer using a narrow precorrelator filter was determined experimentally. The measured sensitivity was the same as the theoretical radiometer using a full-wave, square-law detector. The sensitivity of the radiometer was independent (within the experimental error) of whether a half-wave square-law, linear, or intermediate-law detector was used.

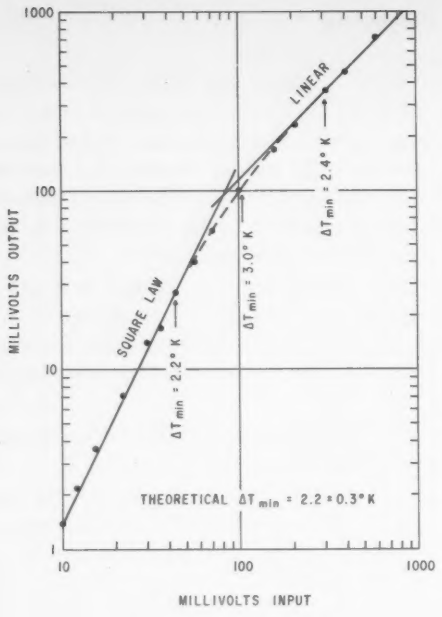

FIGURE 2. *Detector law.*

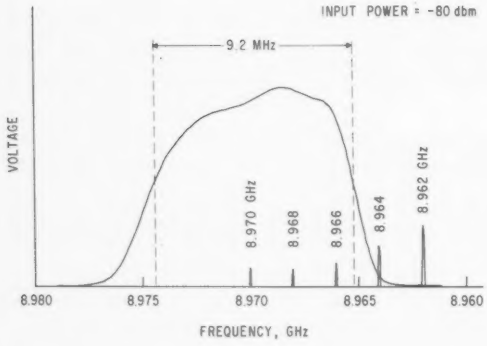

FIGURE 3. *Amplifier voltage response.*

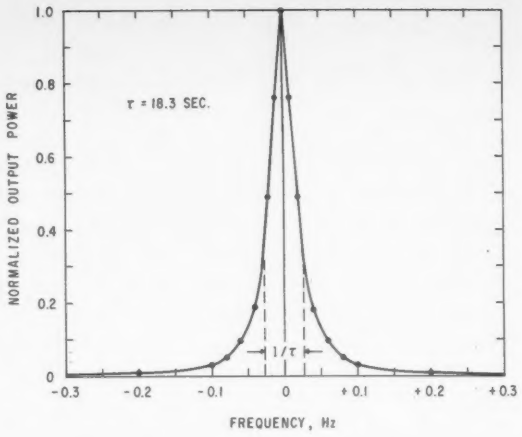

FIGURE 4. *Power response of the low pass filter.*

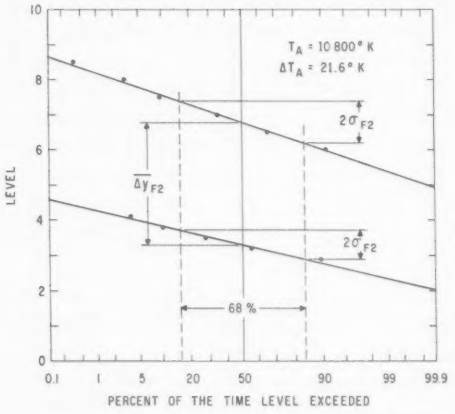

FIGURE 5. *Data plotted on probability paper.*

TABLE 3. *Parameters of the Dicke radiometer under test*

Predetection bandwidth (B)	9.2 MHz ± 10%
Postdetection integrating time (τ)	18 sec ± 10%
Receiver noise temperature (T_n)	750 °K ± 5%
Maximum switch transmission (α)	$(2.57)^{-1}$ ± 4%
Switch temperature (T_{SW})	295 °K
Noise sources ($T_1 \simeq T_2$)	10,800 ± 2.5%
Switching frequency (ν_0)	1000 Hz
Switching waveform	Square wave
Microwave frequency (local oscillator)	9 GHz
ΔT_{min} (theory)	2.3 °K ± 15%
ΔT_{min} (experimental)	2.3 °K ± 20%

The author thanks Charles L. Trembath and Douglas W. Schulze for carrying out the experimental measurements and Bernice K. Bender for the bandwidth computer program. Discussions with John J. Faris and Glenn F. Engen were very useful. Comments by M. E. Tiuri and the use of a preprint and comments by Walter A. Johnson were helpful. This research was supported by the Advanced Research Projects Agency under Project DEFENDER and was monitored by Charles M. Herzfeld under ARPA Order No. 515.

7. Appendix A. Equivalent Statements for B and τ and Notation Conversion for Literature

Various statements are used in the literature for B and τ. This section gives the definition used in this paper in alternate forms which are easier to compare with the literature.

Using the Wiener-Khintchine Theorem, (7), and assuming the order of integration can be interchanged, the following relationships can be proven:

$$G(0)\bigstar G(0)=\int_{-\infty}^{\infty}G^2(\nu)d\nu, \tag{A-1}$$

$$\int_{-\infty}^{\infty}G(\nu)\bigstar G(\nu)d\nu=\left[\int_{-\infty}^{\infty}G(\nu)d\nu\right]^2, \tag{A-2}$$

$$g(0)=\int_{-\infty}^{\infty}G(\nu)d\nu, \tag{A-3}$$

$$H(0)=\int_{-\infty}^{\infty}h(t)dt, \tag{A-4}$$

and Parsevals relation,

$$\int_{-\infty}^{\infty}H(\nu)H^*(\nu)d\nu=\int_{-\infty}^{\infty}h^2(t)dt, \tag{A-5}$$

where $g(t)$ is the Fourier transform (autocorrelation function) of the power response $G(\nu)$, and $h(t)$ and $H(\nu)$ are a Fourier transform pair, with $h(t)$ a real function.

If instead of using frequency ν in hertz (cycles per second) as a parameter, the angular frequency $\omega=2\pi\nu$ is used, then the following conversions may be used:

$$\nu=\omega/(2\pi),$$

$$G_\nu(\nu)=2\pi G_\omega(\omega),$$

$$W_\nu(\nu)=2\pi W_\omega(\omega),$$

$$Y_\nu(\nu)=2\pi Y_\omega(\omega),$$

$$H_\nu(\nu)=2\pi H_\omega(\omega),$$

$$G_\nu(\nu)\bigstar G_\nu(\nu)=2\pi G_\omega(\omega)\bigstar G_\omega(\omega),$$

where the subscripts ν and ω are introduced to distinguish a difference in functional form. This subscript will now be dropped. The functional form appropriate to the function used is under-

stood. The conversion from $W(\nu)$ to $W(\omega)$ is chosen so that

$$W(\nu)d\nu = W(\omega)d\omega.$$

In the ω notation,

$$Y(\omega) = (2\pi)^{-1} \int_{-\infty}^{\infty} e^{-j\omega t} y(t)dt,$$

and

$$W(\omega) = \underset{T\to\infty}{\text{Lim}} (2\pi/T)Y(\omega)Y^*(\omega).$$

The conversion system above is not unique. The easiest way to determine what system a given author is using is by examining the form used for the Wiener-Khintchine theorem, or statements which include the autocorrelation function. The autocorrelation function is universally defined in a manner equivalent to (9).

7.1. Equivalent Statements for B

The definition of B is in (52):

$$B = \frac{\left[\int_{-\infty}^{\infty} G_A(\nu)d\nu\right]^2}{2G_A(0)\bigstar G_A(0)}. \tag{A-6}$$

Using (A–2),

$$B = \frac{\int_{-\infty}^{\infty} G_A(\nu)\bigstar G_A(\nu)d\nu}{2G_A(0)\bigstar G_A(0)}, \tag{A-7}$$

or (A–1),

$$B = \frac{\left[\int_{-\infty}^{\infty} G_A(\nu)d\nu\right]^2}{2\int_{-\infty}^{\infty} G_A^2(\nu)d\nu}. \tag{A-8}$$

Beginning with (A–8), noting that $G_A(\nu) \equiv H_A(\nu)H_A^*(\nu)$, and converting to ω notation,

$$B = \frac{\left[\int_{-\infty}^{\infty} |H_A(\omega)|^2 d\omega\right]^2}{4\pi\int_{-\infty}^{\infty} |H_A(\omega)|^4 d\omega}. \tag{A-9}$$

Beginning with (A–8), applying (A–3) to the numerator and (A–5) to the denominator,

$$B = \frac{g_A^2(0)}{2\int_{-\infty}^{\infty} g_A^2(t)dt}. \tag{A-10}$$

Using a normalized autocorrelation function, $\rho_A(t)=g_A(t)/g_A(0)$,

$$(2B)^{-1}=\int_{-\infty}^{\infty}\rho_A^2(t)dt. \tag{A-11}$$

7.2. Equivalent Statements for τ

The definition of τ is from (65):

$$\tau^{-1}=\int_{-\infty}^{\infty}G_{F2}(\nu)d\nu/G_{F2}(0). \tag{A-12}$$

Noting that $G_{F2}(\nu)\equiv H_{F2}(\nu)H_{F2}^*(\nu)$ and converting to the ω convention,

$$\tau^{-1}=\frac{\int_{-\infty}^{\infty}|H_{F2}(\omega)|^2d\omega}{2\pi H_{F2}^2(\omega=0)}. \tag{A-13}$$

Using (A–4), and (A–5), and assuming a causal system such that $h(t)=0$ for $t<0$,

$$\tau^{-1}=\frac{\int_{-\infty}^{\infty}h_{F2}^2(t)dt}{\left[\int_{-\infty}^{\infty}h_{F2}(t)dt\right]^2}. \tag{A-14}$$

7.3. Literature Conversion

Several representative statements from the literature referring to the minimum resolvable change in temperature for a radiometer near balance ($T_1=T_2$) and for $\Delta T_{\min}\leq T_n$ will be converted to the notation of this paper.

a. Dicke [1946]

Dicke's [3] equation (21) for square-wave modulation and cosine correlation is,

$$\frac{\Delta T}{T}=\frac{\pi}{2}N\frac{\left\{\left[\int_{-\infty}^{\infty}|F(\omega)|^4d\omega\right]\left[\int_{-\infty}^{\infty}|S(\omega)|^2d\omega\right]\right\}^{1/2}}{S(0)\int_{-\infty}^{\infty}|F(\omega)|^2d\omega}. \tag{A-15}$$

Using (A–9) and (A–13) and the following conversions,

$$\Delta T=\Delta T_{\min},$$

$$T=T_1=T_2,$$

$$N=(T_n+T_1)/T_1 \text{ (for } T_1=290\ ^\circ\text{K}),$$

$$F(\omega)=H_A(\omega),$$

$$S(\omega)=H_{F2}(\omega),$$

and (A–15) becomes

$$\Delta T_{\min}=\pi(T_1+T_n)(8B\tau)^{-1/2}.$$

b. Goldstein [1955, 1956]

For voltage sinusoidal modulation and sinusoidal correlation Goldstein [4, 5] obtains

$$\sigma_{Id}^2 = 4\sigma_n^2 \sqrt{\gamma/\alpha}. \tag{A-16}$$

Goldstein's work corresponds to $T_1 = T_2 = 0$ °K and

$$\sigma_{Id}^2 = k\Delta T_{\min},$$

$$\sigma_n^2 = kT_n,$$

$$\gamma = (2\tau)^{-1},$$

$$\alpha = B,$$

where k is Boltzman's constant. Thus (A-16) becomes

$$\Delta T_{\min} = 4T_n(2B\tau)^{-1/2}.$$

c. Bunkin and Karlov [1955]

For square-wave modulation and sinusoidal correlation, Bunkin and Karlov obtain [17]

$$\delta T = \pi(T_{\text{in}} + T_e)\left\{\frac{1}{\Delta\omega}\frac{\Delta\Omega_1\Delta\Omega}{\Delta\Omega_1 + \Delta\Omega}\left[1 + \frac{\Delta T}{T_{\text{in}} + T_e} + \frac{1}{2}\frac{\Delta T^2}{(T_{\text{in}} + T_e)^2}\right]\right\}^{1/2}. \tag{A-17}$$

If the precorrelator bandwidth $\Delta\Omega_1$ is much greater than the postcorrelator low pass filter bandwidth $\Delta\Omega$, then

$$\frac{\Delta\Omega_1\Delta\Omega}{\Delta\Omega_1 + \Delta\Omega} \approx \Delta\Omega.$$

Using the following conversions

$$\delta T = \Delta T_{\min},$$

$$T_{\text{in}} = T_n,$$

$$T_e = T_1,$$

$$\Delta\omega = 2\pi B,$$

$$\Delta\Omega = \pi/\tau,$$

for $\Delta T \ll 1$, (A-17) becomes

$$\Delta T_{\min} = \pi(T_1 + T_n)(2B\tau)^{-1/2}.$$

d. Kelly, Lyons, and Root [1958, 1963]

For square-wave modulation and detection, (49) and (31) of Kelly, Lyons, and Root [12] becomes

$$\Delta T = 2[T_2 + T_n]\sqrt{\frac{1 + \Gamma(0)}{B\tau}}. \tag{A-18}$$

Equations (A–11) and (A–14) are used to establish the conversion for B and τ. Using the following conversions,

$$\Delta T = \Delta T_{\min},$$

$$T_2 = T_2 = T_1,$$

$$T_n = T_n,$$

$$\Gamma(0) = 0, \text{ (for zero gain fluctuations)}$$

$$B = B,$$

$$\tau = \tau,$$

(A–18) becomes

$$\Delta T_{\min} = 2(T_1 + T_n)(B\tau)^{-1/2}.$$

e. Knight [1962]

For rectangular modulation and rectangular correlation, Knight [9] obtains

$$\frac{S}{N} = \frac{2\pi\,\alpha(\sigma_R^2 - \sigma_S^2)^2}{2\Gamma\sigma_N^4}\left(\frac{a}{a+b}\right)\left(1 - \frac{a}{a+b}\right), \tag{A–19}$$

where the 2π omitted in Knight's eq (4) is added. The appropriate resolution criterion is $S/N = 1$. With this condition, then

$$\sigma_R^2 - \sigma_S^2 = k\Delta T_{\min},$$

$$\sigma_N^2 = kT_n,$$

$$a/(a+b) = d,$$

$$\Gamma = \pi/\tau,$$

$$\alpha = B,$$

and (A–19) becomes

$$\Delta T_{\min} = T_n[B\tau d(1-d)]^{-1/2}$$

8. Appendix B. Theorems on the Fourier Transform

Several theorems involving the Fourier transform of the time function $y_x(t)$ and $y_z(t)$ of zero mean are proved in this appendix:

$$\lim_{T\to\infty} \frac{Y_x(\nu)Y_z^*(\nu)}{T} = 0, \tag{B–1}$$

for $y_x(t)$ uncorrelated with $y_z(t)$, and

$$\operatorname*{Lim}_{T\to\infty}\frac{1}{T}\,Y_{xz}(\nu)Y^*_{x'z'}(\nu')=0, \tag{B-2}$$

unless $y_x(t)\equiv y'_x(t)$, $y_z(t)\equiv y'_z(t)$, and $\nu=\nu'$, and

$$\bar{y}=\operatorname*{Lim}_{T\to\infty}\frac{Y(0)}{T}, \tag{B-3}$$

and

$$\operatorname*{Lim}_{T\to\infty}\frac{Y_{xx}(0)}{T}=\int_{-\infty}^{\infty}W_x(\nu)d\nu, \tag{B-4}$$

and

$$Y_x(\nu+p\nu_0)\bigstar Y_z(\nu+q\nu_0)=Y_{xz}(\nu+p\nu_0+q\nu_0), \tag{B-5}$$

and

$$P_{i,r}=\frac{1}{\Theta}\int_{-\Theta/2}^{\Theta/2}a_i^2(t)e^{j2\pi r\nu_0 t}dt, \tag{B-6}$$

and

$$P_{i,r}=\sum_{m=-\infty}^{\infty}A_{i,m}A_{i,r-m}, \tag{B-7}$$

and

$$Q_{i,0}=\sum_m P_{i,m}P^*_{i,m}, \tag{B-8}$$

and

$$V_{ij,0}=\sum_m U_{ij,m}U^*_{ij,m}, \tag{B-9}$$

where $P_{i,r}$ and $A_{i,p}$ are defined in (18) and (12) respectively, and $\Theta=\nu_0^{-1}$ is one period of the periodic signal $p(t)$, and

$$\sum_\alpha C_\alpha P_{1,-\alpha}=\overline{c(t)p_1(t)} \tag{B-10}$$

where

$$\overline{c(t)p_1(t)}\equiv\frac{1}{\Theta}\int_{-\Theta/2}^{\Theta/2}c(t)p_1(t)dt. \tag{B-11}$$

8.1. Theorem 1

Taking the inverse transform (3) *of the left-hand side of* (B–1), *then taking inverse transform of* $\mathrm{Y}_1(\nu)$ *and* $\mathrm{Y}_2(\nu)$ *and interchanging the order of integration, one obtains* (Lim $\mathrm{T}\to\infty$ *is understood*)

$$\mathrm{T}^{-1}\int_{-\infty}^{\infty}\mathrm{e}^{\mathrm{j}2\pi\nu t}\mathrm{Y}_1(\nu)\mathrm{Y}_2^*(\nu)\mathrm{d}\nu=\mathrm{T}^{-1}\iint\mathrm{y}_1(\mathrm{t}')\mathrm{y}_2(\mathrm{t}')\mathrm{dt}'\mathrm{dt}''\int_{-\infty}^{\infty}\mathrm{e}^{\mathrm{j}2\pi\nu(\mathrm{t}-\mathrm{t}'+\mathrm{t}'')}\mathrm{d}\nu.$$

The integration over ν yields the Dirac delta function $\delta(t-t'+t'')$ [24].

Thus integrating over t',

$$T^{-1}\int e^{j2\pi\nu t}Y_1(\nu)Y_2^*(\nu)d\nu = T^{-1}\int_{-\infty}^{\infty} y_1(t+t'')y_2(t'')dt''.$$

If $y_1(t)$ and $y_2(t)$ are not correlated, then the integral on the right is finite, and when divided by T tends to zero as $T\to\infty$. Thus, the left-hand side is zero, the Fourier transform is also zero and (B–1) is proved.

8.2. Theorem 2

The theorem is proved in a manner analogous to theorem 1.

8.3. Theorem 3

By definition,

$$\bar{y} = \operatorname*{Lim}_{T\to\infty}\frac{1}{T}\int_{-T/2}^{T/2} y(t)dt.$$

The function $y(t)$ is truncated so that $y(t)$ equals zero for $|t| > T/2$. Thus,

$$\bar{y} = \operatorname*{Lim}_{T\to\infty}\frac{1}{T}\int_{-\infty}^{\infty} y(t)dt.$$

Taking the Fourier transform of $y(t)$ and interchanging the order of integration,

$$\bar{y} = \operatorname*{Lim}_{T\to\infty}\frac{1}{T}\int_{-\infty}^{\infty} Y(\nu)d\nu\int_{-\infty}^{\infty} e^{j2\pi\nu t}dt.$$

The integration over time yields the δ-function of ν. Subsequent integration over ν yields (B–3).

8.4. Theorem 4

Let $Y_{xz}(\nu)$ be the Fourier transform of $y_x(t)y_z(t)$ where $y_x(t)$ and $y_z(t)$ are random variables with zero mean:

$$Y_{xz}(\nu) = \int_{-\infty}^{\infty} e^{-j2\pi\nu t}y_x(t)y_z(t)dt.$$

If $y_x(t)$ is not correlated to $y_z(t)$ or $e^{-j2\pi\nu t}$, then the mean of the product is zero. Thus, $Y_{xz}(\nu)$ is finite and if divided by T, will approach zero as $T\to\infty$. If $y_z(t)\equiv y_x(t)$, then

$$Y_{xx}(\nu) = \int_{-T/2}^{T/2} e^{-j2\pi\nu t}y_x^2(t)dt,$$

where the limits of the integral are taken from $-T/2$ to $T/2$. This does not change the value of the integral because $y(t)=0$ for $|t|\geq T/2$. When $y_x^2(t)$ is rewritten as $\overline{y_x^2}+[y_x^2(t)-\overline{y_x^2}]$ and the above equation is divided by T (the limit $T\to\infty$ being understood),

$$T^{-1}Y_{xx}(\nu) = T^{-1}\left\{\overline{y_x^2}\int_{-T/2}^{T/2} e^{-j2\pi\nu t}dt + \int_{-T/2}^{T/2} e^{-j2\pi\nu t}[y_x^2(t)-\overline{y_x^2}]dt\right\}.$$

247-602 O-67—5

The integral in the second term is finite and the term goes to zero as $T \to \infty$. *The first term on the right-hand side goes to zero unless* $\nu = 0$. *For* $\nu = 0$ *the term approaches* $\overline{y_x^2}$. *Thus,*

$$\lim_{T \to \infty} Y_{xz}(\nu) = \begin{cases} \overline{y_x^2} & \text{for } \nu = 0 \text{ and } x = z, \\ 0 & \text{otherwise.} \end{cases}$$

Using (10) yields (B–4).

8.5. Theorem 5

Using the definition of convolution, eq (5),

$$Y_x(\nu + m\nu_0) \bigstar Y_z(\nu + q\nu_0) \equiv \int_{-\infty}^{\infty} Y_x(\nu' + m\nu_0) Y_z(\nu - \nu' + q\nu_0) d\nu'.$$

Taking the Fourier transform and interchanging the order of integrations,

$$Y_x(\nu + m\nu_0) \bigstar Y_z(\nu + q\nu_0) = \int \int_{-\infty}^{\infty} e^{-j2\pi[m\nu_0 t + \nu t' + q\nu_0 t']} y_x(t) y_z(t') dt\, dt' \cdot \int_{-\infty}^{\infty} e^{-j2\pi\nu''(t-t')} d\nu'.$$

The integration over ν' *yields* $\delta(t - t')$, *then the result of integrating over* t' *is identified as* $Y_{xz}(\nu + m\nu_0 + q\nu_0)$.

8.6. Theorem 6

To obtain (B–6), both sides of (18) are multiplied by $e^{j2\pi r\nu_0 t}$ *and then integrated over a period, using for* $p_i(t)$ *the equivalent* $a_i^2(t)$ *as noted in (14).*

8.7. Theorem 7

Using (B–6) and (12),

$$P_{i,r} = \frac{1}{\Theta} \sum_{m,s} \int_{-\Theta/2}^{\Theta/2} [A_{i,m} e^{jm2\pi\nu_0 t}][A_{i,s} e^{j(s-r)2\pi\nu_0 t}] dt.$$

Due to the orthogonality of different Fourier components, the integral has nonzero value only when $s = r - m$. *This leads directly to (B–7).*

8.8. Theorems 8, 9, 10, and 11

The proof of (B–8), (B–9), and (B–10) are analogous to the proof of (B–7). Equations (13), through (21) are needed for various definitions.

9. Appendix C. Radiometer Using an IF Amplifier

A schematic for the IF amplifier is shown in figure C–1. Instead of the amplifier shown in figure 1, now a mixer, local oscillator, and IF amplifier are used. The amplifier noise temperature T_n of figure 1 is now interpreted as the noise temperature of the mixer-IF amplifier as referred to the input of the *mixer*. Using the same notation convention as the body of the paper,

$$\begin{aligned} y_{LO}(t) &= \eta \cos 2\pi\nu_1 t, \\ y_{SM}(t) &= \eta y_S(t) \cos 2\pi\nu_1 t, \\ y_A(t) &= h_A(t) \bigstar y_{SM}(t), \end{aligned} \qquad \text{(C–1)}$$

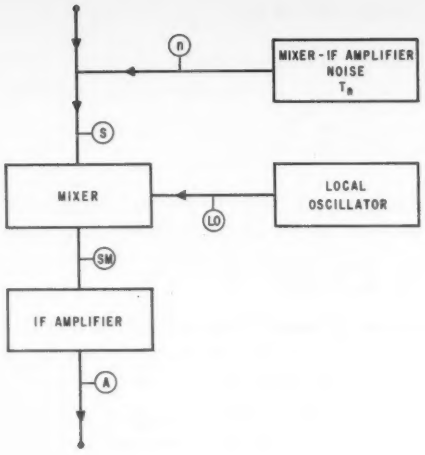

FIGURE C-1. *IF amplifier.*

where η is the amplitude of the local oscillator of frequency ν_1. From (C-1), it is clear that an ideal balanced mixer is assumed. Taking the Fourier transform,

$$Y_{SM}(\nu)=\tfrac{1}{2}\eta\,[Y_S(\nu+\nu_1)+Y_S(\nu-\nu_1)], \tag{C-2}$$

$$Y_A(\nu)=H_A(\nu)Y_{SM}(\nu). \tag{C-3}$$

Applying (6),

$$W_{SM}(\nu)=(\eta^2/4)[W_S(\nu+\nu_1)+W_S(\nu-\nu_1)], \tag{C-4}$$

$$W_A(\nu)=G_A(\nu)W_{SM}(\nu). \tag{C-5}$$

9.1. Calculation of $\overline{y_{F2}}$

The calculation of $\overline{y_{F2}}$ proceeds in a manner similar to section 3.5 except (C-2) and (C-3) are used in place of (29). Thus, instead of (46), now we have,

$$Y_A(\nu)=\tfrac{1}{2}\eta\sum_{i,p}A_{i,-p}[Y_{i\bigstar A}(\nu+p\nu_0+\nu_1)+Y_{i\bigstar A}(\nu+p\nu_0-\nu_1)]. \tag{C-6}$$

Substituting (C-6) into (30) will give terms of the type [see eq (47)],

$$Y_x(\nu+m\nu_0\pm\nu_1)\bigstar Y_z(\nu+q\nu_0\mp\nu_1)=Y_{xz}(\nu+m\nu_0+q\nu_0)$$

and

$$Y_x(\nu+m\nu_0\pm\nu_1)\bigstar Y_z(\nu+q\nu_0\pm\nu_1)=Y_{xz}(\nu+m\nu_0+q\nu_0\pm 2\nu_1). \tag{C-7}$$

Using an argument similar to that used to obtain (48), noting that the terms like (C-7) do not contribute,

$$\lim_{T\to\infty}\frac{Y_D(m\nu_0)}{T}=\frac{1}{2}\eta^2\sum_{i,q}A_{i,q}A_{i,-q-m}K_{i\bigstar A}. \tag{C-8}$$

Equation (C-8) is identical to (48) except for the multiplicative constant $\frac{1}{2}\eta^2$. Thus the remainder of the calculation is unchanged except that the gain functions λ of (51) now contain $\frac{1}{2}\eta^2$. Thus,

$$\lambda=\tfrac{1}{4}\eta^2 kH_{F2}(0)[2G_A(0)\bigstar G_A(0)]^{1/2}. \tag{C-9}$$

9.2. Calculation of σ_{F2}

The calculation of σ_{F2} proceeds in a manner similar to section 3.5 except (C–4) and (C–5) are used in place of (37). Because $W_S(\nu+\nu_1)=W_S(\nu-\nu_1)$, (C–4) and (C–5) combined become,

$$W_A(\nu)=\tfrac{1}{2}\eta^2 G_A(\nu)W_S(\nu).$$

Thus the calculation is similar except $W_S(\nu)$ is replaced by $\frac{1}{2}\eta^2 W_S(\nu)$. If (C–9) is used for the definition of λ, then the statement of $\overline{y_{F2}}$ and σ_{F2} in (50) and (64) are otherwise unchanged.

9.3. Comments

The bandwidth B is defined in a similar manner whether the amplifier is at the signal frequency or an IF frequency. For an IF amplifying system, B is the bandwidth of the IF amplifier. If for some reason the signal were only in the signal channel of the IF amplifier (the noise remains in both channels), then T_1 and T_2 would be replaced by $\frac{1}{2}T_1$ and $\frac{1}{2}T_2$, but no other changes. Thus, the single channel IF radiometer would be equivalent (as far as sensitivity is concerned) to a similar double-channel IF radiometer except it would have twice the amplifier noise temperature.

10. References

[1] J. S. Wells, W. C. Daywitt, and C. K. S. Miller, Measurement of effective temperatures of microwave noise sources, IEEE Trans. on Instr. and Meas. **IM–13,** 17–28 (Mar. 1964).

[2] D. F. Wait, and C. L. Trembath, A comparison between a switched and a correlation radiometer for cryogenic noise source measurements, ISA Conference, Los Angeles, California, Preprint No. 14.4–3–65 (Oct. 1965).

[3] R. H. Dicke, The measurement of thermal radiation at microwave frequencies, Rev. Sci. Inst. **17,** 268–275 (July 1946).

[4] S. J. Goldstein, Jr., A comparison of two radiometer circuits, Proc. IRE **43,** 1663–1666 (Nov. 1955).

[5] S. J. Goldstein, Jr., A comparison of two radiometer circuits, Proc. IRE **44,** 366 (Mar. 1956).

[6] L. D. Strom, The theoretical sensitivity of the microwave radiometer, a problem in non-stationary noise analysis, Doctoral Thesis, University of Texas (1957).

[7] L. D. Strom, The theoretical sensitivity of the Dicke radiometer, Proc. IRE **45,** No. 9, 1291–1292 (1957).

[8] P. D. Strum, Considerations in high-sensitivity microwave radiometry, Proc. IRE **46,** 43–53 (Jan. 1958).

[9] J. Knight, A general expression for the output of a Dicke-type radiometer, Proc. IRE **50,** No. 12, 2497–2498 (1962).

[10] W. A. Johnson, Effect of modulation-correlation choices on Dicke radiometer performance, Proc. IEEE **52,** 1242–1243 (1964).

[11] E. J. Kelly, D. H. Lyons, and W. L. Root, The theory of the radiometer, MIT Lincoln Lab. Group 312 Group Report 47.16 (May 1958).

[12] E. J. Kelly, D. H. Lyons, and W. L. Root, The sensitivity of radiometric measurements, J. Soc. Indust. Appl. Math. **11,** 235–257 (1963).

[13] R. S. Colvin, A study of radio astronomy receivers, Stanford Radio Astronomy Institute Publication **18A,** Stanford Electronics Labs., Stanford University [AF 18(603)–53] (Oct. 1961).

[14] M. E. Tiuri, Radio astronomy receivers, IEEE Trans. on Mil. Electro. **MIL–8,** 264–272 (1964).

[15] S. O. Rice, Mathematical analysis of random noise, Bell Sys. Tech. J. **23,** 282–332 (1944); Bell Sys. Tech. J. **24,** 46–156 (1945).

[16] W. Selove, A dc comparison radiometer, Rev. Sci. Instr. **25,** No. 2, 120–123 (Feb. 1954).

[17] F. V. Bunkin, and N. V. Karlov, On the question of sensitivity of radiometers (in Russian), Zhur. Tekh. Fiz. **25,** 430–435, 733–741 (1955).

[18] G. D. Ward, and J. M. Richardson, Analysis of a microwave radiometer for precise standardization of noise sources, J. Res. NBS **67C** (Engr. and Instr.), No. 2, 139–159 (1963).

[19] J. L. Lawson, and G. E. Uhlenbeck, Threshold signals **24,** MIT Rad. Lab. Series (McGraw-Hill Book Co., New York, N.Y., 1950).

[20] Y. W. Lee, Statistical theory of communication (John Wiley & Sons, Inc., New York, N.Y., 1960).

[21] H. Nyquist, Thermal agitation of electric charge in conductors, Phys. Rev. **32,** 110–113 (1928).

[22] B. M. Oliver, Thermal and quantum noise, Proc. IEEE **53,** 436–454 (1965).

[23] M. J. Lighthill, Fourier analysis and generalized functions, Cambridge (1960), or A. Messiah, Quantum mechanics (North Holland Publishing Co., Amsterdam, Holland), p. 468 (1961).

[24] D. F. Wait, Noise from passive multiports, to be published.

(Paper 71C2–252)

JOURNAL OF RESEARCH of the National Bureau of Standards — C. Engineering and Instrumentation
Vol. 71C, No. 2, April–June 1967

Sensitivity of a Correlation Radiometer*

John J. Faris**

Institute for Basic Standards, National Bureau of Standards, Boulder, Colo. 80302

(November 14, 1966)

The correlation radiometer is analyzed to determine the sensitivity that can be obtained under various operating conditions.

The radiometer using a sine wave comparison signal is analyzed and compared with the usual radiometer that employs a random noise for the comparison signal. It is found that the radiometer employing the sine wave comparison signal is the more sensitive of the two circuits, particularly in the case that the effective temperature of the input noise signal is greater than the effective input temperature of the amplifiers.

It is shown that if nonidentical amplifiers are used in the correlation circuit, the properties of the radiometer are determined by the portion of the amplifier response functions in the frequency interval that the two response functions overlap. The effect of amplifier gain fluctuations are considered, and although the correlation scheme reduces the effect of gain fluctuations, it is shown that they still do contribute to the output fluctuations of the radiometer.

Calculations are included showing that the effect of a differential phase shift between the two channels is a reduction in radiometer sensitivity. The same conclusion is reached concerning the effect of a differential time delay.

Finally, it is shown that if the comparison signal and the input signal have the same statistical properties, the requirements on the multiplier are less stringent than if the two signals have different statistical properties.

Key Words: Correlation radiometer, differential time delay, gain fluctuations, imperfect multiplier, noise comparison, nonidentical amplifiers, sine-wave comparison signal.

1. Introduction

The use of correlation techniques in radiometry has been suggested recently by several workers [Strum, 1958; Blum, 1959; Colvin, 1961; Allred, 1962]. One of the major reasons for this interest is that by using correlation techniques, it is possible to build a radiometer in which amplifier gain fluctuations contribute less to the fluctuations present in the output of the instrument than they do in the conventional radiometer; thus, the correlation radiometer might be expected to be superior to the conventional radiometer under conditions in which gain fluctuations are important. Strum [1958] has pointed out that as the noise level in a conventional radiometer system is reduced, the fluctuations due to changes in amplifier gain become more serious; therefore, at cryogenic temperatures it is very important to reduce this contribution to the total radiometer fluctuation. Thus, it was felt to be desirable to calculate the sensitivity obtainable from instruments of this type.

The analysis was carried out on the correlation receiver shown in figure 1. Although several different types of correlation receivers have been suggested in the literature, the operation of all of them is quite similar to the one chosen here. Therefore, the results obtained here should be applicable with appropriate modifications to many of the correlation radiometer circuits in the literature.

The first problem to be considered (see sec. 2) is the calculation of the sensitivity of a radiometer with amplifiers whose gain and passband are identical but with different effective tempera-

*This research was supported by the Advanced Research Projects Agency under Project DEFENDER and was monitored by M. I. Witow under ARPA Order No. 515.

**Radio Standards Laboratory, NBS Laboratories, Boulder, Colo. 80302. Permanent address, Colo. State University, Ft. Collins, Colo. 80521.

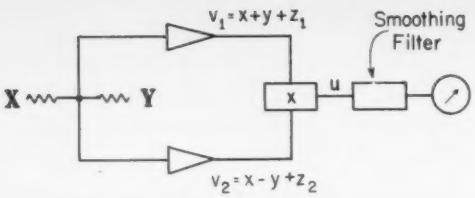

FIGURE 1. *Radiometer circuit.*

tures at the input circuit. These calculations are carried out for two types of input signals: (1) both input signals consist of white noise and, (2) one input signal is white noise and the other is sinusoidal. The first case was selected because it corresponds to the problem considered by Colvin [1961], and the second was chosen because it was the problem considered by Allred [1962]. Throughout this calculation, all filters are assumed to have a square passband. This assumption is made because it allows the results of the calculation to be written rather explicitly and thus it is easy to see the physical significance of the results. When it is desired to apply these results to a real radiometer with filters that are not square, it is only necessary to use the formalism of Colvin [1959] that expresses the effective bandwidth of a filter in terms of a convolution integral. Thus, this generalization can be carried out rather simply.

Section 3 is an analysis of the correlation radiometer in which it is assumed that the two amplifiers have different gains and different response curves.

Section 4 deals with the same circuit, but here the effect of variation in phase and in time delay of the signals in the two amplifiers is considered.

Finally, section 5 deals with some effects produced by an imperfect multiplier.

2. Sensitivity of an Ideal Correlation Radiometer

The circuit to be analyzed is shown in figure 1. Two noise sources, designated X and Y, are connected to opposite arms of a matched hybrid junction. The signals from the other pair of arms are applied to amplifiers whose transfer functions are $R_1(\omega)$ and $R_2(\omega)$ respectively. The outputs of the amplifiers are multiplied together and the product is filtered with a smoothing filter (low pass filter). The output of the smoothing filter is displayed on a d-c instrument.

As the following analysis will show, the average value of the deflection of the output instrument is proportional to the difference in noise temperature of the two sources, X and Y. Thus, when the two noise sources have the same effective temperature, the average value of the output deflection is zero and the radiometer is said to be balanced. The instantaneous deflection is a stochastic function of the time; thus the random fluctuations of the output deflection produce an uncertainty in the experimental conditions that correspond to a balance.

The sensitivity of a radiometer is usually defined as the change in temperature of one of the noise sources that will produce a deflection whose magnitude is equal to the root mean square of the output fluctuation. Therefore, in order to calculate the sensitivity of a radiometer it is necessary to obtain expressions for both the rms value of the output fluctuation and the change in average deflection per degree change in effective temperature of one of the noise sources.

In this section the assumption will be made that the two amplifiers have the same power transfer function, and for simplicity, a "square passband" will be assumed.

If $x(t)$ is the signal voltage due to source X that leaves each amplifier, and $y(t)$ is the signal voltage due to source Y that leaves amplifier 1, the signal voltage $-y(t)$ due to source Y must leave amplifier 2. It will be further assumed that the amplifiers introduce noise voltages z_1 and z_2 respectively.

Since the random functions $x(t)$, $y(t)$, $z_1(t)$, and $z_2(t)$ represent noise from physically separate noise generators, it will be assumed that they are mutually independent. It is also assumed that each is a second order, stationary Gaussian process possessing a continuous spectral density function. These assumptions imply that the processes are ergodic so that time averages and ensemble averages coincide. It is also assumed that each of these functions has zero mean.

If the output of amplifier 1 is designated by v_1 and the output of amplifier 2 by v_2, then

$$v_1 = x + y + z_1 \tag{1}$$

and

$$v_2 = x - y + z_2. \tag{1a}$$

The multiplier will be assumed to have a response law such that

$$u = a v_1 v_2 \tag{2}$$

where u is the voltage output and a is a constant of proportionality.

For any random quantity ξ, let $\overline{\xi}$ be the expectation or ensemble average of ξ. (This is the equivalent of the notation $E(\xi)$ used in the literature of mathematical statistics.) Using the independence and normality of the random processes and the fact that each process has zero mean, the autocorrelation function of u is

$$\psi_u(\tau) = \overline{u(t)u(t+\tau)} = a^2\, \overline{v_1(t)v_2(t)v_1(t+\tau)v_2(t+\tau)}$$

$$= a^2\, \overline{[x^2(t) - y^2(t) + z_1(t)(x(t) - y(t)) + z_2(t)(x(t) + y(t)) + z_1(t)z_2(t)][x^2(t+\tau) - y^2(t+\tau) + \ldots .]}.$$

$$\psi_u(\tau) = a^2[\psi_{x^2}(\tau) + \psi_{y^2}(\tau) - 2\psi_x(0)\psi_y(0) + \psi_{z_1}(\tau)(\psi_x(\tau) + \psi_y(\tau)) + \psi_{z_2}(\tau)(\psi_x(\tau) + \psi_y(\tau)) + \psi_{z_1}(\tau)\psi_{z_2}(\tau)]. \tag{3}$$

If ξ_i, $i = 1, 2, 3, 4$ are Gaussian variables, each with zero mean and

$$\overline{\xi_i \xi_j} = \sigma_{ij}$$

then

$$\overline{\xi_1 \xi_2 \xi_3 \xi_4} = \sigma_{12}\sigma_{34} + \sigma_{13}\sigma_{24} + \sigma_{14}\sigma_{23}. \tag{4}$$

Setting $\xi_1 = \xi_2 = x(t)$ and $\xi_3 = \xi_4 = x(t+\tau)$, there results

$$\psi_{x^2}(\tau) \equiv \overline{x^2(t)x^2(t+\tau)} = 2\psi_x^2(\tau) + \psi_x^2(0). \tag{5}$$

When (4) is applied to (3), the result is

$$a^{-2}\psi_u(\tau) = 2[\psi_x^2(\tau) + \psi_y^2(\tau)] + [\psi_x(0) - \Psi_y(0)]^2 + \psi_{z_1}(\tau)[\psi_x(\tau) + \psi_y(\tau)]$$

$$+ \psi_{z_2}(\tau)[\psi_x(\tau) + \psi_y(\tau)] + \psi_{z_1}(\tau)\psi_{z_2}(\tau). \tag{6}$$

The Fourier transform of the autocorrelation function of a process is the spectral density of the process. Further, the Fourier transform of a product of functions is the convolution of the Fourier transforms. Thus, designating the spectral density by Q, and the convolution operation by $*$,

$$a^{-2}Q_u(f) = [\psi_x(0) - \psi_y(0)]^2\delta(f) + 2[Q_x * Q_x(f) + Q_y * Q_y(f)]$$

$$+ [Q_{z_1} + Q_{z_2}] * [Q_x + Q_y](f) + Q_{z_1} * Q_{z_2}(f). \tag{7}$$

Case I. Consider both X and Y to be white noise generators at temperature T_x and T_y respectively. When the spectral densities are evaluated, it is necessary to consider the power division that takes place at the hybrid junction. These spectral densities are (see appendix)

$$Q_x * Q_x \approx \frac{1}{8}(kT_x)^2 B, \tag{8}$$

$$Q_x * Q_{z_1} \approx \frac{1}{4} k^2 T_x T_{z_1} B, \tag{8a}$$

$$Q_{z_1} * Q_{z_2} \approx \frac{1}{2} k^2 T_{z_1} T_{z_2} B. \tag{8b}$$

Thus, using Q' to designate the portion of the spectral density that contributes to fluctuations, this portion of (7) becomes

$$Q'_u = \frac{a^2 k^2 B}{4}[T_x^2 + T_y^2 + T_x(T_{z_1} + T_{z_2}) + T_y(T_{z_1} + T_{z_2}) + 2T_{z_1}T_{z_2}]. \tag{9}$$

With the assumption that the two amplifiers have the same effective noise temperature, this becomes

$$Q'_u = \frac{a^2 k^2 B}{4}[T_x^2 + T_y^2 + 2T_x T_z + 2T_y T_z + 2T_z^2]. \tag{10}$$

If the smoothing filter has a power response $G(f)$, the output power spectrum from the smoothing filter is

$$W(f) = G(f)Q'_u(f). \tag{11}$$

It is well known that integrating a power spectrum over all frequencies results in the mean square of the output voltage or current; so if the output voltage from the smoothing filter is $w(t)$, and $G(f)$ represents a square pass filter of width b, then

$$\overline{w(t)^2} = \int_{-\infty}^{\infty} W(f)df = \frac{1}{2} a^2 k^2 G_0 bB[T_x^2 + T_y^2 + 2T_z^2 + 2(T_x T_z + T_y T_z)] \tag{12}$$

where G_0 is the power response of the filter at zero frequency. The fluctuations at balance are required, so the balance condition is substituted into $\overline{w^2}$. The balance occurs when $T_x = T_y$, so for balance

$$\overline{w^2} = a^2 k^2 G_0 bB(T_x + T_z)^2. \tag{13}$$

Therefore, in terms of an rms voltage

$$w_{\text{rms}} = \overline{(w^2)}^{1/2} = ak(G_0 bB)^{1/2}(T_x + T_z). \tag{14}$$

Next, we calculate the deflection arising from a certain imbalance of the input signals. From (2)

$$u = av_1 v_2 = a(x + y + z_1)(x - y + z_2),$$

$$= a[x^2 - y^2 + z_1 z_2 + z_1(x - y) + z_2(x + y)]. \tag{15}$$

Since $x(t)$, $y(t)$, $z_1(t)$ and $z_2(t)$ are all uncorrelated, when (15) is averaged over time, the result is

$$\bar{u} = a(\overline{x^2} - \overline{y^2}). \tag{16}$$

Again applying the theorem that the integral of the power spectrum over all frequencies is the average square of a function, (16) becomes

$$\begin{aligned}\bar{u} &= a\left[\int Q_x df - \int Q_y df\right], \\ &= \frac{akB}{2}\,[T_x - T_y].\end{aligned} \tag{17}$$

In order to examine the effect of a small imbalance, set

$$T_y = T_x + \Delta T. \tag{18}$$

Then

$$u + \Delta u = \frac{akB}{2}\,[T_x - (T_x + \Delta T)].$$

Since $u = 0$ when $T_x = T_y$,

$$|\Delta u| = \frac{akB}{2}\,\Delta T. \tag{19}$$

The resulting signal at the output of the smoothing filter is

$$|\Delta w| = G_0^{1/2}|\Delta u| = \frac{a}{2}\,G_0^{1/2}kB\Delta T. \tag{20}$$

As is usual in radiometer calculations, the assumption is made that the minimum detectable signal occurs when the deflection is equal to w_{rms}. Thus, equating the right-hand sides of (14) and (20), the condition corresponding to minimum detectable signal results; i.e.,

$$ak(G_0bB)^{1/2}(T_x + T_z) = \frac{a}{2}\,G_0^{1/2}kB\Delta T. \tag{21}$$

Thus, the minimum detectable temperature difference is

$$\Delta T = 2(b/B)^{1/2}(T_x + T_z). \tag{22}$$

Case II. Let Y produce a sinusoidal signal, so that

$$Q_y(f) = \frac{v^2}{4}\,[\delta(f - f_0) + \delta(f + f_0)]. \tag{23}$$

The expression for $\psi_{x^2-y^2}$ is needed, so it will be calculated first. From the previous calculation, it is known that

$$\psi_{x^2-y^2} = \psi_{x^2} + \psi_{y^2} - 2\overline{x^2y^2}.$$

Thus, it is necessary to compute ψ_{y^2}:

$$\begin{aligned}\psi_{y^2} &= \overline{y^2(t)y^2(t+\tau)}, \\ &= \overline{\frac{v^4}{4}\cos^2\omega_0 t\,\cos^2\omega_0(t+\tau)},\end{aligned} \tag{24}$$

$$\psi_{y^2} = \frac{v^4}{4}\left[\frac{3}{8}\cos^2\omega_0\tau + \frac{1}{8}\sin^2\omega_0\tau\right]. \tag{25}$$

Making use of the above and (5), the result is

$$\psi_{x^2-y^2}=\overline{x^2}^2+2(\psi_x)^2+\frac{v^4}{4}\left(\frac{3}{8}\cos^2\omega_0\tau+\frac{1}{8}\sin^2\omega_0\tau\right)-2\overline{x^2}\frac{v^2}{4}. \tag{26}$$

From this, the power spectral density is

$$Q_{x^2-y^2}=\int\psi_{x^2-y^2}e^{-i\omega\tau}d\tau,$$

$$=\left(\overline{x^2}^2-\overline{x^2}\frac{v^2}{2}\right)\delta(f)+2(Q_x*Q_x)+\frac{v^4}{4}\left[\frac{1}{4}\delta(f)+\frac{1}{16}\delta(f-2f_0)+\frac{1}{16}\delta(f+2f_0)\right]. \tag{27}$$

Therefore

$$Q_u=a^2Q_{v_1v_2}=a^2\left[Q_{x^2-y^2}+Q_{z_1(x-y)}+Q_{z_2(x+y)}+Q_{z_1z_2}\right] \tag{28}$$

$$=a^2\left\{\left(\overline{x^2}-\frac{v^2}{4}\right)^2\delta(f)+\frac{v^4}{64}\left[\delta(f-2f_0)+\delta(f+2f_0)\right]+2(Q_x*Q_x)\right.$$

$$\left.+Q_{z_1}*(Q_x+Q_y)+Q_{z_2}*(Q_x+Q_y)+Q_{z_1}*Q_{z_2}\right\}. \tag{29}$$

Since the present calculation is to compute the fluctuations occurring in this radiometer, only the terms that contribute to the fluctuation need be considered; therefore they will be expressed as

$$Q_u'=a^2\{2(Q_x*Q_x)+(Q_{z_1}+Q_{z_2})*(Q_x+Q_y)+Q_{z_1}*Q_{z_2}\}, \tag{30}$$

where $Q_u'(f)$ denotes the fluctuating portion of Q_u.

All of the evaluations of the convolutions that occur in (30) can be taken from (8), except $Q_y*Q_{z_1}$; which is,

$$Q_y*Q_{z_1}=Q_{z_1}*Q_y=\int Q_{z_1}(f')Q_y(f-f')df',$$

where Q_y is given in (23). Thus,

$$Q_y*Q_{z_1}=\int Q_{z_1}(f')\frac{v^2}{4}\left[\delta(f-f'+f_0)+\delta(f-f'-f_0)\right]df',$$

$$=\frac{v^2}{4}\left[Q_{z_1}(f+f_0)+Q_{z_1}(f-f_0)\right]. \tag{31}$$

Since Q_{z_1} is assumed to be constant through the passband, when f_0 is in the passband and f is small, this convolution becomes

$$Q_y*Q_{z_1}=\frac{v^2}{4}kT_{z_1}. \tag{32}$$

Therefore

$$Q_u'=a^2\left\{\frac{1}{4}(kT_x)^2+\frac{1}{4}k^2BT_x(T_{z_1}+T_{z_2})+\frac{1}{4}v^2k(T_{z_1}+T_{z_2})+\frac{1}{2}k^2T_{z_1}T_{z_2}B\right\}. \tag{33}$$

By analogy with the previous calculation, the spectral density of the output of the filter can be written as

$$W(f)=G(f)Q_u(f),$$

and

$$\overline{w^2}=\int_{-\infty}^{\infty} W(f)df=a^2G_0(2b)\left\{\frac{1}{4}(kT_x)^2B+\frac{1}{4}k^2BT_x(T_{z_1}+T_{z_2})+\frac{1}{4}v^2k(T_{z_1}+T_{z_2})+\frac{1}{2}k^2T_{z_1}T_{z_2}B\right\}. \quad (34)$$

The d-c term of (29) indicates that the system is balanced when $kT_xB=v^2/2$. Also, to simplify the expression, it will be assumed that $T_{z_1}=T_{z_2}$. Then, at balance

$$\overline{w^2}=a^2G_0bk^2B\left(\frac{1}{2}T_x^2+2T_xT_z+T_z^2\right). \quad (35)$$

By analogy with the previous calculation, a root mean square fluctuation amplitude may be defined by

$$w_{\text{rms}}=ak(G_0bB)^{1/2}\left(\frac{1}{2}T_x^2+2T_xT_z+T_z^2\right)^{1/2}. \quad (36)$$

As mentioned previously, in order to arrive at the radiometer sensitivity, two parameters must be computed. The first is w_{rms}, which is given in (36). The second is the change in deflection due to a small change in temperature of the thermal source. The deflection sensitivity will be the same as it was in the previous calculation, so it is

$$|\Delta w|=G_0^{1/2}\frac{akB}{2}\Delta T.$$

Again, the minimum change in temperature that is observable will be taken to be a change that produces a deflection equal to the w_{rms}. Therefore

$$G_0^{1/2}\frac{akB}{2}\Delta T=ak(G_0B)^{1/2}\left(\frac{1}{2}T_x^2+2T_xT_z+T_z^2\right)^{1/2},$$

and the final result is

$$\Delta T=2\left(\frac{b}{B}\right)^{1/2}\left(\frac{1}{2}T_x^2+2T_xT_z+T_z^2\right)^{1/2}. \quad (37)$$

When this result is compared with (22), the sensitivity of a radiometer with both signals assumed to be white noise, it is evident that this instrument has a somewhat higher sensitivity. This is particularly true in the case that the input signal is the dominant noise in the system and thus sets the fluctuation level. In this case the improvement in sensitivity approaches $\sqrt{2}$.

3. Radiometer With Dissimilar Amplifiers

In section 2 the assumption was made that the two amplifiers were identical, except that they were allowed to have different effective temperatures. Here the more general problem, in which the two amplifiers may differ with respect to other parameters, will be considered.

The considerations are limited at first to a case in which the two amplifiers have the same shape of gain function but with differing gain amplitudes. If $H_1(\omega)$ is the complex voltage gain of the first amplifier, then the complex voltage gain of the second will be taken to have the form

$$H_2(\omega, t) = [1 + \alpha(t)]H_1(\omega). \tag{38}$$

where $\alpha(t)$ is a stochastic function.

If $x_1(t)$ is the signal resulting from amplifying the signal from the source X (this signal is $l(t)$) with the first amplifier and $x_2(t)$ is the result of amplifying $l(t)$ with the second amplifier, then a straightforward Fourier analysis shows that

$$x_2(t) = [1 + \alpha(t)]x_1(t), \tag{39}$$

and a similar relationship occurs for the signals $y_1(t)$ and $y_2(t)$ that arise from the signal $m(t)$ from the source Y. This notation is summarized in figure 2.

The most general form of the autocorrelation function of the sum of two random functions is

$$\begin{aligned}\psi_{a\pm b} &= \overline{[a(t) \pm b(t)][a(t+\tau) \pm b(t+\tau)]}, \\ &= \psi_a + \psi_b \pm \overline{a(t)b(t+\tau) + b(t)a(t+\tau)}.\end{aligned} \tag{40}$$

From this it follows that

$$\begin{aligned}\psi_{(x_1+y_1)(x_2-y_2)} = \psi_{x_1x_2} + \psi_{x_1y_2} + \psi_{y_1x_2} + \psi_{y_1y_2} - 2\overline{x_1x_2y_1y_2} \\ - \overline{x_1(t)y_1(t+\tau)y_2(t)x_2(t+\tau)} + \overline{y_1(t)x_1(t+\tau)x_2(t)y_2(t+\tau)}.\end{aligned} \tag{41}$$

From (39) it follows that

$$\begin{aligned}\psi_{x_1x_2} &= \overline{x_1(t)x_2(t)x_1(t+\tau)x_2(t+\tau)}, \\ &= \overline{x_1^2(t)x_1^2(t+\tau)[1+\alpha(t)][1+\alpha(t+\tau)]}, \\ &= \psi_{x_1^2}(1 + \psi_\alpha + 2\bar{\alpha}).\end{aligned} \tag{42}$$

By means of a similar line of reasoning, every term in (41) can be put into a form similar to that in (42). Thus,

$$\psi_{(x_1+y_1)(x_2-y_2)} = \psi_{(x_1+y_1)(x_1-y_1)}(1 + \psi_\alpha + 2\bar{\alpha}), \tag{43}$$

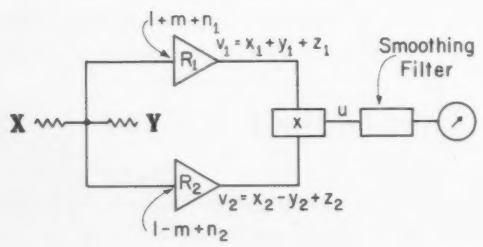

FIGURE 2. *Radiometer circuit with terminology for section 3.*

again

$$\psi_{z_1(x_2-y_2)}=(\psi_{z_1x_1}+\psi_{z_1y_1})(1+\psi_\alpha+2\overline{\alpha}), \tag{44}$$

and in the same way

$$\psi_{z_2(x_2-y_2)}=(\psi_{z_1^1x_1}+\psi_{z_1^1y_1})(1+\psi_\alpha+2\overline{\alpha}), \tag{45}$$

and

$$\psi_{z_1z_2}=\psi_{z_1z_1^1}(1+\psi_\alpha+2\overline{\alpha}), \tag{46}$$

where z_1^1 is the signal that would result if the noise signal $n_2(t)$ (the equivalent noise generated in the input of the second amplifier) were amplified by the first amplifier.

When these terms are all collected together, the result is

$$\psi_{v_1v_2}=(1+\psi_\alpha+2\overline{\alpha})\{(x_1^2-y_1^2)^2+\psi_{x_1}^2+\psi_{y_1}^2+\psi_{z_1x_1}+\psi_{z_1y_1}+\psi_{z_1^1x_1}+\psi_{z_1y_1}+\psi_{z_1^1z_1}\}. \tag{47}$$

Notice that in this case the second and third terms of (41) are cancelled by the sixth term.

In order to simplify the analysis, we will consider two cases: (1) α a constant, independent of time, and (2) $\alpha(t)$ a random variable with $\overline{\alpha}=0$.

Case I. When α is a constant independent of time, it is elementary to show that

$$\left.\begin{aligned}\psi_\alpha&=\alpha^2\\ \overline{\alpha}&=\alpha\end{aligned}\right\}. \tag{48}$$

Thus

$$\psi_{v_1v_2}=(1+\alpha)^2\{(x_1^2-y_1^2)^2+2(\psi_{x_1}^2+\psi_{y_1}^2)+\psi_{z_1x_1}+\psi_{z_1y_1}+\psi_{z_1^1x_1}+\psi_{z_1^1y_1}+\psi_{z_1z_1^1}\}. \tag{49}$$

Therefore, both the d-c and the fluctuation terms are multiplied by $(1+\alpha)^2$. Since this affects both the fluctuations and the deflection by the same amount, the sensitivity is not changed.

Case II. Assume that $\alpha(t)$ is a random function of time, such that $\overline{\alpha}=0$. At balance the term $\overline{(x_1^2-y_1^2)}=0$, so using a prime to denote quantities evaluated at the balance point, the result is

$$\psi'_{v_1v_2}=(1+\psi_\alpha)\{2(\psi_{x_1}^2+\psi_{y_1}^2)+\psi_{z_1x_1}+\psi_{z_1y_1}+\psi_{z_1^1x_1}+\psi_{z_1^1y_1}+\psi_{z_1^1z_1}\}. \tag{50}$$

From this the spectral density is

$$Q'_{v_1v_2}=(1+Q_\alpha)*\{2(Q_{x_1}*Q_{x_1}+Q_{y_1}*Q_{y_1})+Q_{z_1}*(Q_{x_1}+Q_{y_1})+Q_{z_1^1}*(Q_{x_1}+Q_{y_1})+Q_{z_1^1}*Q_{z_1}\}. \tag{51}$$

Notice that (51) is similar to the result that is obtained in the case of identical amplifiers; the only difference is that the present result is the convolution of the original result with $(1+Q_\alpha)$.

The spectral density of the multiplier output is

$$Q_u=a^2Q_{v_1v_2},$$

where $Q_{v_1v_2}$ is given by (51). The spectral density at the output of the low pass filter is

$$W(f)=G(f)Q_u(f),$$

$$=a^2G(f)(1+Q_\alpha)*\{2(Q_{x_1}*Q_{y_1}+Q_{y_1}*Q_{y_1})+Q_{z_1}*(Q_{x_1}+Q_{y_1})+Q_{z_1}^1*(Q_{x_1}+Q_{y_1})+Q_{z_1^1}*Q_{z_1}\}. \tag{52}$$

Following the same line of reasoning that was used from (11) to (14), the root mean square fluctuation on the output can be seen to be

$$w_{\text{rms}}=\left[\int_{-\infty}^{\infty}W(f)df\right]^{1/2},$$

$$=\left[\int_{-\infty}^{\infty}a^2G(f)(1+Q_\alpha)*\{2(Q_{x_1}*Q_{x_1}+Q_{y_1}*Q_{y_1})+Q_{z_1}*(Q_{x_1}+Q_{y_1})\right.$$

$$\left.+Q_{z_1}^1*(Q_{x_1}+Q_{y_1})+Q_{z_1^1}*Q_{z_1}\}df\right]^{1/2}. \tag{53}$$

To see the effect of the gain fluctuations, consider that the amplifiers have a square bandpass of bandwidth B. Then,

$$Q_{x_1}*Q_{x_1}=2Q_i^2R_1^2B,$$

where

$$R_1(\omega)=H_1(\omega)\ H_1^*(\omega),$$

is the power gain of the amplifier, and

$$Q_\alpha*Q_{x_1}*Q_{x_1}=\int_{-\infty}^{\infty}2Q_i^2R_1^2BQ_\alpha(f-f')df'=2Q_i^2R_1^2B\overline{\alpha^2}. \tag{54}$$

Thus the term $(1+Q_\alpha)*(Q_{x_1}*Q_{x_1})$ can be written as $2Q_i^2R_1^2B(1+\overline{\alpha^2})$. Each term in (53) will produce the same effect, so the result is

$$w_{\text{rms}}=(1+\overline{\alpha^2})^{1/2}w_{\text{rms}}(0), \tag{55}$$

where $w_{\text{rms}}(0)$ is the fluctuation level that occurs when there are no gain fluctuations, i.e., when $\alpha=0$.

Since gain fluctuations increase the fluctuation level of the output but have no effect on the average deflection, it is evident that this effect results in a reduction in radiometer sensitivity by the factor $(1+\overline{\alpha^2})^{1/2}$.

While the above expression for the reduction in radiometer sensitivity has been derived only in the case of white noise and amplifiers with square bandpass, examination of the integral that leads to (54) shows that the result will be qualitatively similar even in a less idealized case.

The next consideration will be to calculate the sensitivity of a radiometer with differing amplifier gain functions (transfer functions). In general these amplifiers could have differing center frequencies, and also the shape of the gain-frequency functions could differ.

The average square output can be expressed as

$$\overline{w(t)^2}=\int_{-\infty}^{\infty}G(f)Q_u df \tag{56}$$

where $G(f)$ is the power transfer function of the low pass filter. The input to the filter is given by

$$u = av_1v_2 = a(x_1 + y_1 + z_1)(x_2 - y_2 + z_2). \tag{2}$$

By means of the theorem expressed in (4), the autocorrelation function of u can be put into the form

$$a^{-2}\psi_u = (\overline{x_1x_2} - \overline{y_1y_2})^2 + (\psi_{x_1} + \psi_{y_1} + \psi_{z_1})(\psi_{x_2} + \psi_{y_2} + \psi_{z_2})$$
$$+ \overline{x_1(t)x_2(t+\tau)}\ \overline{x_2(t)x_1(t+\tau)} + \overline{y_1(t)y_2(t+\tau)}\ \overline{y_2(t)y_1(t+\tau)}$$
$$- \overline{x_2(t)x_1(t+\tau)}\ \overline{y_1(t)y_2(t+\tau)} - \overline{x_1(t)x_2(t+\tau)}\ \overline{y_2(t)y_1(t+\tau)}. \tag{57}$$

Recalling that

$$Q_{x_1} = R_1Q_l = H_1H_1^*Q_l,$$

and similar relationships exist for the other variables, the spectral density of u becomes

$$a^{-2}Q_u = (\overline{x_1x_2} - \overline{y_1y_2})^2\delta(f) + (R_1Q_l + R_1Q_m + R_1Q_{n_1}) * (R_2Q_l + R_2Q_m + R_2Q_{n_2})$$
$$+ \mathrm{Re}\{[(H_1H_2^*Q_l) * (H_2H_1^*Q_l)] + [(H_1H_2^*Q_m) * (H_2H_1^*Q_m)]$$
$$- [(H_2H_1^*Q_l) * (H_1H_2^*Q_m)] - [(H_1H_2^*Q_l) * (H_2H_1^*Q_m)]\}. \tag{58}$$

The form of the last term arises from the theory of cross-spectra [Goodman, 1957; Korn and Korn, 1961].

The complete expression for the spectral density of the multiplier output is obtained by evaluating (58). From the resulting expression the fluctuation amplitude of the radiometer can be obtained by following the same procedure used previously.

Next it is necessary to calculate the average deflection resulting from a particular combination of input signals. This can be obtained by evaluating (2) of the simple theory in this more general case.

First, consider

$$\bar{u} = a\overline{v_1v_2} = a(\overline{x_1 + y_1 + z_1})(\overline{x_2 - y_2 + z_2}). \tag{2}$$

Of the six random variables that appear in the right-hand term of (2), the only correlations that are not zero are the partial correlations of x_1 with x_2 and of y_1 with y_2. Therefore this expression reduces to

$$\bar{u} = a(\overline{x_1x_2} - \overline{y_1y_2}). \tag{59}$$

Equation (59) must be evaluated in terms of the transfer functions of the two amplifiers, $H_1(f) + H_2(f)$, and the spectral densities of the noise outputs of the two noise sources. The Fourier transform of the random function l is

$$S_l(f) = \int l(t)e^{-2\pi ift}dt. \tag{60}$$

In the theory of cross-correlations, it is shown that [Korn and Korn, 1961] the time average of the cross correlation of x_1 and x_2 can be expressed as

$$\langle x_1x_2\rangle = \int \mathrm{Re}\left[\lim_{T\to\infty}\frac{1}{T}(S_{x_1}S_{x_2}^*)\right]df = \lim_{T\to\infty}\frac{1}{2T}\int (S_{x_1}S_{x_2}^* + S_{x_1}^*S_{x_2})df = \frac{1}{2}\int (H_1H_2^* + H_1^*H_2)Q_l df, \tag{61}$$

where the symbol $\langle\ \rangle$ is used to indicate a time average. The final form of (61) results from the fact that $S_{x_1}=H_1S_I$, etc. Also, due to the fact that the random processes are ergodic, the time average in (61) may be replaced by an ensemble average.

In the same way

$$\overline{y_1y_2}=\frac{1}{2}\int (H_1H_2^*+H_2H_1^*)Q_m df. \tag{62}$$

Therefore,

$$\bar{u}=a[\overline{x_1x_2}-\overline{y_1y_2}]=\frac{a}{2}\int (H_1H_2^*+H_2H_1^*)(Q_I-Q_m)df. \tag{63}$$

The above expression leads to the following conclusions: (1) In case the two sources have the same form of spectral density over the amplifier bandwidth, balance occurs independent of the amplifier response curves. Thus, for white noise, balance occurs when $T_I=T_m$. (2) In case Q_I and Q_m have different forms, balance occurs where

$$\int (H_1H_2^*+H_2H_1^*)Q_I df=\int (H_1H_2^*+H_2H_1^*)Q_m df. \tag{64}$$

An expression for $\Delta\bar{u}$, the change in $\bar{u}$ due to a deviation from balance, is required. In the case where both signals consist of white noise,

$$Q_I-Q_m=\frac{1}{4}k(T_I-T_m). \tag{65}$$

Next, the assumption is made that

$$T_m=T_I-\Delta T,$$

then,

$$Q_I-Q_m=\frac{1}{4}k[T_I-(T_I-\Delta T)]=\frac{1}{4}k\Delta T. \tag{66}$$

In this case

$$\Delta\bar{u}=\frac{a}{8}k\Delta T\int (H_1H_2^*+H_2H_1^*)df. \tag{67}$$

If the smoothing filter has a response function at zero frequency given by G_0, then

$$\Delta\bar{w}=G_0^{1/2}\Delta\bar{u}=\frac{a}{8}G_0^{1/2}k\Delta T\int (H_1H_2^*+H_2H_1^*)df. \tag{68}$$

Again the assumption is made that the minimum detectable change in deflection is a change equal to the rms value of the fluctuations. The minimum detectable value of ΔT is evaluated by equating the right-hand side of (68) and the square root of $\overline{w^2}$. Using the fact that

$$w_{\text{rms}}=(\overline{w^2})^{1/2}=\left[\int_{-\infty}^{\infty} W(f)df\right]^{1/2},$$

the result is

$$\left[\int_{-\infty}^{\infty} G(f)Q_w'(f)df\right]^{1/2}=\frac{a}{8}G_0^{1/2}k\Delta T\int (H_1H_2^*+H_2H_1^*)df. \tag{69}$$

When this solved for ΔT, the result is

$$\Delta T = \frac{\left[\int_{-\infty}^{\infty} G(f) Q_u'(f) df\right]^{1/2}}{\frac{a}{8} G_0^{1/2} k \int (H_1 H_2^* + H_2 H_1^*) df}. \tag{70}$$

Equation (70) is the general expression for the sensitivity of a correlation radiometer with amplifiers with differing complex gain functions. In order to interpret this result and obtain a feeling for the importance of the various parameters, it is convenient to look at two examples. First the case of two amplifiers with square gain functions centered on the same frequency f_0; the first amplifier with bandwidth B_1 and gain R_1^0 and the second with bandwidth B_2 and gain R_2^0 will be considered. To be specific, it will be assumed that $B_1 > B_2$. It will be assumed that no phase shifts occur in these amplifiers.

In order to evaluate (70) it is necessary to evaluate the various terms of (58), recalling that the numerator of (70) contains only fluctuation terms; i.e., any d-c contributions must be ignored. It is reasonable to evaluate the convolution integrals that occur with the restriction that f is small enough that B_2 is enclosed within B_1. When these evaluations are carried out with the assumptions that the radiometer is balanced and also that the low pass filter has a square passband of width b, the result is

$$[\text{numerator of (70)}] = a G_0^{1/2} b^{1/2} (B_2 R_1^0 R_2^0)^{1/2} k (T_l + T_n).$$

When this is compared to the similar result from the simple theory, for example (14), it is evident that the bandwidth that sets the fluctuation level is B_2, the narrower of the two amplifier bandwidths. Also, the amplifier gains appear as the product $R_1^0 R_2^0$.

The denominator of (70) must also be evaluated under the same conditions. This involves evaluating the integral

$$\int (H_1 H_2^* + H_2 H_1^*) df, \tag{71}$$

where H_1 and H_2 are the discontinuous real functions as defined above. When this is carried out, the result is

$$[\text{denominator of (70)}] = \frac{a}{8} G_0^{1/2} k (4 R_1^0 R_2^0 B_2).$$

These results lead to

$$\Delta T = 2 \left(\frac{b}{B_2}\right)^{1/2} (T_l + T_n). \tag{72}$$

Thus, in this case the same sort of expression is obtained as in the case of the simple theory except that the bandwidth of the narrowest amplifier sets the sensitivity.

Finally the case of two amplifiers with square bandpass with identical bandwidth but tuned to slightly different center frequencies will be considered. Again phase shifts will be neglected, the complex gains will be treated as real positive functions, and the radiometer will be assumed to be balanced. The resulting sensitivity is

$$\Delta T = 2 \left(\frac{b}{B_0}\right)^{1/2} (T_l + T_n) \tag{73}$$

where B_0 is the "overlap bandwidth" or the frequency interval common to both amplifiers.

247-602 O-67—6

4. Effect of Variation in Time Delay and Phase in the Amplifiers of a Correlation Type Radiometer

Here it will be assumed that a differential variation in time delay can occur to the signals in the two amplifiers. Thus, at any instant the multiplier is comparing voltages corresponding to two different instants of time. Therefore, the multiplier output can be expressed as

$$u(t) = v_1(t)v_2(t+\tau), \tag{74}$$

where τ is the time delay difference in the two signal channels. In order to simplify this analysis, the assumption will be made that the two radiometer channels are identical except for the difference in time delay. Thus the voltages that are multiplied together are

$$v_1(t) = x(t) + y(t) + z_1(t),$$

$$v_2(t+\tau) = x(t+\tau) - y(t+\tau) + z_2(t+\tau). \tag{75}$$

Equation (7) shows that the fluctuation level of the radiometer depends only on convolutions of power spectra. Since these are not a function of τ, the fluctuation level does not vary as a result of a differential time delay. Therefore, the change in sensitivity will be related to the change in average deflection caused by the time delay.

The change in average deflection can be obtained from

$$\overline{u(t,\tau)} = \overline{[x(t)+y(t)+z_1(t)]\,[x(t+\tau)-y(t+\tau)+z_2(t+\tau)]}$$

$$= \overline{x(t)x(t+\tau)} - \overline{y(t)y(t+\tau)} = \psi_x(\tau) - \psi_y(\tau). \tag{76}$$

The Wiener-Khintchine theorem allows this to be put into the form

$$\overline{u(t,\tau)} = \int (Q_x - Q_y)e^{i\omega\tau}df. \tag{77}$$

In order to be able to evaluate the above integral, it is convenient to consider that both sources generate white noise and the amplifiers have square bandpass of width B centered on f_0. Thus, in this case,

$$\bar{u}(\tau) = (Q_x - Q_y)\left[\int_{-f_0-B/2}^{-f_0+B/2} e^{i\omega\tau}df + \int_{f_0-B/2}^{f_0+B/2} e^{i\omega\tau}df\right],$$

$$= 2B(Q_x - Q_y)\cos 2\pi\tau f_0 \frac{\sin \pi\tau B}{\pi\tau B}. \tag{78}$$

This can be put in more convenient form by noting that

$$\bar{u}(0) = 2B(Q_x - Q_y).$$

Thus

$$\bar{u}(\tau) = \bar{u}(0)\cos 2\pi\tau f_0 \frac{\sin \pi\tau B}{\pi\tau B}. \tag{79}$$

For the usual case in which $B \ll f_0$ and τ is on the order of $1/f_0$, this can be approximated by

$$\bar{u}(\tau) \approx \bar{u}(0)\cos 2\pi\tau f_0. \tag{80}$$

Thus, in the case of white noise sources and square bandpass amplifiers, time delay variations will not influence the balance point. They will affect sensitivity, however. For maximum sensitivity, it is important to keep the difference in time delay in the two amplifiers small enough that cos $2\pi\tau f_0$ is approximately unity.

A somewhat related question is the effect of a differential phase change in the two amplifiers. Again assuming white noise sources and amplifiers that are identical except for the phase shift, the average deflection can be computed by means of (63). With the assumption that

$$R_2 = R_1 e^{i\phi}, \tag{81}$$

this equation becomes

$$\bar{u}(\phi) = \frac{a}{2}(Q_l - Q_m) R_1 (2 \cos \phi).$$

This can again be expressed in the form

$$\bar{u}(\phi) = \bar{u}(0) \cos \phi. \tag{82}$$

5. Some Effects of Using an Imperfect Multiplier

The simplest form of multiplier to multiply two microwave signals together is probably that shown in figure 3. The input signals (v_1 and v_2) are applied to two opposite arms of a hybrid junction. The other pair of opposite arms are terminated by square law detectors. The outputs from these detectors are applied to a difference amplifier. In case the hybrid T is matched, the detectors have the same sensitivity and their reflection coefficient is zero; and, if they are assumed to have a perfect square law envelope response, the output voltage z will be

$$z = t_1 - t_2 = \alpha\left(\frac{v_1 + v_2}{\sqrt{2}}\right)^2 - \alpha\left(\frac{v_1 - v_2}{\sqrt{2}}\right)^2, \tag{83}$$

where α is the coefficient of proportionality in the multiplier law. Thus,

$$z = 2\alpha v_1 v_2. \tag{84}$$

In an actual multiplier constructed on this principle, the ideal conditions suggested above will be only approximated. Thus, the output will not be an accurate multiplication of the input signals. A scattering matrix analysis of the multiplier junction indicates that if the junction is matched and perfect, the wave arriving at the detectors is equal to that assumed in the ideal case as long as either pair of leads are terminated in matched loads. Since the detectors (if bolometers) can be quite accurately matched, this will probably not be the phenomenon that sets the multiplier accuracy. This accuracy can depend on the accuracy of the "square law" of the detectors, however.

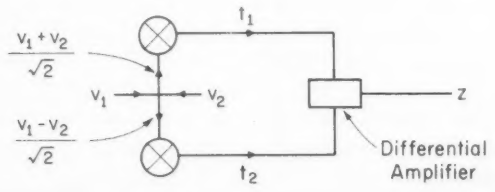

FIGURE 3. *Microwave multiplier.*

In order to investigate the effect of the detector law on the multiplier accuracy, assume that both detectors follow the same law. If one detector is more sensitive than the other, the incoming signal can be attenuated, so that, referred to the input of the attenuator, the two detectors are assumed to have the same law with the same numerical coefficients. Thus, the voltages from the detectors can be expressed as power series

$$t_1=\sum_n a_n\left(\frac{v_1+v_2}{\sqrt{2}}\right)^n, \tag{85a}$$

$$t_2=\sum_n a_n\left(\frac{v_1-v_2}{\sqrt{2}}\right)^n. \tag{85b}$$

Then the multiplier output is

$$z=t_1-t_2=\sum_n a_n\left[\left(\frac{v_1+v_2}{\sqrt{2}}\right)^n-\left(\frac{v_1-v_2}{\sqrt{2}}\right)^n\right]. \tag{86}$$

These terms may be expanded with the binomial theorem: the result is

$$z=2\left[\frac{a_1}{2^{1/2}}\,v_2+\frac{a_2}{2^{2/2}}\,(2v_1v_2)+\frac{a_3}{2^{3/2}}\,(3v_1^2v_2+v_2^3)+\frac{a_4}{2^{4/2}}\,(4v_1^3v_2+4v_1v_2^3)+\ldots\right]. \tag{87}$$

The smoothing filter provides an estimate of the average of the multiplier output; thus it is necessary to compute $\bar{z}$. This is,

$$\bar{z}=2[a_2\overline{(v_1v_2)}+a_4\overline{(v_1^3v_2+v_1v_2^3)}+\ldots],$$

$$=2[a_2\overline{(x+y+z_1)(x-y+z_2)}+a_4\{\overline{(x+y+z_1)^3(x-y+z_2)}+\overline{(x+y+z_1)(x-y+z_2)^3}\}+\ldots],$$

$$=2[a_2(\overline{x^2}-\overline{y^2})+2a_4(\overline{x^4}-\overline{y^4})+3a_4(\overline{x^2}-\overline{y^2})\,(\overline{z_1^2}+\overline{z_2^2})+\ldots]. \tag{88}$$

The result is that if $\overline{x^4}-\overline{y^4}=0$ at the same conditions that $\overline{x^2}-\overline{y^2}=0$, the balance condition is not affected by any term up to the fourth in the crystal law expansion. This would be the case if both x and y are signals with the same statistical properties; for example, if both are thermal noise sources, they both possess Gaussian statistics.

However, in the case that the two signals have different statistical properties, $(\overline{x^4}-\overline{y^4})$ would not necessarily equal zero when $(\overline{x^2}-\overline{y^2})$ does. Thus, in this case, it is important to select detectors that are accurately square law.

6. Conclusions

The sensitivity of a correlation radiometer has been computed under a variety of conditions. In section 2 a very simplified calculation is used to derive the usual expression for the sensitivity of the radiometer. This is followed by a calculation of the sensitivity of a radiometer of the type suggested by Allred (1962) in which the unknown noise signal is balanced against a sinusoidal reference signal. By performing these two calculations in an analogous manner, it is particularly easy to compare the sensitivities that result. In the case that the output fluctuations are predominately due to the input noise signals, Allred's radiometer is more sensitive than the conventional circuit that compares two noise signals.

The first part of section 3 demonstrates that it is not necessary for the two amplifiers to have the same gain. The calculation shows that the product of the gains is the parameter that determines the output amplitude, instead of the individual amplifier gains. Next, it is shown that gain fluctuations produce a decrease in sensitivity. The last part of this section is concerned with the effect of using two dissimilar amplifiers. A general expression is obtained for the sensitivity of a radiometer with amplifiers with arbitrary gain functions. This expression is evaluated for the case of amplifiers with square bandpass and no phase shifts. It is shown that under these conditions, whether the two amplifiers have the same bandpass and different center frequencies or whether they have the same center frequency and different bandwidths, the sensitivity is determined by the "overlap" bandwidth.

Section 4 deals with the effect of a differential time delay or differential phase shift in the two radiometer channels. It is shown that both of these effects result in a decrease of sensitivity.

Finally in section 5 it is shown that, if the multiplier carries out the multiplication operation by forming the difference of the squares of the sum and difference of the two input signals, errors can result if the "square law" elements do not have a perfect square law response and if the two input voltages have differing statistical distributions. Thus, the radiometer proposed by Allred, in which the comparison signal is sinusoidal, places a more stringent requirement on the multiplier than does the more usual correlation radiometer, in which both input signals are Gaussian noise.

The author gratefully acknowledges many helpful discussions with D. F. Wait and G. F. Engen. M. M. Siddiqui's comments on the manuscript proved to be very helpful.

7. References

Allred, C. M. (1962), A precision noise spectral density comparator, J. Res. NBS **66C** (Engr. and Instr.), No. 4, 323–330.

Blum, E. J. (1959), Sensibilité des radioteléscopes et recepteurs a correlation, Annales d' Astrophysique **22,** No. 2, 140–163.

Colvin, R. S. (1959), Faint signal limitations of radiometers, Inst. of Radio Engr., WESCON Convention Record **3,** Pt. 8, 52–58.

Colvin, R. S. (1961), A study of radio-astronomy receivers; Stanford Radio Astronomy Institute Publication No. 18A (Stanford University, Stanford, Calif.).

Goodman, N. R. (Mar. 1957), On the joint estimation of the spectra, cospectrum and quadrature spectrum of a two-dimensional stationary Gaussian process, Engineering Statistics Laboratory Scientific paper No. 10, New York University, p. 23.

Korn, G. A. and T. M. Korn (1961), Mathematical Handbook for Scientists and Engineers (McGraw-Hill Book Co., Inc., New York, N.Y.).

8. Appendix—Evaluation of Convolution Integrals

Assume a random signal with white spectral density amplified by an amplifier with square passband as shown in figure A–1.

If the spectral density of the input signal is Q_0 as measured, the amplitude of Q_x is $RQ_0/2$, where R is the power gain of the amplifier. The division by 2 occurs because the spectral density is assumed to be split equally between the positive and negative frequency regions. Then,

$$Q_x * Q_x = \int Q_x(f-f')Q_x(f')df'.$$

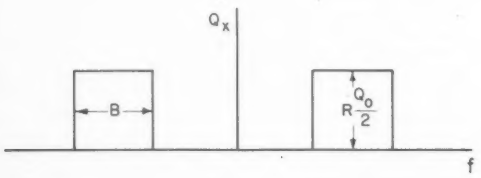

FIGURE A–1. *Square spectral density.*

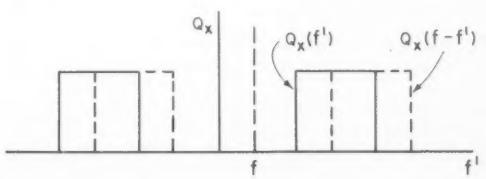

FIGURE A–2. *Functions appearing in integrand of convolution integral.*

The value of this integral for small values of the parameter f is required. The term $Q_x(f-f')$ has the same shape as $Q_x(f')$ except that it is displaced an amount f and inverted on the frequency axis, as shown in figure A–2. Since the integrand is the product of these two functions, the value of the integral is the product of the amplitudes of these functions times the frequency interval over which the product is nonzero. Thus,

$$Q_x * Q_x = \left(R\frac{Q_0}{2}\right)^2 2(B-f) \tag{A-1}$$

for $f < B$.

In this paper, the value of this integral is required under the condition that $f \ll B$. To this approximation, the result is

$$Q_x * Q_x = 2B\left(R\frac{Q_0}{2}\right)^2. \tag{A-2}$$

In general, the convolutions of the other spectral densities appearing in this paper are evaluated in the same way. The reason that the various convolutions of power spectra that are used have differing numerical coefficients is that the hybrid junction at the input of the radiometer divides the input powers; however, the noise powers appearing due to the effective input temperatures of the amplifiers do not undergo this power division.

(Paper 71C1–253)

JOURNAL OF RESEARCH of the National Bureau of Standards—C. Engineering and Instrumentation
Vol. 71C, No. 2, April–June 1967

Publications of the National Bureau of Standards*

Selected Abstracts

Research on crystal growth and characterization at the National Bureau of Standards June 1966, ed. H. C. Allen, Jr., *Tech. 293 (Aug. 26, 1966), 25 cents.*

The National Bureau of Standards with partial support from the Advanced Research Projects Agency of the Department of Defense is continuing a wide program of studies involving crystalline materials. These include investigation of methods and theory of growth, study of detection and effects of defects, determination of physical properties, refinement of chemical analysis, and determination of stability relations and atomic structure. The types of materials range from organic compounds, through metals, and inorganic salts to refractory oxides. This report summarizes progress in those projects wholly or partially supported by ARPA.

Key Words: Crystal growth, crystal characterization, and crystalline materials.

A sensitive recording NMR ultrasonic spectrometer, L. W. James, *Tech. Note 344 (Sept. 7, 1966), 20 cents.*
Instrumentation is described for automatically obtaining a continuous recording of ultrasonic absorption lines. Ultrasonic power is added to the crystal lattice by a transducer mounted on a single crystal of the sample. The interaction of the ultrasonics with the nuclear spin system is recorded by using a pulse NMR system in conjunction with a boxcar integrator. This technique is more sensitive and provides more easily interpretable results than earlier systems.

Standard Reference Materials: Viscosity of a standard lead-silica glass, A. Napolitano and E. G. Hawkins, *Misc. Publ. 260–11 (Nov. 7, 1966), 25 cents.*
The viscosity of a lead-silica glass has been measured at the National Bureau of Standards and seven other laboratories. Determinations were made in the range of 10^2 to 10^{15} poises (1350–400 °C). Measurements were made by the rotating cylinder, restrained sphere, fiber-elongation, and beam-bending methods. The results have been critically evaluated and the glass has been issued as Standard Reference Material No. 711.

Key Words: Beam bending, fiber elongation, glass, glass standard, glass viscosity, lead-silica glass, restrained sphere, rotating cylinders, standard, standard reference material, viscosity, viscosity standard.

Thermal conductivity of selected materials, R. W. Powell, C. Y. Ho, and P. E. Liley, *NSRDS-NBS 8 (Nov. 25, 1966), $1.00.*
The work presented in this report consists of the critical evaluation and analysis of the available thermal conductivity data on eleven metals and nine nonmetals for the solid state, on seven fluids for both the liquid and gaseous states and on two for the liquid state only. The materials studied were selected primarily for their potential applicability as reference standards or because of their technical importance. The temperature range for which values are given often exceeds that for which these values are known with a high degree of certainty.

Key Words: Thermal conductivity, solids, metals, liquids, gases.

Notes on the state-of-the-art of benefit-cost analysis as related to transportation systems, J. D. Crumlish, *Tech. Note 294 (Nov. 1, 1966), 30 cents.*

This review of benefit-cost analysis as a tool for evaluating alternative courses of action describes the technique, discusses a number of benefit-cost studies, and indicates the difficulties inherent in this area of applied economics. The author concentrates on the application of the technique to large scale transport problems, reviews the literature and indicates in his conclusions where the technique can be helpful and where there is little chance for its success.
An accompanying matrix of benefit-cost studies and a commentary thereon is supplied by Marsha Geier, an NBS economist. Miss Geier's literature search failed to produce any analytic methods which were comprehensive, theoretically justifiable, operational or significant. This finding tended to support the views of the author. (Introduction by Alan J. Goldman, Applied Mathematics Division, Institute for Basic Standards, National Bureau of Standards.)

Key Words: Benefit-cost analysis; transportation economics; transport systems; systems analysis; state of the art.

Calculation of the heating value of a sample of high purity methane for use as a reference material, G. T. Armstrong, *Tech. Note 299 (Dec. 15, 1966), 25 cents.*
The heat of combustion of CH_4 has been recalculated in kJ $(mol)^{-1}$, Btu $(mol)^{-1}$, Btu $(cu\ ft)^{-1}$ (dry basis) and Btu $(std.\ cu\ ft)^{-1}$ (saturated basis), using the best available experimental determinations of the heat of combustion and other measured quantities and the most recent generally accepted physical constants and defined physical units. The calculations are outlined in detail. The resulting quantities are applied to calculation of the heat of combustion of a reference sample of CH_4 submitted for analysis of composition and certification of heating value by the Institute of Gas Technology.

A standard for accurate phase-angle measurements at audio frequencies, W. W. Scott, Jr., *Tech. Note 347 (Oct. 14, 1966), 25 cents.*
A method is described for the measurement of phase angles from 0° to 360° (except for a band ± 10° about the 180° point) with an uncertainty at audio frequencies of ± 0.05° to ± 0.01°, depending on the phase-angle. The method utilizes readily available equipment which may be assembled and connected to serve as a standard. The principal advantage of this standard is in its potentially broad frequency-response; namely, 10 Hz to 10 kHz or higher. It makes use of inductive voltage dividers and thermal voltage converters to compare voltage magnitudes, which are related to phase-angle by the law of cosines. The thermal voltage converters are compared with each other before each phase-angle measurement. Their outputs are connected so that short-time power supply variations do not affect the measurements. The repeatability of measurements with this standard at a phase-angle of 60° is within a range of 0.001°. A model has been built which shows good measurement precision, but it has not been thoroughly tested or studied at many frequencies and phase-angles for sources of error. This report serves as a record of the development work completed on this standard to date.

Key Words: Audio frequency, inductive voltage divider, measurement, phase-angle, thermal voltage converter, standard.

A new near-zone electric field-strength meter, F. M. Greene, *(Proc. 8th IEEE Symp. Electromagnetic Compatibility, San Francisco, Calif., July 11–13, 1966), Symposium Digest New Ideas for Electromagnetic Compatibility, 1966.*
The National Bureau of Standards has recently completed the development of prototype instrumentation for measuring the electric-field components of complex, high-level, near-zone electromagnetic

fields from 0.1 to 1000 volts per meter, at frequencies from 150 kHz to 30 MHz with a present uncertainty of less than ±2 dB. The successful design of the NBS meters is based on the use of a novel form of telemetry, employing a completely non-metallic electrical transmission line, which apparently has not been fully exploited heretofore. This avoids the perturbing effects on the field being measured, usually caused by field-strength meters employing metallic ore transmission lines.

Key Words: Device, electro-explosive ordnance—field, near-zone electromagnetic—hazards, electromagnetic radiation—line, nonmetallic electrical transmission—meter, electric field-strength—telemetry, novel form.

New standard for the calibration of microphones, W. Koidan, *Mag. Std.* **37,** *No. 5, 141–144 (May 1966).*
This article discusses the background, contents and use of a new American Standard, Calibration of Microphones, S1.10–1966, published by the American Standards Association, Incorporated.

Key Words: Calibration, microphones, Standard.

Resistance to weathering, H. T. Arni, *ASTM Significance of Tests of Concrete and Concrete Making Materials, Am. Soc. Testing Mater. Spec. Tech. Publ. 169A, pp. 261–274 (1966).*
Deterioration of concrete due to physical processes produced by exposure to natural weathering is discussed. The most recent theories on the mechanisms of freezing-and-thawing damage are presented, and freezing-and-thawing tests now specified and proposed are discussed. The effects of de-icing chemicals and of weathering processes other than freezing and thawing are also considered.

Key Words: Concrete, de-icing scaling, durability, freezing-and-thawing, weathering.

Survey of infrared measurement techniques and computational methods in radiant heat transfer, S. T. Dunn, J. C. Richmond, and J. F. Parmer, *J. Spacecraft Rockets* **3,** *No. 7, 961–975 (July 1966).*
This paper is an analysis of 133 replies to a questionnaire sent to all known workers in the field of thermal radiation property measurements and radiant heat transfer computations. The questions were designed to obtain information on the current state of the art in these fields. In addition, the authors have supplemented the information obtained from the questionnaire to give a broad overall picture of the current status and future needs in each area covered. A brief summary of Russian literature in the field of thermal radiation property measurements is also included.

Key Words: Computational methods, emissivity, emittance measurements, radiant heat transfer, reflectance measurements, thermal radiation.

Optical methods of temperature measurement, G. A. Hornbeck, *J. Appl. Opt. Lead Article* **5,** *No. 2, 179 (Feb. 1966).*
The history of the laws of thermal radiation is briefly reviewed, and the theoretical relations basic to some of the optical methods of temperature measurement are given. Comments on a number of optical methods are presented, as well as a selected reference with each method where more detail is available. In conclusion, several problems, in areas of uncertainty in the field of optical methods of temperature measurement, are suggested in the belief that a solution to these problems will greatly enhance the technical value of this field.

Key Words: Boltzmann, Draper, Jeans, Kirchoff, optical, Planck, pyrometry, radiance, Rayleigh, Stefan, temperature, Wien.

Infrasonic waves from aurorae, K. Maeda and J. M. Young, *Nature* **207,** *No. 4994, 279–281 (July 1965).*
The effects of atmospheric thermal structure on the free-field propagation of auroral infrasound are discussed. Experimental data illustrating dispersion and near-sinusoidal oscillations near the Bruunt frequency are shown. The effects of the large positive lapse rate layers, especially the one in the thermosphere, on atmospheric resonances are given particular attention.

Magnetic core permeability measurement techniques, R. D. Harrington and A. L. Rasmussen, *Proc. Magnetic Core Conf.* **7,** *11–24 (1965).*
Techniques for measuring the initial complex permeability of magnetic cores in the frequency range from 1 kHz to 50 MHz are briefly discussed. Emphasis is directed toward studies recently carried out at the National Bureau of Standards.
At frequencies below 100 kHz, either a demountable coil or a specially designed Maxwell bridge is used for obtaining core data. The frequency range from 100 kHz to about 50 MHz is most conveniently covered through the use of the radio frequency permeameter. A brief survey of the development of the permeameter with a description of some recent measurements indicating that this method may be used to frequencies even greater than 50 MHz is given.
It has been found that toroidal coils are preferable to the permeameter for obtaining accurate measurements of the temperature coefficient of permeability. A brief description is given of a method for evaluating the inductance and resistance changes of such coils using a bridge as a null indicating device. The technique is capable of measuring temperature coefficients of permeability of the order of one 10^{-6} per degree centigrade.

An examination of the effects of heat transfer and compressible flow on the performance of laminar flowmeters, F. W. Ruegg and H. H. Allion, *Proc. Flow Measurement Conf., Am. Soc. Mech. Eng. Fluid Meters Golden Anniversary, Pittsburgh, Pa., Sept. 26–28, 1966, pp. 253–273 (1966).*
Laminar meters are now widely used for measurement of gas flow, and high accuracy can be achieved with proper calibration and use. It has been found necessary to modify Poiseuille's law for laminar flow to explain the performance of meters over the wide range of flow conditions encountered. A one-dimensional flow analysis is used to derive the effects of meter shape, heat transfer, and compressibility of the gas on meter performance. A relationship between the meter flow coefficient and the similarity parameters of Reynolds number, Prandtl number, Mach number, and Knudsen number is given in a form that is convenient for both the calibrator and user of the meter. The small but significant effects predicted are compared with experimental results.

Key Words: Compressible flow, flowmeter, gas meter, heat transfer, laminar flow, meter calibration.

Roofing research, T. H. Boone, *Military Engr.* **385,** *344–345 (Sept.-Oct. 1966).*
The Building Research Division of the National Bureau of Standards has for many years studied roof systems, constituent materials and components. Highlights of the roofing research in the last five years and a brief résumé of the results of this research are given. Description of some of the newly developed roofing systems and the present status of roofing research are also discussed.

Key Words: Liquid-applied coatings; membrane movements; prefabricated sheets; radiative cooling; roofing research; solar heating.

A new guide for photographers, C. S. McCamy, *Mag. Stds.* **37,** *No. 8, 223–224 (Aug. 1966).*
The new "American Standard Photographic Exposure Guide" presents and relates data which provide means of calculating camera settings for daylight and moonlight exposure of black-and-white and color films. The Appendix gives guidance for photographing sunsets, clouds, the moon, artificial satellites, rainbows, cities at night, fireworks, lightning, aurora, stars, and eclipses. The standard is based on extensive picture tests.

Key Words: Camera, crystal, diffraction, dislocation, topography, x-ray.

A simple non-scanning camera for x-ray diffraction contrast topography, H. P. Layer and R. D. Deslattes, *J. Appl. Phys.* **37,** *No. 9, 3631–3632 (Aug. 1966).*
A new x-ray topographical camera has been developed that is applicable to both Laue and Bragg geometries for normal and anomalous transmission, that results in a significant reduction of experimental complexity along with quite acceptable exposure times.

Key Words: Camera, diffraction, dislocation, topography, x-ray.

Studies of some exploding wire light sources, E. C. Cassidy and S. Abramowitz, *J. SMPTE* **75,** *No. 8, 735–737 (Aug. 1966).*
Continuous and time-resolved measurements of the spectral distribution of light emitted by various exploding wire systems have been obtained by use of a high-speed drum camera and a rotating shutter, respectively. Results from experiments with several systems show the effects of environment, pressure, energy, and wire material on the spectrum. Various intermediate species, produced by the explosion, are determined spectroscopically.

Key Words: A10, A1H, aluminum, atomic spectra, electrical discharges, exploding wires, light sources, time-resolved spectroscopy, titanium TiO.

A device for use in applying strain gages to cylindrical specimens, T. W. Butler and R. L. Bloss, *Experimental Mechanics* **6,** *No. 10, 528 (Oct. 1966).*
A simple device is described which applies a uniform pressure to the exterior of a cylindrical specimen. This device has been used in connection with a regulated air supply to apply pressure while curing strain gage installations.

Key Words: Adhesive, application, curing, cylinder, installation, strain gage.

Calibration and use of laminar flowmeters, H. H. Allion, (*Proc. 25th Annual Gas Measurement Short Course, Aug. 25, 1965*), *West Virginia Univ. Tech. Bull.* **77,** *pp. 34–43 (1965).*
The laminar meters discussed are made of one or more uniform passages each having a depth or diameter small in relation to its length. Resistance to flow is largely viscous and may be analyzed in a fairly simple fashion in the incompressible case. For gas flow in these meters, treatment of the effects of deviations from incompressible theory is quite complex; however, errors resulting from ignoring these deviations when predicting meter response at other than calibration conditions are apparently less than the measurement errors over a fairly wide range of conditions. In some applications linear response and independence from pressure level may be approximated closely.

Key Words: Accuracy, calibration, compressible flow, differential meter and effects, fluid meter, incompressible flow, laminar flow, Mach number, Reynolds number, viscous flow, volumetric flow.

Embrittlement of high strength AISI 4340 steel in boiling NaCl solution, H. L. Logan and J. M. Wehrung, *Corrosion* **22,** *No. 9, 265–269 (Sept. 1966).*
The resistance of high strength AISI 4340 steel tubing, quenched in oil and tempered at 425 °F, to corrosive media has been investigated. The exterior surface of the specimen was exposed to boiling NaCl, the interior cavity was evacuated and the specimen was subjected to a tensile stress. Specimens failed, with little evidence that cracking was developing, after several hours exposure and after hydrogen had penetrated through the specimen wall. The appearance of the initial fracture and its mode of development indicate that it originated within the specimen wall. The data indicate that failure resulted from hydrogen embrittlement.

Key Words: Boiling sodium chloride solution, delayed failure, high strength steel, hydrogen embrittlement, hydrogen diffusion, internal initiation, stress-corrosion.

Some effects of notch geometry on the tensile behavior of annealed type 310 stainless steel, G. W. Geil, *J. Materials* **1,** *No. 3, 583–608 (Sept. 1966).*
A study was made of the influence of notch geometry (angle, depth and root radius) on the tensile deformation and fracture characteristics of circumferentially notched cylindrical tensile specimens of annealed 310 stainless steel at ambient temperatures. Specimens with a root radius of 0.05 inch or less and theoretical stress concentration factors of 1.6 or greater, regardless of notch angle or depth, exhibited cracking at small plastic strains. These strains were generally much smaller than the strains at maximum load. The cracking slowly increased in depth in a discontinuous manner with increase in applied stress and extension of the specimen until a condition of plastic instability was reached, resulting in a final rapid fracture of the specimen. Notched specimens with a root radius of 0.10 inch or greater, and theoretical stress concentration factors less than 1.6 did not exhibit any cracking at the root of the notch prior to the final rapid fracture.

Key Words: Fracture, initial cracking, multiaxial stresses, notch geometry, 310 stainless steel, stress concentrations, tensile deformation, workhardening.

A nonmagnetic laboratory for the National Bureau of Standards, F. K. Harris, *IEEE Spectrum* **3,** *No. 11, 85–87 (Nov. 1966).*
Plans are discussed for a nonmagnetic laboratory to be built on the Gaithersburg campus of the National Bureau of Standards for absolute electrical measurements and other purposes. The operation of the NBS current balances and the proton gyromagnetic ratio apparatus is briefly reviewed, and a short history of the national electrical units since the creation of the Bureau is included.

Key Words: Absolute ampere determination, calculable inductor, current balance, national electrical units, nonmagnetic facility, pellat dynamometer, proton precession frequency.

A scattering chamber for use with cooled large area lithium-compensated silicon radiation detectors, W. R. Dodge, J. A. Coleman and S. R. Domen, *Nucl. Instr. Methods* **42,** *181–187 (July 1966).*
A scattering chamber designed to be used with large area lithium-compensated silicon radiation detectors has been constructed. The chamber has provision for cooling a circular array of detectors to 77 °K to achieve short charge collection times and good resolution. The apparatus was designed to be used with the NBS 180-MeV synchrotron in photoproton experiments in the 2 to 35 MeV proton energy interval.

Key Words: Detector telescope, large area detectors, photonuclear physics apparatus, scattering chamber, semiconductor detectors.

Lithium-compensated silicon focal plane detectors for electron scattering spectrometers, W. R. Dodge, J. A. Coleman, S. R. Domen and J. K. Whittaker, *Rev. Sci. Instr.* **37,** *No. 9, 1151–1159 (Sept. 1966).*
In order to utilize the inherent resolving power of a double-focusing, 169.8°, 76.2-cm radius-of-curvature magnetic spectrometer being constructed at the National Bureau of Standards for elastic- and inelastic-electron nuclear scattering studies, focal plane counters were needed whose dimension along the direction of momentum dispersion was 1-mm. This paper describes the fabrication techniques and performance of lithium-compensated silicon $1 \times 1 \times 60$-mm radiation detectors which seem well suited for use as focal plane detectors for the above spectrometer. Differential and integral pulse height distributions for 10–40 MeV electrons incident on the counters are presented as a function of the temperature and bias voltage. Effects due to the finite width of the counters are discussed. A tunnel diode discriminator which provides the desired binary information to the NBS data processing system is described.

Key Words: Electron scattering, focal plane detectors, lithium-compensated silicon, low temperature radiation detectors, photonuclear physics apparatus, rectangular counters, spectrometer.

Measurement of the mean energy required to create an electron-hole pair in silicon between 6 and 77 °K, W. R. Dodge, S. R. Domen, T. F. Leedy, and D. M. Skopik, *Phys. Rev. Letters* **17,** *No. 12, 653–655 (Sept. 19, 1966).*
Relative values of the mean energy required to create an electron-hole pair with ^{207}Bi conversion electrons between 6 and 77 °K have been measured. The data show that ϵ exhibits no first order variation with temperature from 6 to 77 °K. Previous measurements had yielded values as high as $5.22 \pm .02$ eV/electron-hole pair at 20 °K.

Key Words: Energy require to create an electron-hole pair, low temperature, recombination, Shockley theory of ϵ, silicon radiation detectors, trapping.

Multiple diffraction in the Weissenberg methods, A. Santoro and M. Zocchi, *Acta Cryst.* **21,** *Pt. 3, 293–297 (Sept. 1966).*
The conditions for multiple diffraction due to symmetry have been derived for the Weissenberg geometry, for the various crystal systems and for the most commonly used rotation axes.

It is shown that the equal-cone method is the most appropriate in intensity measurements.

Key Words: Crystal structure, diffraction, multiple diffraction, Weissenberg method.

Other NBS Publications

J. Res. NBS 71A (Phys. and Chem.), No. 2, (Mar.–Apr. 1967), $1.00.

Relative enthalpy of beryllium 1:1-aluminate, $BeO \cdot Al_2O_3$, from 273 to 1173 °K. Thermodynamic properties from 273 to 2150 °K. D. A. Ditmars and T. B. Douglas.

Relative enthalpy of beryllium 1:3-aluminate, $BeO \cdot 3Al_2O_3$, from 273 to 1173 °K. Thermodynamic properties from 273 to 2150 °K. D. A. Ditmars and T. B. Douglas.

The heats of combustion of polytetrafluoroethylene (Teflon) and graphite in elemental fluorine. E. S. Domalski and G. T. Armstrong.

Phase relations in the systems TiO_2-IrO_2 and SnO_2-IrO_2 in air. C. L. McDaniel and S. J. Schneider.

Sample purity and the N.Q.R. of Cl^{35} in $KClO_3$ at 0 °C. D. B. Utton.

Techniques for the growth of large single crystals of potassium of high purity. H. J. Foster and P. H. E. Meijer.

Synthesis of *α*-L-fucose-*1*-^{14}C (6-deoxy-L-galactose-*1*-^{14}C. H. S. Isbell, H. L. Frush, and N. B. Holt.

Deuterium isotopes effects in *α*-*β* in the pyranose-furanose interconversions. H. S. Isbell and C. W. R. Wade.

Calculated transition strengths between the configurations $5d^8$ 6s and $5d^8$ 6*p* in Au III. H. Mendlowitz.

Hartree-Fock multiplet strengths for K I, Ca II, and Sc III. A. W. Weiss.

Oscillator strengths for the helium isoelectronic sequence. A. W. Weiss.

Solvent effects on the ultraviolet absorption of polystyrene. V. M. Story, D. McIntyre, and J. H. O'Mara.

J. Res. NBS 71B (Math. and Math. Phys.), No. 1 (Jan.–Mar. 1967), 75 cents.

Algorithms for frames and lineality spaces of cones. R. J. B. Wets and C. Witzgall.

The coefficients of the powers of a polynomial. M. Newman.

Stable evaluation of polynomials. C. Mesztenyi and C. Witzgall.

On involutions. O. Shisha and C. B. Mehr.

Minimum number of subsets to distinguish individual elements. P. R. Meyers.

E-transforms. F. M. Ragab.

Three observations on nonnegative matrices. A. J. Hoffman.

Additional remarks on a theorem of M. Riesz. J. M. Smith.

Standard Reference Materials: Determination of oxygen in ferrous materials SRM 1090, 1091, and 1092, O. Menis and J. T. Sterling, Misc. Publ. 260–14 (Sept. 23, 1966), 30 cents.

Critical Phenomena, Proceedings of a conference held in Washington, D.C., April 1965, ed. M. S. Green and J. V. Sengers, Misc. Publ. 273 (Dec. 1, 1966), $2.50.

Hydraulic research in the United States 1966, ed. H. K. Middleton and G. Kulin, Misc. Publ. 280 (Sept. 8, 1966), $1.50.

High temperature properties and decomposition of inorganic salts. Part I. Sulfates, K. H. Stern and E. L. Weise, NSRDS–NBS7 (Oct. 1, 1966), 35 cents.

Mat-formed wood particleboard, CS236–66 (Apr. 15, 1966), 10 cents.

A survey of some empirical and semi-empirical interatomic and intermolecular potentials, B. M. Axilrod, Tech. Note 246 (Oct. 3, 1966), 40 cents.

Disclosures on: A transrotor engine, high temperature platinum resistance thermometer, dynamic analog correlation system, and combination metering and safety valve for filling sonde balloons with hydrogen, ed. D. Robbins and A. J. Englert, Tech. Note 295 (Oct. 21, 1966), 25 cents.

Observed phase-front distortion in simulated earth-to-space microwave transmissions, H. B. Janes and M. C. Thompson, Jr., Tech. Note 339 (May 12, 1966), 50 cents. (Formerly Central Radio Propagation Laboratory of the National Bureau of Standards, now Environmental Science Services Administration, Boulder, Colo.)

The long-term performance of two rubidium vapor frequency standards, B. E. Blair and A. H. Morgan, Tech. Note 341 (June 22, 1966), 25 cents.

Hydromagnetic wave propagation near 1 c/s in the upper atmosphere and the properties and interpretation of Pc 1 micropulsations, J. A. Dawson, Tech. Note 342 (June 30, 1966), 40 cents. (Formerly Central Radio Propagation Laboratory of the National Bureau of Standards, now Environmental Science Services Administration, Boulder, Colo.)

On the natural shift of a resonance frequency, R. J. Harrach, Tech. Note 346 (Sept. 29, 1966), 25 cents.

Electrochemical analysis: studies of acids, bases, and salts by EMF, conductance, optical, and kinetic methods, July 1965 to June 1966, ed. R. G. Bates, Tech. Note 400 (Sept. 6, 1966), 55 cents.

Activities of the NBS Spectrochemical Analysis Section July 1965 through June 1966, ed. B. F. Scribner, Tech. Note 401 (Sept. 30, 1966), 55 cents.

Microchemical Analysis Section: summary of activities July 1965 to June 1966, ed. J. K. Taylor, Tech. Note 403 (Sept. 1, 1966), 50 cents.

Organic chemistry: air pollution studies; kinetic behavior of sugars in solution; carbon-14- and tritium-labeled carbohydrates; characterization of chemical structures, phenylhydrazono-phenylazo tautomerism; synthesis of research materials, cyclopentitols and related substances; novel research materials; standard reference materials (organic), July 1965 through June 1966, ed. H. S. Isbell, Tech. Note 405 (Sept. 30, 1966), 60 cents.

Superconductive materials and some of their properties, B. W. Roberts, Tech. Note 408 (Sept. 26, 1966), 45 cents.

Fortran programs for the calculation of Wigner 3*j*, 6*j*, and 9*j* coefficients for angular momenta 80, R. S. Caswell and L. C. Maximon, Tech. Note 409 (Nov. 15, 1966), 40 cents.

Improved Fortran program for single particle energy levels and wave functions in nuclear structure calculations, R. S. Caswell, Tech. Note 410 (Sept. 30, 1966), 25 cents.

Analysis of lanolin in soap, F. J. Linnig, Soap Chem. Specialties **XVLL**, No. 7, 55–57 (July 1966).

Analytical applications of microwave spectroscopy, D. R. Lide, Jr., Book, Advances in Analytical Chemistry and Instrumentation 5, 235–277 (Interscience Publ., New York, N.Y., 1966).

Chemical substructure searching with linear notations, B. A. Marron, G. R. Boltsky, and S. J. Tauber, J. Chem. Doc. **6,** 92–95 (May 1966).

Determination of glycerol in paper, E. L. Graminski and B. W. Forshee, Tappi **49,** No. 7, 324–326 (July 1966).

Electron spin resonance studies of the reaction of water-soluble polymers with hydroxyl radicals, F. Sicilio, M. Dousset, R. E. Florin, and L. A. Wall (Proc. 150th American Chemical Society Meeting, Atlantic City, N.J., Sept. 12–17, 1965), Polymer Preprint **6,** No. 2, 958–964 (Sept. 1965).

Experimental and theoretical studies of photoionization efficiency curves for C_2H_2 and C_2D_2, R. Botter, V. H. Dibeler, J. A. Walker, and H. M. Rosenstock, J. Chem. Phys. **44,** No. 3, 1271–1278 (Feb. 1966).

Gas-phase radiolysis and photolysis of neopentane, S. G. Lias and P. Ausloos, J. Chem. Phys. **43,** No. 8, 2748–2759 (Oct. 1965).

Identification of inclusions with the electron probe microanalyzer, K. F. J. Heinrich, Am. Soc. Testing Mater. Spec. Tech. Publ. **393** (Jan. 1966).

Intramolecular insertion of isobutylidene in the vacuum ultraviolet photolysis of isobutane, E. Tschuikow-Roux and J. R. McNesby, Trans. Faraday Soc. **62,** No. 524, 2158–2163 (Aug. 1966).

Investigation of polymer pyrolysis with thermogravimetry, J. H. Flynn and L. A. Wall (Proc. 150th American Chemical Society Meeting, Atlantic City, N.J., Sept. 12–17, 1965), Polymer Preprint **6,** No. 2, 945–955 (Sept. 1965).

Mass spectrometric study of the reactions of O atoms with NO and NO_2, Erratum, J. T. Herron, J. Chem. Phys. **44,** No. 9, 3645 (May 1966).

Oxidation of asphalt flux with oxides of nitrogen, P. G. Campbell and J. R. Wright, Am. Chem. Soc. Div. Petroleum Chem. **10,** No. 1, 79–89 (Mar. 1965).

Phenylhydrazono-phenylazo tautomerism. Part I. xylo-4,5,6-trihydroxy-2-oxo-1, 3-bis(phenylhydrazono) cyclohexane and 4-

oxo-1-phenyl-5-phenylazo-3-pyridazine derivatives, H. S. Isbell and A. J. Fatiadi, Carbohydrate Res. **2,** No. 2, 204–215 (June 1966).

Polymerization and pyrolysis of poly-1, 2-dihydronaphthalene, L. A. Wall, L. J. Fetters, and S. Straus (Proc. 150th American Chemical Society Meeting, Atlantic City, N.J., Sept. 12–17, 1965), Polymer Preprint **6,** No. 2, 930–939 (Sept. 1965).

Radiation-induced polymerization at high pressure of 3,3,3-trifluoropropene; 4,4,4,3,3-pentafluorobutene-1; and 5,5,5,4,4,3,3,-heptafluoropentene-1, D. W. Brown (Proc. 150th American Chemical Society Meeting, Atlantic City, N.J., Sept. 12–17, 1965), Polymer Preprint **6,** No. 2, 965–976 (Sept. 1965).

Solid-vapor equilibrium in the system helium-methane, M. J. Hiza and A. J. Kidnay (Proc. 1965 Cryogenic Engineering Conf., Rice University, Houston, Tex., Aug. 23–25, 1965), Book, Advances in Cryogenic Engineering II, 338–348 (Plenum Press Inc., New York, N.Y., 1966).

Status of light-element heat-capacity calorimetry at the National Bureau of Standards: a review of the high-temperature thermodynamics of the BeO-H_2O system, T. B. Douglas, Proc. 4th Meeting Interagency Chemical Rocket Propulsion Group, Working Group of Thermochemistry, Kennedy Space Flight Center, Florida, Mar. 16–17, 1966, I, No. 108, 27 (Chemistry Propulsion Information Agency, Silver Spring, Md., June 1966).

The crystal and molecular structure of dichloro (1,10-phenanthroline) zinc, C. W. Reimann, S. Block, and A. Perloff, Inorg. Chem. **5,** No. 7, 1185–1189 (July 1966).

The crystal structure of the high temperature form of barium borate, $BaO \cdot B_2O_3$, A. D. Mighell, A. Perloff, and S. Block, Acta Cryst. **20,** pt. 6, 819–823 (June 1966).

The determination of bound styrene in soluble high styrene-butadiene resins, M. A. Post, J. Paint Tech. Eng. Official Digest **38,** No. 497, 335–342 (June 1966).

The determination of heats of formation of refractory compounds, G. T. Armstrong and E. S. Domalski, Proc. 4th Meeting Interagency Chemical Rocket Propulsion Group, Working Group on Thermochemistry, Kennedy Space Flight Center, Florida, March 16–18, 1966, I, No. 108, 15 (Chemistry Propulsion Information Agency, Silver Spring, Md., June 1966).

The determination of mercury in latex paints and paint films containing mercury fungicides, H. W. Berger, J. Paint Technol. **38,** No. 498, 371–376 (July 1966).

The evolution of the accuracy of isotopic analysis by thermal ionization from 2% to 0.2%, W. R. Shields (Proc. Symp. Nuclear Materials Management, IAEA, Vienna, Austria, Aug. 30–Sept. 3, 1965), Book, Nuclear Materials Management, pp. 737–746 (Intern. Atomic Energy Agency, Vienna, Austria, Feb. 1966).

The monomer-polymer equilibrium of alpha-trideuteromethyl-beta, beta-dideuterostyrene, L. J. Fetters and L. A. Wall, (Proc. 150th American Chemical Society Meeting, Atlantic City, N.J., Sept. 12–17, 1965), Polymer Preprint **6,** No. 2, 899–903 (Sept. 1965).

The radiation induced polymerization of hexafluoropropylene at high temperature and pressure, R. E. Lowry, D. W. Brown, and L. A. Wall (Proc. 150th American Chemical Society Meeting, Atlantic City, N.J., Sept. 12–17, 1965), Polymer Preprint **6,** No. 2, 977–984 (Sept. 1965).

Thermal decomposition of hexamethylethane, 2,2,3-trimethylbutane and neopentane in a single pulse shock tube, W. Tsang, J. Chem. Phys. **44,** No. 11, 4283–4295 (June 1, 1966).

Thermolytic chain scission of linear polyethylene and an ethylene-propylene copolymer, H. Yu and L. A. Wall (Proc. 150th American Chemical Society Meeting, Atlantic City, N.J., Sept. 12–17, 1965), Polymer Preprint **6,** No. 2, 940–944 (Sept. 1965).

Vacuum-ultraviolet photolysis of paraffin hydrocarbons, J. R. McNesby, Book, Chemical and Biological Actions of Radiation, **IX,** ch. 2, 39–67 (Masson and Co., Editors and Publ., Paris, France, 1966).

Advances in cryogenic engineering, Book, K. D. Timmerhaus, editor, Proc. 1964 Cryogenic Engineering Conf., University of Pennsylvania, Philadelphia, Pa., Aug. 18–21, 1964, 10, pt. 1 (Plenum Press, Inc., New York, N.Y., 1965).

Apparatus for studying the effects of atmospheric pollution and cyclic dew formation on the deterioration of materials, J. W. Pitts and D. G. Moore, Mater. Res. Std. **6,** No. 7, 328–333 (July 1966).

A cold moderator refrigerator incorporating a high-speed turbine expander, R. O. Voth, M. T. Norton, and W. A. Wilson (Proc. 1965 Cryogenic Engineering Conf., Rice University, Houston, Tex., Aug. 23–25, 1965), Book, Advances in Cryogenic Engineering 11, 126–138 (Plenum Press Inc., New York, N.Y., 1966).

A proposal for a supplement to the patent system, S. Henig, Design News Mag. **21,** No. 1, 84–89 (Jan. 5, 1966).

Bond with reinforcing steel, D. Watstein, ASTM Significance of Tests of Concrete and Concrete Making Materials, Am. Soc. Testing Mater. Spec. Tech. Publ. **169A,** pp. 239–245 (July 1966).

Chemical admixtures, B. E. Foster, ASTM Significance of Tests of Concrete and Concrete Making Materials, Am. Soc. Testing Mater. Spec. Tech. Publ. **169A,** pp. 556–564 (July 1966).

Comparative study of forced convection boiling heat transfer correlations for cryogenic fluids, P. J. Giarratano and R. V. Smith (Proc. 1965 Cryogenic Eng. Conf., Rice University, Houston, Tex., Aug. 23–25, 1965), Book, Advances in Cryogenic Engineering II, 492–506 (Plenum Press Inc., New York, N.Y., 1966).

Floor coverings, T. H. Boone, Book, Building Construction Handbook, 2d edition, ed. F. S. Merritt, Sec. 13, pp. 13–1 – 13–8 (1965).

Free radical microwave absorption meter, H. E. Radford, Rev. Sci. Instr. **37,** No. 6, 790–792 (June 1966).

Instrumentation and measurements, H. E. Bussey and J. E. Gray, Digest of Literature on Dielectrics **28,** ch. I., 1–31 (1964); Natl. Acad. Sci.-Natl. Res. Council Publ. 1324 (Natl. Acad. Sci.-Natl. Res. Council, Washington, D.C., 1965).

International advances in cryogenic engineering, Book, K. D. Timmerhause, editor, Proc. 1964 Cryogenic Engineering Conf., Univ. Pennsylvania, Philadelphia, Pa., Aug. 18–21, 1964, 10, pt. 2 (Plenum Press, Inc., New York, N.Y., 1965).

Liquid-solid mixtures of hydrogen near the triple point, D. B. Mann, P. R. Ludtke, C. F. Sindt, and D. B. Chelton (Proc. 1965 Cryogenic Engineering Conf., Rice University, Houston, Tex., Aug. 23–25, 1965), Book, Advances in Cryogenic Engineering II, 207–217 (Plenum Press, Inc., New York, N.Y., 1966).

Message from outgoing editor, R. W. Beatty, IEEE Trans. Microwave Theory Tech. **MTT-14,** No. 4, 170 (Apr. 1966).

Metals for use in orthopedics, S. J. Rosenberg, Book, Orthotics Etcetra, ed. S. Licht, 9, 77–94 (E. Licht Publ., New Haven, Conn., 1966).

Voluntary product standards – what they mean to the consumer, M. Lonie, J. Home Econ. **58,** No. 1, 22 (Jan. 1966).

New method and problems in combinatorial optimization, A. J. Goldman, Washington Oper. Res. Council Newsletter **5,** No. 8, 4–8 (Apr. 1966).

On the complex structure of the universe, E. H. Brown, J. Math. Phys. **7,** No. 3, 417–425 (Mar. 1966).

Atomic timekeeping and the statistics of precision signal generators, J. A. Barnes, Proc. IEEE **54,** No. 2, 207–220 (Feb. 1966).

A superconducting liquid-level sensor for slush hydrogen use, B. L. Knight, K. D. Timmerhaus, and T. M. Flynn (Proc. 1965 Cryogenic Engineering Conf., Rice University, Houston, Tex., Aug. 23–25, 1965), Book, Advances in Cryogenic Engineering 11, 218–222 (Plenum Press Inc., New York, N.Y., 1966).

Effects of long-term stability on the definition and measurement of short-term stability, J. A. Barnes and D. W. Allan, Proc. IEEE–NASA Symp. Definition and Measurement of Short-Term Frequency Stability, NASA Spec. Publ. No. 80, pp. 119–123 (Nov. 23–24, 1964).

Evaluation of a thallium atomic beam frequency standard at the National Bureau of Standards, R. E. Beehler and D. J. Glaze, IEEE Trans. Instr. Meas. **IM-15,** No. 1 & 2, 55–58 (Mar.-June 1966).

LF-VLF frequency and time services of the National Bureau of Standards, D. H. Andrews, IEEE Trans. Instr. Meas. **IM-14,** No. 4, 233–237 (Dec. 1965).

Quantity control – A tool of industry, and arm of government, M. W. Jensen, Proc. Annual Conf. Society for the Advancement of Food Service Research, Washington, D.C. (Apr. 18, 1966).

Remote positioner for rotary switches, S. B. Lang, and A. M. Gray, Rev. Sci. Instr. **37,** No. 6, 799–801 (June 1966).

The performance and capability of cesium beam frequency standards at the National Bureau of Standards, R. E. Beehler and D. J. Glaze, IEEE Trans. Instr. Meas. **IM-15,** No. 1 & 2, 48–55 (Mar.-June 1966).

Time resolved microwave interferometry on diagnostic tool for decaying plasma afterglows, A. J. Estin and M. M. Anderson, Rev. Sci. Instr. **37,** No. 4, 468–470 (Apr. 1966).

Analyzing liquid H_2 with NMR, C. E. Miller, W. J. Alspach, and T. M. Flynn, Cryogenic Engr. News **1,** No. 8, 66 (June 1966).

Angular dependence of the one-phonon-nuclear quadrupole interactions, R. J. Mahler, J. Phys. Chem. Solids **27,** 871–879 (1966).

A suggested experiment to measure part of the transverse electromagnetic mass of the electron, E. A. Power, Proc. Roy. Soc. (London) **292,** No. 1430, 424–432 (May 31, 1966).

Brillouin scattering in liquids at 4880 Å, S. L. Shapiro, M. McClintock, D. A. Jennings, and R. L. Barger, IEEE Quantum Electronics **QE-2,** No. 5, 89–93 (May 1966).

Calculated line strengths for the transition array for d^2s-d^2p: application to Ni II, H. Mendlowitz, Astrophys. J. **143,** No. 2, 573–590 (Feb. 1966).

Calculated slant-path absorption and distribution of atmospheric water vapor, R. F. Calfee and D. M. Gates, Appl. Opt. **5,** No. 2, 287–292 (Feb. 1966).

Comments on the mechanism of the 377-micron CN laser, H. P. Broida, K. M. Evenson, and T. T. Kikuchi, J. Appl. Phys. **36,** No. 10, 3355 (Oct. 1965).

Comparison of the Lennard-Jones, Exp: 6, and Kihara potential functions from viscosity data of dilute argon, H. J. M. Halney, J. Chem. Phys. **44,** No. 11, 4219–4222 (June 1966).

Direct ratio readings from a universal ratio set, D. Ramaley and J. F. Schafer, Instr. Control Systems **39,** 73–74 (Jan. 1966).

Dielectric relaxation in molecular crystals: multiple site models, J. D. Hoffman, Book, Molecular relaxation processes, Chemical Society Spec. Publ. **20,** pp. 47–60 (The Chemical Society and Academic Press, New York, N.Y., 1966).

Electric quadrupole transition in the $A^1\pi\epsilon X^1\Sigma^+$ system of CO, J. D. Simmons and S. G. Tilford, J. Chem. Phys. **44,** No. 11, 4145–4147 (June 1966).

Electron impact ionization cross section data for atoms, atomic ions, and diatomic molecules: I. Experimental data, L. J. Kieffer and G. H. Dunn, Rev. Mod. Phys. **38,** No. 1, 1–33 (Jan. 1966).

Franck-Condon factors for the ionization of H_2 and D_2, G. H. Dunn, J. Chem. Phys. **44,** No. 7, 2592–2594 (Apr. 1966).

Fundamentals of ultrasonics, M. Greenspan, J. Acoust. Soc. Am. **37,** No. 1, 158–159 (July 1965).

Impact broadening of microwave spectra, A. Ben-Reuven, Phys. Rev. **145,** No. 1, 7–22 (May 1966).

Infrared spectra of HCl, DCl, HBr, and DBr in solid rare-gas matrices, D. E. Mann, N. Acquista, and D. White, J. Chem. Phys. **44,** No. 9, 3453–3467 (May 1966).

Ion mobilities in helium, E. C. Beaty, J. C. Browne, and A. Dalgarno, Phys. Rev. Letters **16,** No. 17, 723–724 (Apr. 1966).

Low-temperature phase transformations, R. P. Reed and J. F. Breedis, Behavior of Materials at Cryogenic Temperatures, Am. Soc. Testing Mater. Spec. Tech. Publ. No. 387, pp. 60–132 (1966).

Low temperature speed of sound in single crystal ice, T. M. Proctor, Jr., J. Acoust. Soc. Am. **39,** No. 5, 972–977 (May 1966).

Measurements of collisional energy transfer between rotational energy levels in CN, K. M. Evenson and H. P. Broida, J. Chem. Phys. **44,** No. 4, 1637–1641 (Feb. 15, 1966).

Measurements of the viscosity of parahydrogen, D. E. Diller (Proc. IXth Intern. Conf. Low Temperature Physics, Columbus, Ohio, Aug. 31-Sept. 4, 1964), Book, Low Temperature Physics, LT9, pt. B, pp. 1227–1229 (Plenum Press, Inc., New York, N.Y., 1965).

Nonlinear diffusion with recombination in an electron beam excited plasma, E. R. Mosburg, Jr., Phys. Fluids **9,** No. 4, 824–826 (Apr. 1966).

Nuclear spin relaxation in liquid hydrogen, C. E. Miller, T. M. Flynn, T. K. Grady, and J. S. Waugh, Physica **32,** No. 2, 244–251 (Feb. 1966).

One dimensional solutions of the Ginzburg-Landau equations for thin superconducting films, V. D. Arp, R. S. Collier, R. A. Kamper, and H. Meissner, Phys. Rev. **145,** No. 1, 231–236 (May 6, 1966).

Physics of the *D* region at high latitudes, G. C. Reid (Proc. NATO Advanced Study Institute, Finse, Norway, April 1965), Book, Electron Density Profiles in Ionosphere and Exosphere, ed. J. Frihagen, pp. 17–26 (North Holland Publ. Co., Amsterdam, The Netherlands, 1966).

Polycrystalline spin wave theory of ferromagnetic resonance compared with the tilting experiment, A. S. Risley, E. G. Johnson, Jr., and H. E. Bussey, J. Appl. Phys. **37,** No. 2, 656–668 (Feb. 1966).

Radiation lifetime of the first $2_{p3/2}$ state of ionized calcium and magnesium by the Hanle effect, W. W. Smith and A. C. Gallagher, Phys. Rev. **145,** No. 1, 26–35 (May 6, 1966).

Saturation effects in the sensitized fluorescence of CaF_2(Ce, Mn), B. L. Danielson, Phys. Rev. **142,** No. 1, 228–230 (Feb. 4, 1966).

Soft x-ray spectrum of Ni and comparison with photoemission and ion neutralization results, J. R. Cuthill, A. J. McAlister, and M. L. Williams, Phys. Rev. Letters **16,** No. 22, 993–995 (May 30, 1966).

Some properties of the long-time values of the probability densities for moderately dense gases, R. A. Piccirelli, J. Math. Phys. **7,** 922 (1966).

Summary of recent determinations of the ultrasonic velocity in fluid parahydrogen, B. A. Younglove, (Proc. IXth Intern. Conf. Low Temperature Physics, Columbus, Ohio, Aug. 31–Sept. 4, 1964), Book, Low Temperature Physics LT9, pt. B., pp. 1223–1226 (Plenum Press Inc., New York, N.Y., 1965).

The Chapman-Enskog solution of the generalized Boltzmann equation, M. S. Green, L. S. Garcia-Colin, and F. Chaos, Physica **32,** 450 (1966).

The flow field of a body-stabilized two-dimensional V-flame, F. W. Ruegg and W. W. Dorsey, Combustion and Flame **10,** No. 1, 1–10 (Dec. 1966).

The role of hydrogen in the stress-corrosion cracking of low carbon steel in a nitrate solution, H. L. Logan and H. T. Yolken, Proc. 2d Intern. Congress Metallic Corrosion, New York, N.Y., March 1963, p. 109 (Natl. Assoc. Corrosion Engr., Houston, Texas, 1966).

The spheroidal method in the theory of the orbit of an artificial satellite, J. P. Vinti, Proc. Symp. Celestial Mechanics, Mathematische Forschungsinstitut, Oberwolfach, Germany, March 1964, pp. 97–111 (1964).

The theory of chromospheric spectrum, J. T. Jefferies, Book, The Solar Spectrum, ed. C. DeJager, pp. 131–150 (D. Reidel Publ. Co., Dordrecht, The Netherlands, 1965).

Thermodynamics of the rigid-rotor at high temperature, J. E. Kilpatrick, Y. Fukuda, and S. Y. Larsen, J. Chem. Phys. **43,** No. 2, 430–432 (July 1965).

Thermophysical properties of metals at cryogenic temperatures, R. L. Powell, Behavior of Materials at Cryogenic Temperatures, Am. Soc. Testing Mater. Spec. Tech. Publ. No. 387, pp. 134–148 (1966).

Vacuum ultraviolet spectrum of neutral silicon, V. Kaufman, L. J. Radziemski, Jr., and K. L. Andres, J. Opt. Soc. Am. **56,** No. 7, 911–915 (July 1966).

Zero-point energy and Lamb shift, E. A. Power, Am. J. Phys. **34,** No. 6, 516–518 (June 1966).

Computed performance of moderate size, super-gain, end-fire antenna arrays, C. O. Stearns, IEEE Trans. Ant. Prop. **AP-14,** No. 2, 241–242 (Mar. 1966).

Electron precipitation and ionospheric radio absorption in the auroral zones, K. L. Hargreaves and R. D. Sharp, Planetary Space Sci. **13,** 1171–1183 (Dec. 1965).

Evidence of long-period acoustic-gravity waves launched into the *F* region by the Alaskan earthquake of March 28, 1964, R. V. Row, J. Geophys. Res. Letter **71,** 343–345 (Jan. 1966).

International URSIGRAM and world days service "report on activities in 1964," A. H. Shapley, URSI Info. Bull. No. 150, pp. 43–55 (May 1965).

Ionospheric effects of particles, G. C. Reid, Proc. COSPAR Polar Cap Panel Symp., Alpach, Austria, 1964, pp. 221–231 (Academic Press Inc., New York, N.Y., 1965).

Linear tuning of a microwave cavity, M. J. Vetter, IEEE Trans. Microwave Theory Tech. **MTT-13,** No. 6, 880 (Nov. 1965).

Observations of ionospheric irregularities and plasma resonances by the fixed-frequency topside sounder satellite, W. Calvert, (Proc. NATO Advanced Study Institute, Finse, Norway, April 1965), Book, Electron Density Profiles in Ionosphere and Exosphere, ed. J. Frihagen, pp. 281–298 (North Holland Publ. Co. Amsterdam, The Netherlands, 1966).

Observations of the equatorial ionosphere using incoherent backscatter, D. T. Farley (Proc. NATO Advanced Study Institute, Finse, Norway, April 1965), Book, Electron Density Profiles in Ionosphere and Exosphere, ed. J. Frihagen, pp. 446–469 (North Holland Publ. Co., Amsterdam, The Netherlands, 1966).

Slow fluctuations between conjugate points in the auroral absorption of cosmic noise, H. J. A. Chivers and J. K. Hargreaves, J. Atmos. Terrest. Phys. **28,** 337–342 (1966).

SPACEWARN—an international mechanism for rapid distribution of information on satellites and space probes, A. H. Shapley, COSPAR Info. Bull. No. 24, pp. 30–55 (July 1965).

Spectral distribution of solar radiation at the earth's surface, D. M. Gates, Science **151,** No. 3710, 523–529 (Feb. 1966).

Statistics of atomic frequency standards, D. W. Allan, Proc. IEEE **54,** No. 2, 221–230 (Feb. 1966).

Swept-frequency antenna gain measurements, R. G. FitzGerrell, IEEE Trans. Ant. Prop. **AP-14,** No. 2, 173–178 (Mar. 1966).

The important atmospheric processes in the *D* region, G. C. Reid, Proc. COSPAR Polar Cap Panel, Alpach, Austria, 1964, pp. 15–19 (Academic Press, Inc., New York, N.Y., 1965).

"Winter anomaly" in ionospheric absorption and stratospheric warnings, A. H. Shapley and W. J. G. Beynon, Nature **206,** 1242–1243 (June 1965).

Dissociation of acetic acid-d_4 in deuterium oxide from 5 to 50° and related isotope effects, M. Paabo, R. G. Bates, and R. A. Robinson, J. Phys. Chem. **70,** 2073–2077 (1966).

Effects of errors in the chemical literature on the compilation of critically evaluated data, W. H. Evans, J. Chem. Doc. **6,** No. 3, 135–136 (Aug. 1966).

Electronically excited NO by photodissociation of NO_2 and NOCl, K. H. Welge, J. Chem. Phys. **45,** No. 4, 113–1117 (Aug. 15, 1966).

Gas-phase photolysis of isopentane at photon energies below and above the ionization energy, A. A. Scala, and P. Ausloos, J. Chem. Phys. **45,** No. 3, 847–854 (Aug. 1, 1966).

Formation of $N_2(A^3\Sigma^+)$ and $N(^2D, ^2P)$ by photodissociation of HN_3 and N_2O and their reactions with NO and N_2O, K. H. Welge, J. Chem. Phys. **45,** No. 1, 166–170 (July 1, 1966).

Glass-molten salt interactions, K. H. Stern, Chem. Rev. **66,** No. 4, 355–372 (July 25, 1966).

Ground state of bis-(acetylacetonato) copper (II), H. C. Allen, Jr., J. Chem. Phys. **45,** No. 2, 553–555 (July 15, 1966).

Interactions in aqueous nonelectrolyte solutions. I. Solute-solvent equilibria, R. H. Stokes and R. A. Robinson, J. Phys. Chem. **70,** 2126–2131 (1966).

K-absorption fine structures of sulfur in gaseous SF_6, R. E. LaVilla and R. D. Deslattes, J. Chem. Phys. **44,** No. 12, 4399–4400 (June 15, 1966).

Losses due to adsorption during filtration of aqueous solutions of polycyclic aromatic hydrocarbons, M. Inscoe, Nature **211,** No. 5053, 1083–1085 (Sept. 3, 1966).

Mass spectrometric study of the rates of the reactions of nitrogen atoms with olefins, J. T. Herron, Phys. Chem. **70,** No. 9, 2803–2807 (Sept. 1966).

Mass-spectrometric study of photoionization. Iv. Ethylene and 1,2-dideuteroethylene, R. Botter, V. H. Dibeler, J. A. Walker, and H. M. Rosenstock, J. Chem. Phys. **45,** No. 4, 1298–1301 (Aug. 15, 1966).

Measurement of photochemical degradation in rigid poly(vinyl chloride) by colour reactions with N,N-dimethyl-*p*-phenylenediamine, J. R. Wright and V. E. Gray, (Proc. Conf. Plastics in Building Structures, London, England, June 14–16, 1965), Plastics Inst. Trans. J. Suppl. **1,** 113–118 (June 14, 1966).

Mossbauer spectrometry, J. R. DeVoe and J. J. Spijkerman, Anal. Chem. **38,** 382R–393R (1966).

Photoionization efficiency curve for SF_6 in the wavelength region 1050 to 600 Å, V. H. Dibeler and J. A. Walker, J. Chem. Phys. **44,** No. 12, 4405–4406 (June 15, 1966).

Photoionization of *n*-butane at 1067–1048 Å. Decomposition of the parent ion and superexcited molecule, P. Ausloos and S. G. Lias, J. Chem. Phys. **45,** No. 2, 524–535 (July 15, 1966).

Study of D_2O ice as a cold-neutron source, J. J. Rush, D. W. Connor, and R. S. Carter, Nucl. Sci. Engr. **25,** 383–389 (1966).

A high directivity, broadband coaxial coupler, P. A. Hudson, IEEE Trans. Microwave Theory Tech. **MTT-14,** No. 6, 293–294 (June 1966).

Development of performance standards, B. E. Foster, Military Engr. **58,** No. 385, 335–336 (Sept.–Oct. 1966).

Roofing research, T. H. Boone, Military Engr. **385,** 344–345 (Sept.–Oct. 1966).

Analysis of multimode experimental data, H. Kurss, IEEE Trans. Ant. Prop. **AP-14,** No. 3, 401–402 (May 1966).

A network-simulation approach to the railroad freight train scheduling and car sorting problem, W. P. Allman, Proc. 4th Intern. Conf. Operational Research, Boston, Mass., Aug. 29–Sept. 2, 1966 (Arthur D. Little Inc., Cambridge, Mass., 1966).

Absorption spectrum of SF_6 in the far ultraviolet by electron impact, J. A. Simpson, C. E. Kuyatt, and S. R. Mileczarek, J. Chem. Phys. **44,** No. 12, 4403–4404 (June 15, 1966).

Chemical and physical mechanisms of salt stress-corrosion cracking in the titanium 8-1-1 alloy, H. L. Logan, M. J. McBee, C. J. Bechtoldt, B. T. Sanderson, and G. M. Ugiansky, (Proc. Stress Corrosion Cracking Symp., Seattle, Washington, Nov. 1965), Am. Soc. Testing Material Spec. Tech. Publ. **397,** pp. 215–229 (1966).

Commission on fundamental spectroscopic data, C. Moore-Sitterly, Trans. Intern. Astron. Union **XIIB,** 173–185 (1966).

Current algebras and matrix elements of the axialvector current, H. J. Lipkin, H. R. Rubinstein, and S. Meshkov, Phys. Rev. **148,** No. 4, 1405–1407 (Aug. 26, 1966).

Electron microscopy of irradiation-induced defect clusters in magnesium fluoride, D. J. Barber, Phys. Stat. Sol. **16,** 531–547 (1966).

Exchange and direct second virial coefficients for hard spheres, M. E. Boyd, S. Y. Larsen, and J. E. Kilpatrick, J. Chem. Phys. **45,** No. 2, 499–508 (July 15, 1966).

Fracture surface energy of soda-lime glass, S. M. Wiederhorn (Proc. Conf. Role of Grain Boundaries and Surface in Ceramics, North Carolina State University, Raleigh, N.C., Nov. 16–18, 1964), Book, Materials Science Research **3,** 503–528 (Plenum Press, Inc., New York, N.Y., 1966).

Heat transfer to a subliming solid-vapor mixture of hydrogen below its triple point, M. C. Jones, T. T. Nagamoto, and J. A. Brennan, AICHE J. **12,** No. 4, 790–795 (July 1966).

Higher symmetries and the 2^+ mesons, D. Horn, J. J. Coyne, S. Meshkov, and J. C. Carter, Phys. Rev. **147,** No. 4, 980–984 (July 29, 1966).

Ionization energies of the neutral rare earths, J. Reader and J. Sugar, J. Opt. Soc. Am. **56,** No. 9, 1189–1194 (Sept. 1966).

L-uncoupling effects on the electron-paramagnetic-resonance spectra of $N^{14}O^{16}$, R. L. Brown and H. E. Radford, Phys. Rev. **147,** No. 1, 6–12 (July 8, 1966).

Magnetization and critical fields of superconducting $SrTiO_3$, E. Ambler, J. H. Colwell, W. R. Hosler, and J. F. Schooley, Phys. Rev. **148,** No. 1, 280–286 (Aug. 5, 1966).

Melting temperatures of copolymers, J. P. Colson and R. K. Eby, J. Appl. Phys. **37,** No. 9, 3511–3514 (Sept. 1966).

Quench defects formed in a low-stacking-fault-energy silver-tin alloy, A. W. Ruff, Jr., and L. K. Ives, J. Appl. Phys. **37,** No. 8, 3073–3079 (July 1966).

Radiation absorption between the ultraviolet and x-ray bands, U. Fano, Science **153,** No. 3735, 522–525 (July 29, 1966).

Structure in the photoionization continuum of SF_6 below 630 Å, K. Codling, J. Chem. Phys. **44,** No. 12, 4401–4402 (June 15, 1966).

SU_3 reaction predictions and symmetry breaking, S. Meshkov, Elementary Particles Conf., Institute for Theoretical Physics, University of Colorado, Boulder, Colo., Summer 1964, Lectures Theoret. Phys. **VII B,** 36–50 (1965).

Triple collision contribution to the transport coefficients of a rigid sphere gas, J. V. Sengers, Phys. Fluids **9,** No. 7, 1333–1347 (July 1966).

Viscoelastic behavior, H. Leaderman, Encyclopaedic Dictionary of Physics **7,** 633–634 (Pergamon Press, Inc., London, England, 1962).

Medium-frequency sky wave propagation in middle and low latitudes, A. F. Barghausen, IEEE Trans. Broadcasting **BC-12,** No. 1, 1–14 (June 1966).

Abstraction of hydrogen atoms from isobutane-d_9 by methylene, M. L. Halberstadt and J. R. McNesby, J. Chem. Phys. **45,** No. 5, 1666–1669 (Sept. 1, 1966).

Chemisorption of nitric oxide on tungsten, J. T. Yates, Jr., and T. E. Madey, J. Chem. Phys. **45,** No. 5, 1623–1634 (Sept. 1, 1966).

Dissociation constant of morpholinum ion and related thermodynamic quantities from 0 to 50°, H. B. Hetzer, R. G. Bates, and R. A. Robinson, J. Phys. Chem. **70,** No. 9, 2869–2872 (Sept. 1966).

Dissociation of 4-aminopyridinium ion in 50% methanol-water and related acidity functions from 10 to 40 °C, M. Paabo, R. A. Robinson, and R. G. Bates, Anal. Chem. **38,** No. 11, 1573–1575 (Oct. 1966).

Electron affinity of tungsten determined by its positive and negative self-surface ionization. M. D. Scheer and J. Fine, Phys. Rev. Letters **17,** No. 6, 283–284 (Aug. 8, 1966).

Kinetics and statistics of structural changes in polyacrylonitrile, K. Noh and H. Yu, J. Polymer Sci. Letters **4B,** No. 10, 721–726 (Oct. 1966).

Mass-spectrometric investigation of the nickel-fluorine surface reaction, J. D. McKinley, J. Chem. Phys. **45,** No. 5, 1690–1693 (Oct. 1, 1966).

Mass-spectrometric study of the rate of the reaction CO + OH, J. T. Herron, J. Chem. Phys. **45,** No. 5, 1854–1855 (Sept. 1, 1966).

Matrix-isolation study of the photolysis of cyanogen azide. II. The symmetric stretching fundamental of the free radical NCN,

D. E. Milligan and M. E. Jacox, J. Chem. Phys. **45,** No. 5, 1387–1391 (Sept. 1, 1966).

Momentum autocorrelation function for systems with finite spatial boundaries, R. Nossal, J. Chem. Phys. **45,** No. 4, 1097–1100 (Aug. 15, 1966).

Pseudonatural orbitals as a basis for the superposition of configurations. I. He_2^+, C. Edmiston and M. Krauss, J. Chem. Phys. **45,** No. 5, 1833–1839 (Sept. 1, 1966).

Translational diffusion in polymer solutions, R. Zwanzig, J. Chem. Phys. **45,** No. 5, 1858–1859 (Sept. 1, 1966).

A simplified method for the prediction of multi-component adsorption equilibria from a single gas isotherms, A. J. Kidnay and A. L. Myers, AIChE J. **12,** No. 5, 981–986 (Sept. 1966).

Coincident summer weather characteristics of six selected cities in the United States, T. Kusuda and P. R. Achenbach, ASHRAE J. **8,** No. 11, 34–42 (Nov. 1966).

Monte Carlo studies of lattice-model polymer chains. I. Correlation functions in the statistical-bead model, P. H. Verdier, J. Chem. Phys. **45,** No. 6, 2118–2121 (Sept. 15, 1966).

Monte Carlo studies of lattice-model polymer chains. II. End-to-end length, P. H. Verdier, J. Chem. Phys. **45,** No. 6, 2122–2128 (Sept. 15, 1966).

A zero-range treatment of the three-body photodisintegration cross section of ^3H and ^3He, J. M. Knight, J. S. O'Connell, and F. Prats, Phys. Letters **22,** No. 3, 322–325 (Aug. 15, 1966).

Anomalous energy spreads in electron beams, J. A. Simpson and C. E. Kuyatt, J. Appl. Phys. **37,** No. 10, 3805–3809 (Sept. 1966).

Bandlike structure from continuum-continuum emission: the He_2 600–Å bands, F. H. Mies and A. L. Smith, J. Chem. Phys. **45,** No. 3, 994–1000 (Aug. 1, 1966).

Classification of the $Y_1(1765)$ and $Y_0(1520)$ resonances in the 1134 representation of SU(6), J. J. Coyne, S. Meshkov, and G. B. Yodh, Phys. Rev. Letters **17,** No. 12, 666–668 (Sept. 19, 1966).

Determination of the effective force constants between a substitutional impurity and its nearest neighbors in an alkali halide crystal, R. A. MacDonald, Phys. Rev. **150,** No. 2, 597–602 (Oct. 14, 1966).

Dielectric constants of $PbMoO_4$ and $CaMoO_4$, W. S. Brower and P. H. Fang, Phys. Rev. **149,** No. 2, 646 (Sept. 16, 1966).

Effect of surface patch fields on field-emission work-function determinations, R. D. Young and H. E. Clark, Phys. Rev. Letters **17,** No. 7, 351–353 (Aug. 15, 1966).

EPR in single crystals of $NiBr_2$, J. S. Wells and D. R. Winder, J. Chem. Phys. **45,** No. 1, 410–411 (July 1, 1966).

Erratum: Statistical model for the beta zirconium hydrides, T. B. Douglas, J. Chem. Phys. **45,** No. 3, 1080 (Aug. 1, 1966).

Microwave spectrum of CF_2, F. X. Powell and D. R. Lide, Jr., J. Chem. Phys. **45,** No. 3, 1067–1068 (Aug. 1, 1966).

Motions of water molecules in potassium ferrocyanide trihydrate, water, and ice: a neutron-scattering study, J. J. Rush, P. S. Leung, and T. I. Taylor, J. Chem. Phys. **45,** No. 4, 1312–1317 (Aug. 15, 1966).

Photodetachment cross section, electron affinity, and structure of the negative hydroxyl ion, L. M. Branscomb, Phys. Rev. **148,** No. 1, 11–18 (Aug. 5, 1966).

The structure of field-evaporated hexagonal close-packed surfaces: rhenium and ruthenium A. J. Melmed, Surface Science **5,** No. 3, 359–379 (Nov. 1966).

Zeeman effect and magnetic hyperfine structure in the low frequency transitions of H_2CO, H. Takuma, K. M. Evenson, and T. Shigenari, J. Phys. Soc. **21,** 1622–1623 (1966).

**Publications for which a price is indicated are available by purchase from the Superintendent of Documents, U.S. Government Printing Office, Washington, D.C. 20402 (foreign postage, one-fourth additional). The NBS nonperiodical series are also available from the Clearinghouse for Federal Scientific and Technical Information, Springfield, Va. 22151. Reprints from outside journals and the NBS Journal of Research may often be obtained directly from the authors.*

U.S. GOVERNMENT PRINTING OFFICE : 1967 OL—247-602

UNIVERSITY MICROFILMS SERIALS SECTION
300 NORTH ZEEB RD
ANN ARBOR MICH

UNITED STATES
GOVERNMENT PRINTING OFFICE
DIVISION OF PUBLIC DOCUMENTS
WASHINGTON, D.C. 20402

OFFICIAL BUSINESS

POSTAGE AND FEES PAID
U.S. GOVERNMENT PRINTING OFFICE

JOURNAL OF RESEARCH of the National Bureau of Standards — Vol. 71C, No. 2 — April–June 1967
C. Engineering and Instrumentation

Contents

	Page
An apparatus for measuring thermal expansion at elevated temperatures. B. D. Rothrock and R. K. Kirby.	85
Determination and smoothing of Fourier coefficients representing piecewise continuous functions. B. A. Peavy.	93
A 2:1 ratio inductive voltage divider with less than 0.1 ppm error to 1 MHz. Cletus A. Hoer and Walter L. Smith.	101
A dual-load flow calorimeter for rf power measurement to 4 GHz. M. L. Crawford and P. A. Hudson.	111
Polymeric materials for dielectric reference specimens. Arnold H. Scott and Joseph R. Kinard, Jr.	119
The sensitivity of the Dicke radiometer. David F. Wait.	127
Sensitivity of a correlation radiometer. John J. Faris.	153
Publications of the National Bureau of Standards.	171

Library of Congress Catalog Card Number: 62–3900

For sale by the Superintendent of Documents, U.S. Government Printing Office, Washington, D.C. 20402. Price 75¢ (single copy). Subscription price: $2.75 a year; 75¢ additional for foreign mailing.
UNITED STATES GOVERNMENT PRINTING OFFICE, WASHINGTON : 1967